# Neuroinflammation and psychosis; antipsychotic medication.

Peter S Bloomfield


Institute of Clinical Sciences - Imperial College London

PhD thesis

# *Declaration of Originality*

The experiments and data analysis performed were part of my own work carried out at the Clinical Sciences Centre. No part of this thesis has been submitted for any other degree or qualification.

Specialist clinical imaging analysis was conducted in collaboration with Mattia Veronese (King's College London) and Sudhakar Selvaraj (Formerly Imperial College London).

Special thanks go to Dirk Dormann for his help with microglial software design.

The methodology discussed relating to the PET modelling in this thesis is published; Turkheimer, FE, Rizzo G, Bloomfield PS, *et al.,* 2015. The methodology of TSPO imaging with positron emission tomography. *Biochemical society transactions*. vol 43; part 4.

**Chapter 3** is in press with the *American Journal of Psychiatry*. Bloomfield PS, Sudhakar S, Veronese V, *et al.,* 2015. Microglial activity in people at ultra high risk of psychosis and in schizophrenia; an [11C]PBR28 PET brain imaging study, *American Journal of Psychiatry (de Paola and Howes, Equal Contribution)*, ISSN:1535-7228

**Chapter 4** is in preparation for publication

**Chapter 5** is in preparation for publication

# *Declaration of Copyright*

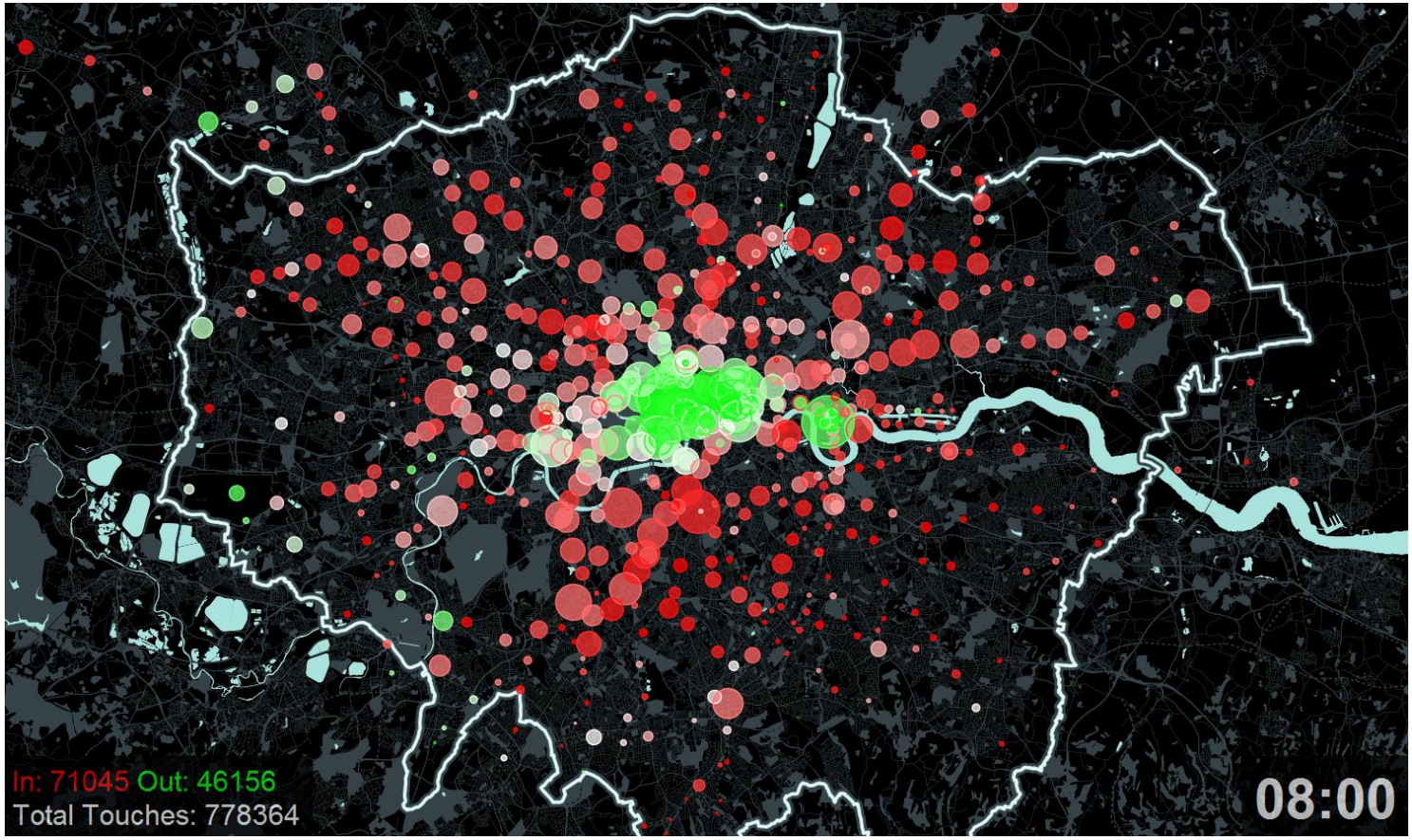


My favourite books start with a map, and as I spent so much time travelling between the IoP and Hammersmith, I decided to use an oyster card contact map of London (8:00-8:10 on a weekday).

(http://mappinglondon.co.uk/wp-content/uploads/2011/07/senseoyster.png (accessed 02/09/15)

# *Abstract*

Neuroinflammation is an early feature of a number of nervous system disorders. Inflammation in the brain is primarily mediated via microglial cells, which are active components of circuit development in the central nervous system. Schizophrenia is a psychiatric illness with deficits in perceptual, cognitive and emotional function. Prior to the onset of psychosis, there is a period of attenuated psychotic symptoms, where individuals experience sub threshold features of psychosis. This 'ultra high risk' period can provide unique opportunities to investigate the development of psychosis. It has been demonstrated through translocator protein (TSPO) positron emission tomographic (PET) imaging that microglial activity is elevated in chronic schizophrenia, however it is unknown whether this elevation is present prior to the onset of psychosis. It is also uncertain what effect antipsychotic medication has on microglia *in vivo*. This thesis is divided between clinical and animal investigation, the results can be split into four findings; Firstly we demonstrate that there is a higher binding of [$^{11}$C]PBR28 (a novel TSPO PET ligand) in ultra high risk subjects and patients with schizophrenia compared to healthy controls. Symptoms in the ultra high risk subjects also correlate with the level of ligand binding. Secondly, brain volumes are not correlated with [$^{11}$C]PBR28 binding or inflammatory cytokine levels in peripheral blood samples. The third finding of this thesis is that antipsychotic drug administration does not appear to alter cortical microglial cells in naïve and systemically inflamed animals. The final finding is that brain volume is reduced by antipsychotic medication. Together these findings demonstrate that inflammation is

present in subjects experiencing subthreshold psychotic symptoms. The animal experiments suggest medicated patients would not be expected to have higher levels of microglial activity than their un-medicated counterparts. Further investigation is needed to determine the mechanism of cortical volume changes after medication and how this relates to TSPO.

# Acknowledgements

*This thesis is dedicated to Gill Madin*

It is hard to know where to start when thanking everyone who has helped both with my work and supporting me generally to get to this point.

Firstly I would like to thank my supervisors, Oliver Howes and Vincenzo De Paola for their support both in terms of my research and ongoing career.

Sudhakar Selvaraj has helped me to learn about and adapt in the clinical world of research, without him I would have struggled incredibly, his moving to the USA is still something I am adjusting to! I will always find it difficult to express how grateful I am to him.

The PET modellers at the IoP and Padova, Mattia, Fet & Gaia, have made analysis of the clinical data possible and they never gave up, even when nothing made sense initially! (Quote Fet's response to PBR28 data analysis, 'It's all fucked!')

I'd like to thank all of Oliver's group and other clinicians who helped with the studies and social elements of my PhD; Ilaria, Michael, Elias, Sameer, Seán, Michelle, Dave Owen & Nicky Kalk. Fede, Graham, Dawn, Lieven, Lucien, Kat, Raquel & Antonio all helped massively with morale in team Hot Lips, as well as with experimental blinding and troubleshooting. My academic mentors, Mark Ungless and Richard Festenstein, both helped to keep me on track with my work and assessments to get me to this point. I'd like to thank all of my year group for their solidarity, but particularly Jo, Ben and ~~Nadia~~.

I think I'll have to thank all my University friends from the various universities in one long list; Dan (who showed me what a real academic CV looked like) & Jess, Bungle

& Marie, Ed & Katie, Kate Horne, George Turner, George & George Martin, Abbie, Dee, Rose & James, Amy, Mo, Daniel, Dru, AJ, Tom Hod, Warran, Ben, Wills, Jamie, Joe, Nick and Sarju Patel, who is sorely missed. I'd like to say a big thank you to my housemates Adrian, Camilo & Ben for putting up with my ramblings over the years. I'm so glad I've managed to stay in touch with my Home friends and have enjoyed all the times we've spend together through to the time of my PhD; Alec & Charis, Piers, Lorrie, Ash, Baz, Ed, Toby, Bill & Anniina, Matt Parish, Rowley, Tom, Mo, Cossie, Coggin and Christine & Dave.

The people I worked with and still see from the Smith Lab at UCL, Andrew, Roshni Dan, Ramona, Nat & Ken, gave me a real taste of research and I value all the help and friendship they've given over the years.

Family play a huge role in life and I'm lucky to have one of the most supportive families ever, so thank you Mum, Dad, Zara, Grandma and Papa (your food parcels and treats have kept me going all the way through university!). My lovely girlfriend Cords has kept me motivated and she's somehow feigned interest through some of the dullest chat a human could ever possibly produce!

Significant teachers at school, some of whom are no longer with us, include; Mr Marsh, Mr Irvine, Dr Dobson, Mr and Mrs Barnard, Mr Norris Mrs Fawcet. Mrs Thewlis gets a special mention, as her spite will always motivate me.

Thanks to Robin Ince for providing me with entertainment in person and via podcast.

Last but by no means least, I give thanks to Gill and David Madin who supported me from a very young age to start to reach my goals. Gill sadly passed away before I started this journey, but I would hope that she'd be proud to see my progress.

# Table of Contents

# *List of figures*

# List of Tables

# *Abbreviations*

2TCM – Two tissue compartment model

2TCM-1K – Two tissue compartment model accounting for endothelial binding

ANOVA – analysis of variance

AP – antipsychotics

ARSAC – Administration of Radioactive Substances Advisory Committee

$Ca^{2+}$ – calcium

CAARMS – Comprehensive assessment of the at risk mental state

CT – Computer tomography

DAPI - 4',6-diamidino-2-phenylindole

DSM – diagnostic and statistical manual of mental disorders

DVR – distribution volume ratio

FGA – First generation antipsychotic

fMRI – functional magnetic resonance imaging

GFAP – Glial fibrillary acidic protein

Hal - Haloperidol

IBA-1 – ionized calcium binding adaptor protein-1

IL-10 – Interleukin 10

IL-12 – Interleukin 12

IL-1β – Interleukin 1β

IL-6 – Interleukin 6

KO – Knockout

LPS – Lipopolysaccharide

MRI – magnetic resonance imaging

MRS – magnetic resonance spectroscopy

NO – nitric oxide

PANSS – Positive and negative syndrome scale

PBR – Peripheral benzodiazepine receptor

PET – Positron emission tomography

PIC – participant identification centre

POB – plasma over blood

PPf – Plasma free fraction

SCID – Structured clinical interview for DSM disorders

SD – standard deviation

SEM – standard error of the mean

SGA – Second generation antipsychotic

TAC – Time activity curve

TNF-α – Tumour necrosis factor α

TSPO – Translocator Protein

Vb – Blood volume

$V_T$ – Volume of distribution

# *Chapter 1 – introduction*

# *Psychosis and Schizophrenia*

## Schizophrenia

The term schizophrenia was first proposed by Eugen Bleuler in 1911 to describe a mental illness with an apparent split of conscious thought segregation from reality (‘schizo’ split, ‘phrene’ mind). It is a chronic disorder of perceptual, cognitive and emotional function. The combination of symptoms is distressing and disabling and has a huge impact on the individual, as well as those providing support. The healthcare burden of schizophrenia is prominent in both developed and developing countries (Howes and Murray, 2014). For the purposes of research, the symptoms of schizophrenia are commonly assessed on the positive and negative syndrome scale (PANSS), which is a summation of the positive (hallucinations and delusions), negative (depressive and social functioning) and general symptoms which comprise the disease state. The aetiology and underlying mechanisms of schizophrenia have not yet been fully elucidated; however dopamine and glutamate are thought to be two main transmitter system abnormalities which contribute to the disease.

## Clinical features and diagnosis of schizophrenia

The diagnosis of schizophrenia is made through clinical interview using a diagnostic schedule such as the diagnostic and statistical manual of mental disorders (DSM IV, a later edition, DSM-5 has been published, however this was not available at the start of the studies presented here (American Psychiatric et al., 2013; Bell, 2001)). The diagnostic criteria for schizophrenia, specified by the American Psychiatric Association in DSM IV are as follows;

“Characteristic symptoms:

A. Two (or more) of the following, each present for a significant portion of time during a 1-month period (or less if successfully treated):

(1) delusions

(2) hallucinations

(3) disorganized speech (e.g., frequent derailment or incoherence

(4) grossly disorganized or catatonic behaviour

(5) negative symptoms, i.e., affective flattening, alogia (poverty of speech), or avolition (lack of motivation) Note: Only one Criterion A symptom is required if delusions are bizarre or hallucinations consist of a voice keeping up a running commentary on the person's behavior or thoughts, or two or more voices conversing with each other.

B. Social/occupational dysfunction: For a significant portion of the time since the onset of the disturbance, one or more major areas of functioning such as work, interpersonal relations, or self-care are markedly below the level achieved prior to the onset (or when the onset is in childhood or adolescence, failure to achieve expected level of interpersonal, academic, or occupational achievement).

C. Duration: Continuous signs of the disturbance persist for at least 6 months. This 6-month period must include at least 1 month of symptoms (or less if successfully treated) that meet Criterion A (i.e., active-phase symptoms) and may include periods of prodromal (symptomatic of the onset) or residual symptoms. During these prodromal or residual periods, the signs of the disturbance may be manifested by only negative symptoms or two or more symptoms listed in Criterion A present in an attenuated form (e.g., odd beliefs, unusual perceptual experiences).

D. Schizoaffective and Mood Disorder exclusion: Schizoaffective Disorder and Mood Disorder With Psychotic Features have been ruled out because either (1) no Major Depressive Episode, Manic Episode, or Mixed Episode have occurred concurrently with the active-phase symptoms; or (2) if mood episodes have occurred during active-phase symptoms, their total duration has been brief relative to the duration of the active and residual periods.

E. Substance/general medical condition exclusion: The disturbance is not due to the direct physiological effects of a substance (e.g., a drug of abuse, a medication) or a general medical condition.

F. Relationship to a Pervasive Developmental Disorder: If there is a history of Autistic Disorder or another Pervasive Developmental Disorder, the additional diagnosis of Schizophrenia is made only if prominent delusions or hallucinations are also present for at least a month (or less if successfully treated).

## Epidemiology

Schizophrenia is estimated to affect more than 21 million people worldwide, with many of these being in developing countries. Half of those with schizophrenia do not receive care for their condition. Those with schizophrenia are 2-2.5 times more likely to die early, often as a result of comorbid illnesses including cardiovascular, metabolic and infectious diseases. For example, the prevalence of diabetes is up to 3 times higher in populations of patients with schizophrenia (WHO statement on schizophrenia and public health http://www.who.int/mental_health/media/en/55.pdf?ua=1 Accessed 19/03/2015).

## Age and sex effects

Sex effects have widely been reported in schizophrenia, both historically from a demographic perspective (Kraepelin, 1893) and in modern investigations using clinical imaging modalities relating to cortical structural differences (Nasrallah et al., 1990). Schizophrenia is more prevalent in men than women (~4:3 ratio men to women (McGrath et al., 2008)), however the reason for this is unknown. A milder progression and better prognosis following diagnosis is observed in female patients (Ochoa, 2012). Indeed a greater proportion of female patients respond to treatment and there is also generally a later onset in women than in men (18-25 in men, 25-35 in women (Ochoa, 2012)). A number of sexual dimorphisms in developmental and mature neurobiology are evident including protein, transmitter and structural differences (Martins-de-Souza et al., 2010). However a sufficient explanation in these differences is currently unknown. Clinical studies generally recruit male and female participants for investigation, however animal literature is largely biased on investigations in male animals (Clayton, 2014), which limits the applicable physiological observations to be applied as clinical theory. Recent policy changes have been considered with the aim of establishing a sex balance for animal studies (Clayton, 2014).

## Ultra High Risk (UHR) for psychosis

Clinical features subthreshold to diagnosis can be a precursor to the development of a specific disorder. This is true of somatic and mental health disorders. Individuals with subthreshold depressive symptoms are at a higher risk of developing major depression than the general population (Cuijpers and Smit, 2004). Indeed the same

effect is apparent with psychosis and psychotic like symptoms. Preventative measures and intervention at this early stage may help prevent the occurrence of a fully developed psychotic disorder. Individuals experiencing these subthreshold symptoms can be identified and provide a unique opportunity for the investigation of psychotic disorder. Not all individuals at ultra high risk (UHR) will transition to psychosis, the literature is variable, with transition rates reported between 15-30% (Cannon et al., 2015; Howes, 2011; Perkins et al., 2014; Wood et al., 2008; Yung et al., 2005), hence longitudinal follow up can provide useful insights into the differences between transitioning individuals and those who stay subthreshold. Onset of features associated with psychosis risk can develop from as early as 15, with psychological symptoms becoming apparent shortly after, the progression of psychosis and the start of treatment is outlined in Figure 1. (adapted from (McGlashan and Hoffman, 2000)). Criteria for risk can be assessed on the 'comprehensive assessment of the at risk mental state' (CAARMS). This clinical scale is similar to the PANSS used for schizophrenia, but assesses the more subtle features of pre-clinical psychotic like and other symptoms seen in the prodrome to psychosis (Yung et al., 2005). The outcome of UHR subjects is difficult to predict, while a modest number of individuals make the transition to first episode psychosis, many return to sub threshold clinical symptoms, and others will be diagnosed with related psychiatric disorders (Yung et al., 2005).

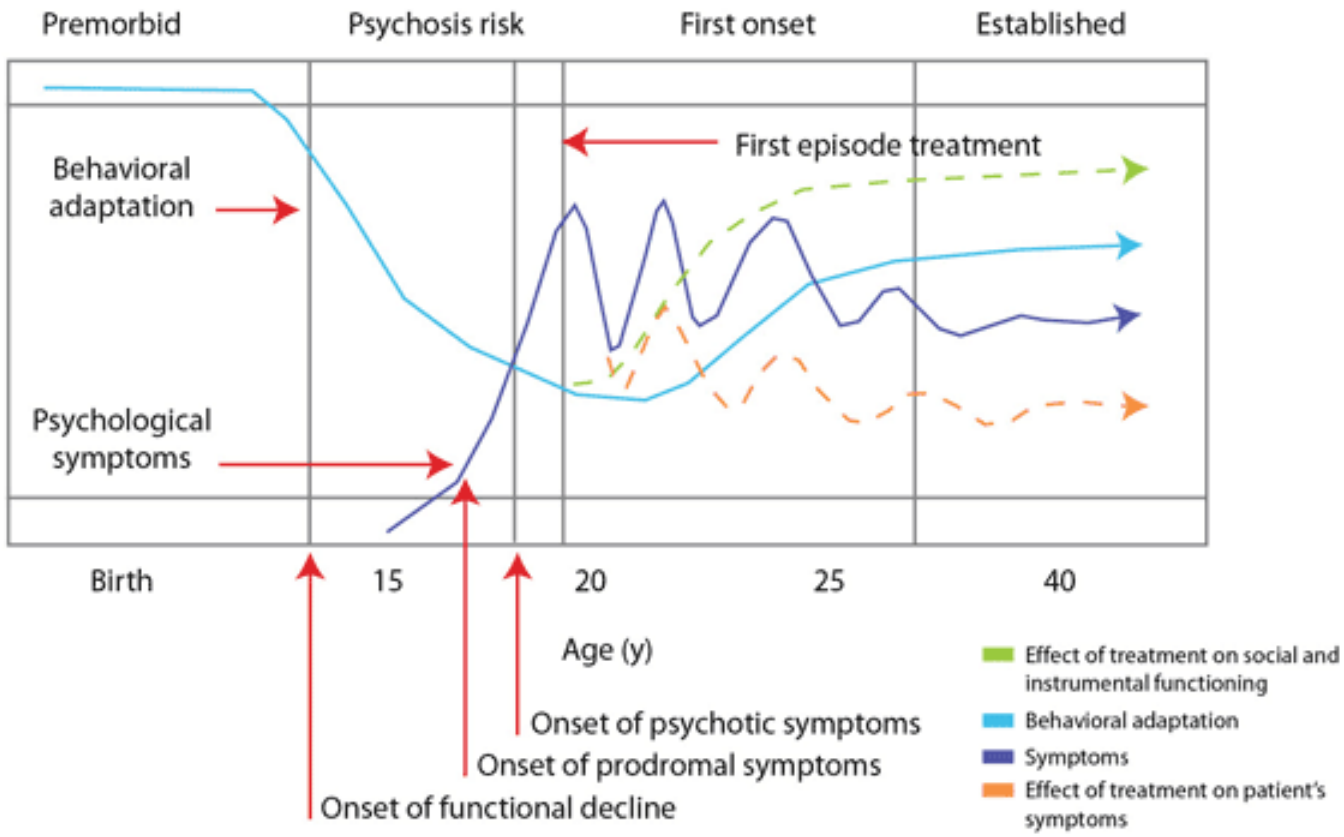


*Figure 1. Onset and progression of psychosis*

Prodromal and high risk subjects are those with psychological symptoms prior to first episode treatment. Adapted from (McGlashan and Hoffman, 2000).

## Grey and white matter alterations in psychosis

In people with psychosis cortical morphology is altered (Cannon et al., 2014). Functional decline and cortical abnormalities correspond developmentally, through prodromal periods, into the first psychotic episode and plateau for a state of maximal chronicity (McGlashan and Hoffman, 2000). Gene pathway analysis of schizophrenia has implicated synaptic and postsynaptic genes (Consortium, 2015). In addition to alterations in connectivity and genetic disruption in synapse associated pathways in established psychosis, gross cortical morphology is also altered in the early stages, when psychotic like symptoms first present (Cannon et al., 2014). Longitudinal imaging of cortical thickness has demonstrated a higher rate of decline in subjects who transition from clinical high risk to first episode psychosis (Cannon et al., 2015). Furthermore, decline in cortical thickness is accompanied by elevated levels of inflammatory plasma markers (Cannon et al., 2014; Perkins et al., 2014). Grey and white matter are both disrupted in psychosis and schizophrenia, however grey matter appears to have a more severe course of decline (Wood et al., 2008). The directionality of change differs between grey and white matter, with grey matter reducing in volume (Pantelis et al., 2003a) and white matter increasing in volume in the prodrome (Walterfang et al., 2008).

## Transmitter abnormalities

Similar to the modifications seen in cortical morphology, there appears to be an alteration in prodromal cortical transmitter function. Dopaminergic transmitter dynamics are markedly altered in schizophrenia (Abi-Dargham et al., 2002; Seeman

and Kapur, 2000), which broadly relate, but are not confined, to striatal hyperdopaminergia and prefrontal cortical hypodopaminergia (Howes and Kapur, 2009) and elevated striatal dopamine synthesis capacity (Bose et al., 2008; Howes, 2011), which are predictive of the transition of high risk subjects to first episode psychosis (Howes, 2011). Alongside dopamine, hypofunctional glutamate signalling, particularly through the NMDA receptors, is apparent in schizophrenia (Howes et al., 2015). The dopamine and glutamate hypotheses likely both hold explanations for the pathophysiology of schizophrenia, however PET evidence of glutamate disruption has not been possible to acquire, as reliable techniques are not currently available. MRS (magnetic resonance spectroscopy) has however been able to demonstrate a difference in glutamate in the prefrontal cortex of patients with schizophrenia and the prodrome (Fusar-Poli et al., 2011; Marsman et al., 2013; Stone et al., 2010).

## Antipsychotic drugs

Antipsychotic medications are prescribed to individuals experiencing psychotic symptoms and are the primary treatment for patients with schizophrenia. As well as being used to treat schizophrenia, many individuals with early stage symptoms of psychosis are prescribed low doses of these drugs to ameliorate symptoms (Miyamoto et al., 2004). Antipsychotic drugs are also prescribed to those with depression (Pisa et al., 2014), and used in the treatment of traumatic brain injury (Elovic, 2008) and dementia (Park et al., 2015b). While the positive symptoms associated with psychosis are improved by drug treatment, the full consequences of antipsychotic drug treatment are not entirely understood. Antipsychotic drugs can

be divided into a number of subtypes, based around when they were first synthesized or their constitutive receptor occupancy. First generation (or typical) antipsychotics (FGAs) such as haloperidol were the earliest antipsychotics to be prescribed. The primary mode of action for a FGA is at the D2 dopamine receptor, where the drug acts as a competitive antagonist. The dopamine hypothesis of schizophrenia, where hyperdopaminergia acts as the cause of the positive symptoms of schizophrenia, arose from the discovery of FGA action on D2 receptors (Seeman and Kapur, 2000). Second generation antipsychotics (SGAs) also have a dopaminergic action, however SGAs are far less specific in their action, often with serotonergic augmentation (Miyamoto et al., 2004). The broader spectrum of antagonism has been useful in addressing the positive and negative symptoms together (Miyamoto et al., 2012). The cortical consequences of antipsychostic drugs have been investigated *in vivo* and *in vitro*, however the results have often conflicted or have not been investigated independently of a disease model. Non-human primate investigation of haloperidol and olanzapine demonstrated an 8-11% reduction in the cortex of all treated animals (Dorph-Petersen et al., 2005). More recently investigations using microMRI in rats dosed with antipsychotics has demonstrated how, over a number of weeks, animals receiving haloperidol exhibit distinct reductions in cortical volume (Vernon et al., 2011). Later in this chapter we will see more literature relating to the action of antipsychotic medication in more detail. When assessing cortical changes associated with psychosis and schizophrenia, it is difficult to separate antipsychotic associated changes and those changes arising from the progression of the disease. Hence high risk for psychosis subjects can provide insights to the separation of disease and medication.

## *Microglia and Neuroinflammation*

There are 3 main classes of glia in the CNS (oligodendrocytes, astrocytes and microglia) which perform distinct functions. Oligodendrocytes provide myelination of neurons in the CNS, astrocytes are involved in transmitter metabolism and ion homeostasis, as well as being reactive to inflammatory stimuli (Zhang, 2001). Microglia have a myeloid origin and act as the residing immune cells of the brain and spinal cord, however recent evidence has demonstrated wider roles for the cells.

Neuroinflammation is broadly characterised as a response within the central nervous system mediated by either resident or infiltrating inflammatory cells. The subtleties of these glia have been debated for over a century and have an incredibly diverse morphological and physiological range. After Ramon y Cajal's initial observations of the cells in 1913 (Cajal, (1913) ), del Rio-Hortega further investigated the cellular microglial phenotype as well as suggesting a potential phagocytic function in the CNS (del Río-Hortega, 1918).

## Microglial origin and developmental involvement

The blood brain barrier (BBB) segregates the brain parenchyma from the blood borne immune protection of white blood cells, hence this intrinsic population of cells is required for health and immune protection. These unique cells are derived from a haematopoietic cell lineage and share the same progenitor as granulo/mono-cytic cells (including dendritic cells Figure 2 (Ransohoff and Cardona, 2010)).

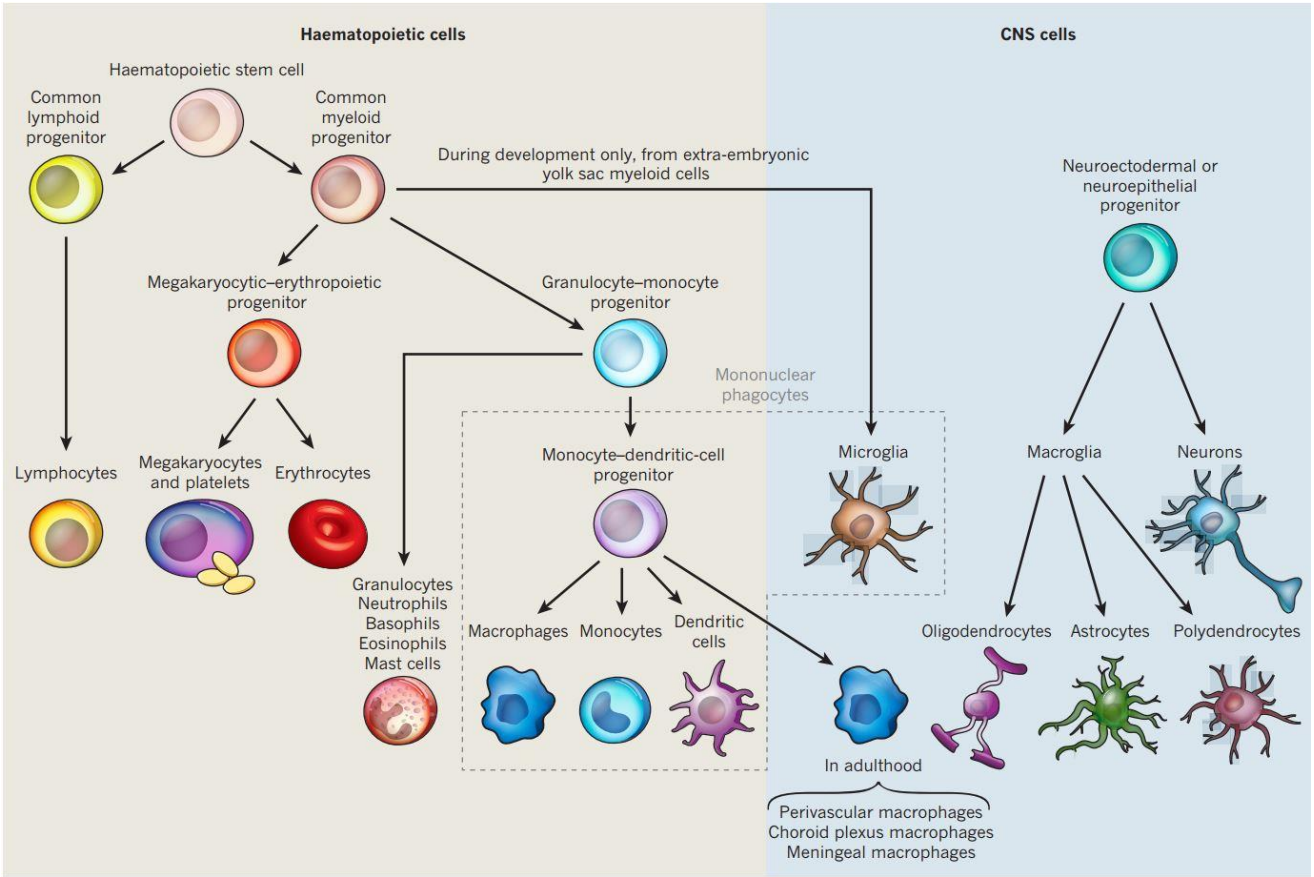


*Figure 2. Myeloid origins of microglial cells*

Unlike other CNS cells, microglia originate from a myeloid cell lineage rather than neuroectodermal. Adapted from (Ransohoff and Cardona, 2010).

While microglia are components of the CNS, they are mononuclear cells that share many common traits with blood borne immune cells. Although initially segregated from the ectoderm located neuronal and macroglial origin, microglia can be observed migrating, or in close proximity, to ectodermal tissue between E7 and E9 (Ginhoux et al., 2010). Microglia are active pruners of synapses in the postnatal brain, engulfing synaptic elements with their processes, providing a more concise synaptic network. Indeed, mice with deficient microglial signalling (through a CX3CR1 KO (knockout)) have reduced amounts of developmental synaptic pruning (Paolicelli et al., 2011).

## Types of response

In healthy brain tissue, microglia are present in a ‘quiescent’ state, where the cell morphology consists of a relatively small soma and ramified processes extending out into the local environment (Figure 3).

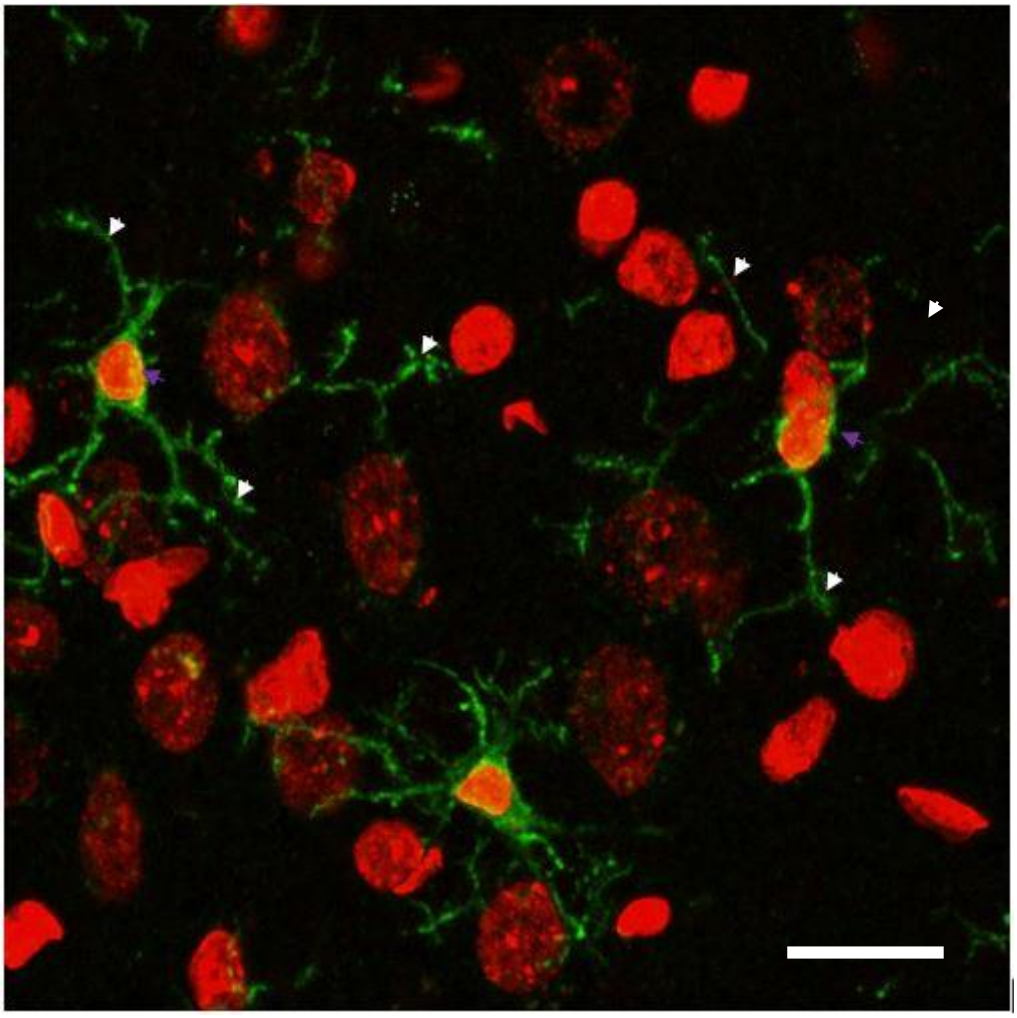

*Figure 3. Ramified microglia*

Ramified microglia (green, nuclei in red) in healthy rat brain tissue, with ramified processes (white arrows) and minimal soma area (Purple arrows). Image from control rat brain tissue stained with Iba-1 for microglia and DAPI nuclei. Scale bar = 20 µm.

The microglial soma will generally be present in a hull of a 5-10 μm radius, whereas the processes can extend into the local environment depending on the state of activity (Lawson, 1990;). As will be discussed, the functions carried out in this morphological context are comparatively diverse. Microglial cell morphology changes rapidly depending on environmental signals, which can be chemical or physical in nature. Many examples in the literature refer to M1 and M2 response phenotypes of microglia. This terminology has arisen from myeloid cell lineage response patterns, where the characteristics of microglia have been thought of in terms of their association with inflammation and types of inflammatory response. In a broad sense, the M1 response is pro-inflammatory and associated with tissue destructive activity. The M2 response is thought to be an anti-inflammatory response with neuro-protective features serving to reduce inflammation (Turtzo et al., 2014).

## Microglial signalling

Microglia are a highly motile cell type, which respond to and release chemokines and cytokines. Peripheral levels of cytokines are often observed alongside central evidence of microglial activity (Kettenmann et al., 2011). Whether the peripheral cytokines are as a result of central release, or vice-versa, is unknown. However, it is unlikely that such levels would be produced purely as a result of the central cellular activity, rather a state of systemic inflammation would potentially link central and peripheral processes (Dieset et al., 2015; Reuben et al., 2002). Microglia have a vast range of receptors expressed on their membrane (Table 1) and can respond to neurotransmitters (Domercq et al., 2013; Mead et al., 2012; Pocock and Kettenmann, 2007) as well as other, more primarily inflammatory signals. The

response of microglial cells to these signals have been investigated *in vitro* and *in vivo* to demonstrate how diverse their responses can be. It has long been established that microglial cells stimulated *in vitro* undergo a distinct membrane depolarization (Kettenmann et al., 1993). The utility of this depolarization remains unknown. More recent experiments have revealed an NMDA receptor association with the membrane potential as it is altered with the administration of MK801, an NMDA receptor antagonist (Morkuniene et al., 2015).

| Receptor | Subtypes | Functional activity including; |
|---|---|---|
| Glutamate /AMPA mRNA flop variants of GluR2 and GluR4 Glutamate (metabotropic) | mRNA flip variants of GluRs 1–4, Modulate TNF-α release. NR1 subunit expressed after transient forebrain ischaemia mGluR1 and mGluR5a mRNA | GluR1 and GluR3 in flip form. No functional activity shown so far. Agonist 1S,3R-ACPD induces increased Ca2+. |
| GABA | GABA(B), GABA(B1a), GABA(B1b) and GABA(B2) proteins | Stimulation of GABAB leads to activation of a K+ conductance; attenuates LPS-induced interleukin release. |
| ATP & purinergic | Gi/Go-coupled P2Y (Y1, Y2 Y4 and Y12), P2X (X1, X4 and X7) P2Y8 and P2X6 mRNA and protein | Modulate movement of microglial fine processes. Activation induces chemotaxis. mRNA and receptor protein is upregulated on microglia after neuronal injury; functions as a mediator of microglial phagocytosis; responds to UDP. |

| | | |
|---|---|---|
| | | Triggers TNF-α release. Modulates superoxide production. Activation implicated in neuropathic pain pathways. Activation induces chemotaxis. |
| Adenosine | A2aA3 | Induces expression of NGF, COX-2 mRNA and synthesis of PGE2.<br>Suppresses LPS-induced TNF-α release. |
| Cholinergic | α7 nAChR subunit | ACh or nicotine inhibits LPS-induced TNF-α release.<br>Nicotine attenuates gp120 or IFNγ-induced microglia activation. |
| Cannabinoid | CB2 receptor expressed in perivascular microglia<br>CB1 CB2 and abn-CBD | Activation reduces microglial toxicity and cytokine secretion.<br>Present on cultured microglia.<br>Non-specific activation of cannabinoid receptors suppresses microglial activation and neurotoxicity. |
| Adrenergic | mRNA for α1 α2 β1 and β2 (but not β3) | Agonists decrease mRNA for IL-6 and TNF-α. Functional noradrenergic receptors identified on cultured microglia and in acutely isolated brain slices; |

| | | |
|---|---|---|
| | | modulates membrane currents; suppresses cytokine and NO release. |
| Dopamine | D1- and D2-like receptors, expression inferred from function | Functional dopamine receptors identified on cultured microglia and in acutely isolated brain slices; modulates membrane currents; suppresses NO release; promotes migration. |
| Opioid | MOR and KOR mRNA | Evidence of MOR and KOR function and an opioid-receptor-independent pathway.<br>Agonists induce ameboid phenotype in microglia, chemotaxis and BDNF-gene expression.<br>Morphine inhibits C5a and RANTES chemotaxis and LPS- or IL-1β-induced production of RANTES. |
| Neuropeptides | neurokinin-1 (NK-1)<br>B1 and B2<br>VPAC1 | Modulates chemotaxis; activates of NADPH oxidase.<br>Increases microglial motility; releases NO and PGE2.<br>Inhibits production of inflammatory chemokines and cytokines. |

*Table 1. Receptors on microglia*

*Adapted from (Pocock and Kettenmann, 2007).*

## Physiology and morphology

Neuroinflammation is commonly initiated by an insult to the CNS and can be as a result of physical (traumatic injury) or chemical (pathogenic substance) insults. Microglia, for a long time, were considered to be ‘sentinels’, with an observational role as the extent of their habitual function. However it is increasingly evident that a much more elaborate function exists (Tremblay et al., 2011). In the quiescent state microglial cells display a ramified morphology, with numerous processes extending through the local environment.

Figure 4 demonstrates the two traditionally accepted morphological states of microglial cells, ramified and amoeboid (left and right respectively). The cytokines associated with the two broad microglial morphologies in Figure 4 are markers of inflammation, or inflammatory response, particularly associated with neurodegenerative processes. Interleukin 1β (IL-1β) (Lim and Marsland, 2013) and interleukin 6 (IL-6) in the periphery are considered hallmark features of inflammation and are predictive of age related cognitive decline and mortality in psychosis (Reuben et al., 2002). Functional roles of microglia are often associated with tissue repair and phagocytosis of potentially harmful material (Weitz and Town, 2012). These examples demonstrate the complex nature of microglial biology from the CNS and peripheral domains.

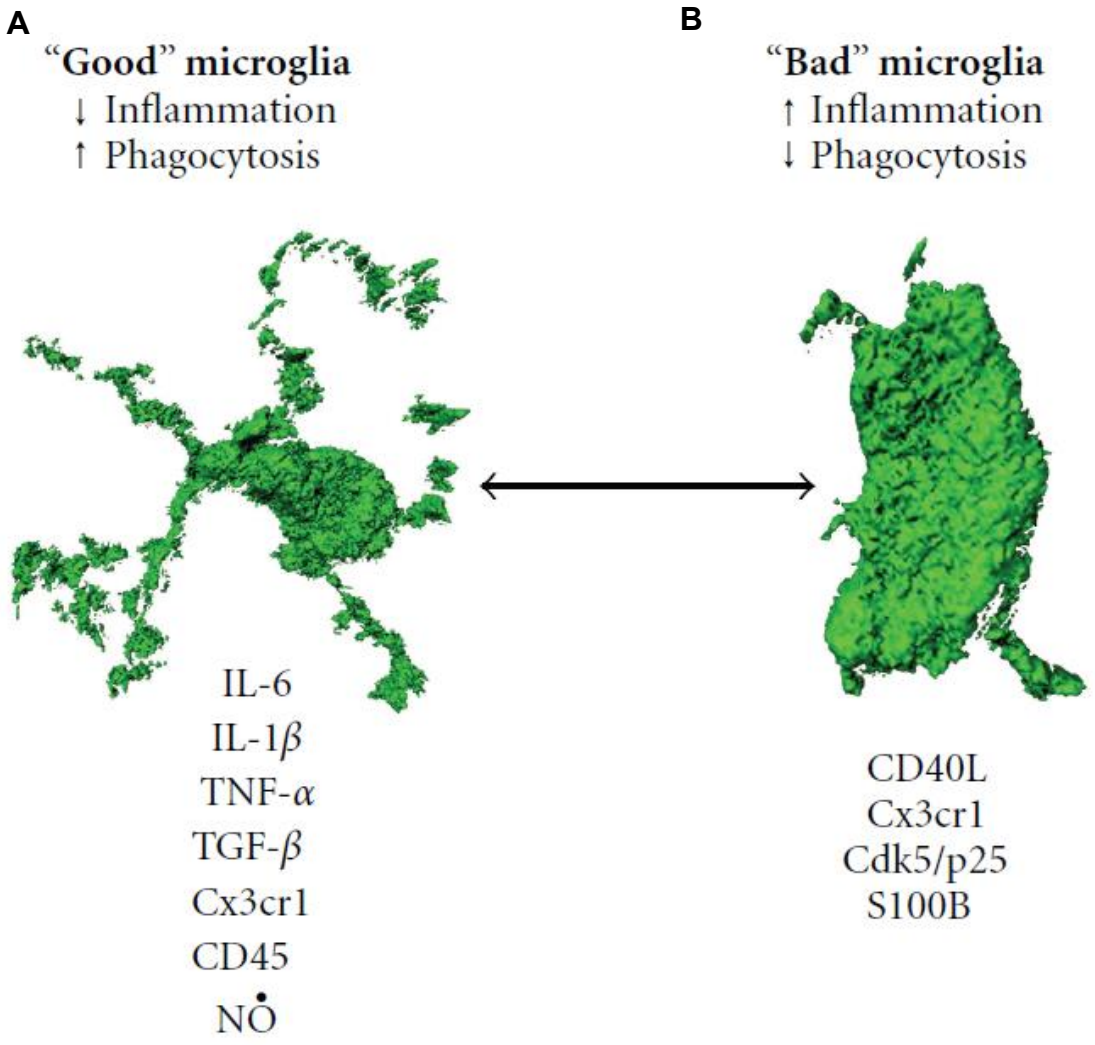


*Figure 4. Microglial morphology*

Microglial cells are thought to largely exist in two morphological states, ramified (A) with processes extending into the surrounding environment, or amoeboid, with a swollen cell body with retracted processes (B) (Weitz and Town, 2012).

It is increasingly clear that the binary model in Figure 4 is a simplified representation and that these are two distinct points on a spectrum of morphology and function. It is unclear how much overlap in function exists on the spectrum between these two points. There are environments where microglia will have cues to be responsive to

inflammation, synaptically involved and phagocytic. It is not currently known how the cellular morphology would be affected in each state. While microglial cells are the primary mediators of a neuroinflammatory response (Chen et al., 2012), they require an initial signal to respond to. In many cases, this signal takes the form of cytokine signalling after an injury. For example tissue damage stimulates the release of cytokines, which in turn attract microglia to the site of injury and cause an activity response (Stence et al., 2001). During plasticity and development, the regulation of microglial activity is not currently known, however plasticity associated microglial activity can be altered experimentally (Parkhurst et al., 2013). While there is a considerable body of literature demonstrating the roles of healthy and diseased function separately, the reality is more likely to be a combination of functions in varying proportions in a context dependent manner.

## Synaptic roles

Traditional function of ramified processes was thought to be for monitoring of extracellular alterations. However, evidence is now accumulating for the involvement of microglia in synaptic dynamics (Nimmerjahn et al., 2005; Paolicelli et al., 2011; Parkhurst et al., 2013; Tremblay et al., 2010). Recent evidence also suggests whole synapses, and neurons, can be phagocytosed by microglial cells (Kettenmann et al., 2013), the trigger for such an extreme response is currently unknown. Microglia are further involved in synaptic processes in the adult brain. Tremblay et al., (2010) demonstrate how altering visual experiences, known to induce plasticity, were able to change the interaction between microglia and synapses. A potential signalling mechanism for plasticity responses is brain derived

neurotrophic factor (BDNF), blocking BDNF signalling can inhibit learning dependent synapse formation (Parkhurst et al., 2013). Microglial cells are restricted to the CNS, being present in both the brain and spinal cord. The density of cells varies across regions, as the local function dictates the morphology of cells as well as the density of the population. Long-range signalling is able to cause a change in microglial cell density depending on their requirement centrally (Mittelbronn, 2001; Savchenko et al., 1997). The distribution of microglia alters over time and with demographic variation in populations. The number of microglia in the cortex are increased with age (Norden and Godbout, 2013) as well as with obesity (Thaler et al., 2013). Similarly, peripheral cytokine levels are elevated in these situations (Lim and Marsland, 2013; Vgontzas et al., 1997), suggesting a potential crosstalk between CNS and the periphery.

## Microglia in schizophrenia

A number of PET and post mortem tissue studies have established that microglial activity is elevated in patients with schizophrenia (see Table 2 & Table 3 respectively). The PET literature varies from regions with higher hippocampal microglial activity (van Berckel et al., 2008), to subtle grey matter elevations (Doorduin et al., 2009) or a symptom correlation (Takano et al., 2010). There is a range of reports of microglial changes in post mortem tissue, with hypertrophic morphology being a key observation (Bayer et al., 1999) although a large amount of controversy is apparent in the studies, with suggestions of an association with suicide (Schnieder et al., 2014; Steiner et al., 2008). It is apparent that microglia play a role in psychosis, or an aspect of psychopathology. A number of animal

models of schizophrenia are based on an immune insult early in the prenatal phase of life, in keeping with neurodevelopmental hypotheses of schizophrenia (Juckel et al., 2011; Zhu et al., 2014).

All of the clinical studies to date have investigated patients with schizophrenia or recent onset psychosis *in vivo*, or end stage schizophrenia in post mortem tissue. Hence it is unclear at which stage of psychosis microglial activity elevation is evident. The stage of psychosis that microglial activity changes are occurring is one aspect of disorder we seek to address in this thesis.

| Reference<br>(Sample size, case/control) | Age in years<br>(case/Ctl) | Medication status | Method of assessment | Disorder status | Methods | Findings (+, ~, -) |
|---|---|---|---|---|---|---|
| (van Berckel et al., 2008)<br>10/10 | 24/23 | Medicated | DSM IV | Recent onset schizophrenia (PANSS) | In vivo PET<br>[$^{11}$C] -(R)- PK11195 | + Grey matter ^ ($p<0.05$) |
| (Doorduin et al., 2009)<br>7/8 | 31/27 | Medicated | DSM IV | Schizophrenia spectrum (PANSS) | In vivo PET<br>[$^{11}$C] -(R)- PK11195 | + Hippocampal ^ ($p=0.004$)<br>30% increase in grey matter |
| (Takano et al., 2010)<br>14/14 | 44/43 | Medicated | DSM IV | Schizophrenia (PANSS) | In vivo PET<br>[$^{11}$C] DAA1106 | ~ Positive symptoms correlation $p<0.0045$ (bonferroni 0.05/11) |
| (Kenk et al., 2015)<br>16/27 | 43/44 | Medicated | DSM IV | Schizophrenia with ongoing symptoms (PANSS) | In vivo PET<br>[$^{18}$F] FEPPA | ~ NS difference |

*Table 2. PET imaging studies of TSPO/microglia in schizophrenia*

| Reference (Sample size, case/ctl) | Age in years (case/Ctl) | Medication status | Disorder status | Methods | Findings (+, ~, -) |
|---|---|---|---|---|---|
| (Bayer et al., 1999) (14/13) | 64/58 | Medicated | Schizophrenia, retrospective assessment with DSM-III | HLA-DR staining | + PFC & hippocampal microglial elevations, particularly in later onset (no stats) |
| (Radewicz, 2000) (8/10) | 84/70 | Medicated | Schizophrenia DSM-III-R | HLA-DR | + dlPFC, ACC ($p$< 0.05) and temporal gyrus ($p$< 0.01) |
| (Steiner et al., 2006) (16/16) | 55/58 | Medicated | Schizophrenia DSM-IV-R | HLA-DR staining | - in ACC and dlPFC, but + in hippocampus. |
| (Steiner et al., 2008) (16/10) | 54/55 | Medicated | Schizophrenia DSM-IV | HLA-DR staining | + in dlPFC, ACC and thalamus ($p$< 0.05) |
| (Kreisl et al., 2013) (45/47) | 55/42 | Medicated | Schizophrenia DSM-IV | [$^3$H]PBR28 autoradiography | + ligand binding in dlPFC ($p$< 0.011) |
| (Schnieder et al., 2014) (25 Suicide/11NonSuicide) | 55/56 | Medicated | Schizophrenia with and without suicide | Iba-1, CD68 staining | + microglia in ventral PFC with suicide (0.033) |

*Table 3. Post mortem tissue analysis of microglia in schizophrenia*

## Antipsychotic medication and microglia

All clinical investigations of microglia in psychosis to date have been confounded by antipsychotic medication. The experimental evidence for antipsychotic-microglial interaction is presented in Table 4. There are 16 investigations across cell culture and animal models demonstrating a range of responses by microglia to a number of antipsychotic medications, both first and second generation. The majority of studies demonstrate an anti-inflammatory action of antipsychotics on microglial cells. In a number of studies antipsychotic medications did not alter microglia either in morphology or physiological response. *In vitro* investigations have demonstrated an anti-inflammatory influence of a number of SGAs in cultured microglia (Bian et al., 2008; Kato et al., 2008; Kato et al., 2007). A recent *in vivo* investigation of the effects of risperidone and minocycline (a tetracycline antibiotic known to inhibit microglial cell activity) on a developmental cortical lesion animal model demonstrated a reduced density of Iba-1 stained cortical microglial cells (Zhu et al., 2014). The evidence to date suggests an anti-inflammatory role of antipsychotic medication, however the *in vivo* evidence has not produced a comprehensive description of morphology or microglial features beyond cell density. It is also unclear how antipsychotic medication influences peripheral cytokine levels and how this corresponds to density or morphology of cortical microglia. It is also unclear how healthy brain tissue and tissue with microglial activity increases would respond to the same treatment. These are further questions we aim to address in this thesis.

| Reference | Experimental model | Medication | Method of assessment | Findings |
|---|---|---|---|---|
| (Näkki et al., 1996) | Ketamine and phencyclidine *in vivo* | Haloperidol | Microglial cell number and HSP70 expression | HSP70 reduced, but microglia were unaffected |
| (Kowalski et al., 2003) | LPS stimulated microglia *in vitro* | Flupentixol, trifluperidol | TNF-α and NO ELISA | Flupentixol and trifluperidol both inhibited production of TNF-α and NO |
| (Labuzek et al., 2005) | LPS stimulated microglia in vitro | Chlorpromazine, loxapine | interleukin-1β (IL-1β) and interleukin-2 (IL-2) release | Both drugs were able to reduce IL-1β and IL-2 release |
| (Hou et al., 2006) | LPS stimulated N9 cells *in vitro* | Haloperidol, Clozapine, Olanzepine | Cell survival and NO production | Olanzepine reduced LPS induced NO production but Clozapine and Haloperidol did not |
| (Kato et al., 2007) | IFNɣ stimulated microglia *in vitro* | Risperidone, Haloperidol | Cytokine ELISA and Nitric oxide (NO) western blot | Haloperidol and Risperidone inhibit NO production. Risperidone also inhibited cytokine production, haloperidol did not |
| (Bian et al., 2008) | IFNɣ stimulated 6-3 microglial cell culture *in vitro* | Perospirone, ziprasidone quetiapine | NO and TNF-α production. Cell viability | All three antipsychotics reduced NO production and all but ziprasidone reduced TNF-α production. Cell viability was not affected. |

| | | | | |
|---|---|---|---|---|
| (Kato et al., 2008) | IFNɣ stimulated 6-3 microglial cell culture *in vitro* | Aripiprazole Quinpirole | NO production, TNF-α production, $Ca^{2+}$ imaging & cell viability | Aripiprazole reduced NO production, but not TNF-α, and Ca2+ concentration. Also promoted cell survival. Quinpirole did not alter any measures |
| (Zheng et al., 2008) | LPS stimulated BV2 microglial culture | Spiperone | NO production, cytokine production, NF-κB production, cell survival | Spiperone reduced production of NO, cytokines and NF-κB. Cell survival was promoted |
| (Hu et al., 2011) | *In vitro* LPS stimulated microglia/neuronal co-culture | Clozapine | Microglial immuno-histochemistry cell counts | Clozapine reduced the LPS induced microglial cell (Iba-1) count elevations |
| (Kato et al., 2011) | Phorbol-myristate-acetate (PMA)-stimulated microglial/neuron co-culture *in vitro* | Aripiprazole | Superoxide production | Aripiprazole reduced PMA induced superoxide production and promoted neuronal cell survival |
| (Seki et al., 2013) | IFNɣ stimulated *in vitro* primary microglia and oligodendrocyte culture | Aripiprazole, Haloperidol | Immunoflourescence and phagocytosis observation | Aripiprazole but not haloperidol prevented microglial associated |

| | | | | |
|---|---|---|---|---|
| | | | | inflammatory action and oligodendrocyte apoptosis |
| (O'Sullivan et al., 2014) | *In vivo* Experimental autoimmune encephalitis (EAE) and *in vitro* macrophage culture | Risperidone | Cytokine measurement, immunohistochemistry of microglia/macrophages and functional deficit assessment | Risperidone reduced cytokine production, in vivo and in vitro. Attenuated physical deficits. Reduces quantity of microglia (Iba-1 and CD68) in tissue sections |
| (Yan et al., 2014) | Transient cerebral ischemia *in vivo* | Risperidone | Microglial immuno-histochemistry cell counts | Risperidone reduced microglial presence (Iba-1) in CA1 hippocampal region |
| (Zhao et al., 2014) | *In vivo* Alzheimer's APP transgenic mice | Quetiapine | Microglial immuno-histochemistry cell counts | Quetiapine reduced hippocampal microglial cell counts (CD11b) |
| (Zhang et al., 2014) | *In vivo* cuprizone induced demyelination | Olanzapine | Microglial immuno-histochemistry cell counts | Olanzapine reduced cuprizone induced elevations of microglia (CD11b) |
| (Zhu et al., 2014) | *In vivo* neonatal hippocampal LPS | Risperidone | Microglial immuno-histochemistry cell counts | Risperidone reduced the number of microglia (Iba-1) in the cortex |

*Table 4. Studies of antipsychotic medication and microglia*

## 18-kDa translocator Protein (TSPO)

Traditionally named the peripheral benzodiazepine receptor (PBR), TSPO is found ubiquitously, but in varying quantity, in the human body and is a protein associated with steroid synthesis and transport (Varga et al., 2009). TSPO is an 18 kDa structure located on the outer membrane of the mitochondrial matrix and is part of a trimeric transmembrane domain and is essential for cholesterol transport (Banati et al., 2014). TSPO is expressed in relatively low levels in the mammalian brain. For example, tissues rich in mitochondria with a high metabolic and hormonal demand, such as the testes and adrenal glands, express a much higher level of TSPO than cortical tissue. In the brain, TSPO is found on microglia, astrocytes and certain subtypes of neurons, including proliferative neurons in the subventricular zone (Varga et al., 2009).

The *in vivo* functional significance of TSPO has been controversial in recent years as the generation of TSPO knockout mice has produced two opposing findings. The initial study reported embryonic lethality with a full TSPO knockout (Papadopoulos et al., 1997), however the more recent investigation demonstrated how TSPO -/- animals were phenotypically normal, with lifespan, growth, cholesterol transport and microglial response to injury appearing unaffected. The only deviation from control was a reduction in production of adenosine triphosphate (ATP), suggested to be a reduction in metabolic activity (Banati et al., 2014). The development of Positron Emission Tomography (PET) as an imaging modality has allowed targeting of molecular markers in both the healthy and diseased brain, chapter 2 will explore the fundamental principles of PET. Ligands binding TSPO are used in PET imaging as

a molecular marker of microglia and neuroinflammation. We will cover the details of TSPO tracers and their application in chapter 2.

## Translational investigation

Fundamental neuroscientific questions are being addressed more comprehensively as technology progresses to allow for investigation of cellular and molecular events. Clinical and basic science have often occurred in isolation of each other, however it is useful and informative to investigate questions from both perspectives. While many argue that animal models of diseases are not valid as representations of disorders, it is possible to model features of diseases to investigate them more thoroughly in a whole organism. Nervous system injuries are relatively easy to model for a direct comparison to a clinical context. Where diseases of cognition, consciousness and perception are the topic of investigation, the situation is less clearly defined. In diseases such as Parkinson's or Alzheimer's, where there are hallmarks of diseases which can be produced in the rodent brain, animal investigation of pathology and it's treatment can greatly inform the clinical context and provide greater opportunities for developing therapeutic targets. Psychiatric illness is particularly difficult to model for functional deficits as psychiatric disorders are diagnosed following structured interview based assessment. While these features aren't assessable in rodent models, the biology underlying the clinical features can be modelled to view network and physiological interactions with better resolution than available clinically. With these approaches in mind, this thesis will address *in vivo* microglial changes associated with antipsychotic medication. Clinical imaging techniques will address microglia in schizophrenia and medication

naïve subjects with early signs of psychotic symptoms. Alongside this, animal investigation of antipsychotic administration on microglial cell density and morphology will serve to further inform the clinical study to determine potential consequences of medication in patients with schizophrenia.

# *Aims and outline of thesis.*

This thesis aims to answer 3 questions;

1. Is neuroinflammation present prior to the onset of psychosis in UHR subjects and patients with chronic schizophrenia? If so, does neuroinflammation relate to the severity of symptoms in UHR subjects and patients with schizophrenia?
2. Is neuroinflammation associated with cortical volume and peripheral inflammation in UHR subjects and patients with schizophrenia?
3. Does antipsychotic drug administration in rats lead to microglial density and morphology changes in the cerebral cortex? If apparent, how do these associate with peripheral levels of cytokines?

These questions will be answered using the clinical imaging and preclinical techniques outlined in the Methods chapter (Chapter 2). The first two experimental chapters of this thesis (Chapters 3 and 4) report results from clinical imaging of UHR and patients with schizophrenia. Chapter 3 will focus on the PET imaging findings and Chapter 4 will relate these to MRI and peripheral inflammatory features. The final experimental chapter (Chapters 5) explores the impact of antipsychotic medication on microglial cells. Chapter 5, assesses the influence of antipsychotic medication on microglial cells and brain volume *in vivo*.

Chapter 6 summarizes the key findings of the thesis and discusses the impact of such findings on the fields of investigation. The comparison of clinical and animal

approaches is also made here. This chapter goes on to discuss the future perspectives as well as providing concluding remarks.

# *Chapter 2 – General methods*

# *Clinical experimental methods*

## Ethics/study approval

The clinical studies contained in this thesis were approved by the research ethics committee at the Hammersmith Hospital, London. The PET study was approved by the Administration of Radioactive Substances Advisory Committee (ARSAC), United Kingdom. The approval for this study was set up for Imanova imaging centre related to the administration of radioactive substances for medical or research purposes. The Ionizing Radiation Regulations (1999) provides guidelines on the levels of radiation participants can receive and participants were monitored to ensure they did not exceed such limits. The patient groups are thoroughly researched, hence we ensured participation in this study would not take subjects yearly exposure >10 mSv (millisieverts). Whole blood and serum samples from participants were collected and stored according to the guidelines of the Human Tissue Act (2004). The clinical study was sponsored by King's College London and the Medical Research Council, researcher indemnity was provided by King's College London. Local research and development committees were consulted for participant identification centre (PIC) approval. The following trusts were used for PIC:

South London and Maudsley Mental Health Trust. West London Mental Health Trust Central and Northwest London Mental Health Trust.

Intervention centres and clinical teams used for PIC were given the research documents and participants were identified in the team meetings, then approached with sanction of the care coordinator.

## *Participants*

Ethical approval was obtained for all clinical experimentation REC: LO/1801

## Clinical cohort recruitment & screening

Healthy volunteers were recruited from advertisements in local London newspapers (The Metro and Evening Standard) as well as posters on site and in local community facilities, such as libraries and general practice clinics. Those who had expressed an interest in previous studies were also contacted for participation.

When a participant had expressed an interest in the study, they were contacted over the telephone for an initial screening of basic background information prior to a more comprehensive face to face screening interview. In the face to face screening interview, informed written consent was taken following an oral and written explanation of the study and participation. Participants were encouraged to ask questions and given as much time as necessary to decide about participation. Following consenting, a psychiatric history was taken and a blood test was taken by a clinician to determine the TSPO binding status prior to scanning. Participants were remunerated for their travel and time.

## Inclusion criteria

All subjects were assessed on the following inclusion criteria;

- All participants will be >18 years old.
- No significant health contra-indications, other than the conditions of mental health being investigated, as determined by a physician. Participants with

other health issues are eligible for inclusion if the condition would not jeopardize or confound the results or integrity of the study.

- The subjects must be capable of giving written informed consent, including compliance with the statements in the consent form.
- The subjects must be able to read, comprehend and record written English.
- A signed, dated written informed consent must be taken

Further to these criteria, patients must have a diagnosis of schizophrenia or schizoaffective disorder, as assessed using DSM IV criteria.
UHR subjects must meet inclusion criteria as assessed with the CAARMS manual (Yung et al., 2005).

## Exclusion criteria

All subjects were assessed for the following exclusion criteria;

- Substance dependence or abuse, including cannabis and alcohol, but not nicotine addiction.
- Benzodiazepine use within 1 month of initial assessment
- Any form of learning disability
- Any neurosurgery or neurological disorder, including epilepsy
- Any serious head injury, resulting in a period of unconsciousness greater than 1 hour.
- Any significant cardiovascular disorder, including;
    - Bleeding or clotting disorders such as DVT or CVA

    - Hypertension – AHA grade II: systolic >160 mm/Hg
    - Arrhythmia or angina
- Previous treatment with ECT (electroconvulsive therapy)
- Pregnancy or attempting to conceive
- Breastfeeding mothers
- Previous exposure to ionizing radiation that would result in the participant's 12 month exposure to exceed 10 mSv following the PET scan
- MRI contraindications.

Control subjects with a first degree relative diagnosed with an Axis 1 psychiatric disorder, or neurodegenerative disorder were also subject to exclusion from this study. Current, or past, history of Major Depression or an Axis 1 disorder was also an exclusion criterion for healthy volunteers.

All participants were initially assessed on SCID (structured clinical interview for DSM disorders) and DSM-IV sub scales, UHR individuals were further assessed with the CAARMS manual and schizophrenic participants with the PANSS.

## *Positron Emission Tomography - principals*

Positron emission tomography (PET) imaging has been used as an experimental tool for research and is starting to be applied clinically for the purpose of diagnosis and treatment. Tumour identification for surgery is the first branch of PET imaging to be applied clinically. The basic principal of PET imaging utilizes gamma radiation and half-life decay of radioactive isotopes which are coupled to ligands which bind to a receptor or protein of interest. PET is a non-invasive three dimensional imaging technique that can be used to investigate the chemistry or molecular biology underlying physiological function. The radioligand injected into subjects for imaging allow a detailed map of a region or organs marked by the ligand. When a receptor or protein in the body is identified for the purpose of research, a corresponding ligand can be produced to bind to it. When this ligand has been produced, a radioactive species can be combined with the ligand so that when bound in the physiological context, gamma radiation can be detected by the PET cameras. Detecting the annihilation radiation with this method of imaging, allows a regionally specific quantitative level of binding to be determined. PET is a unique way to investigate spatiotemporal chemistry and physiology. The question of function often arises when evaluating PET evidence. It is difficult to make functional conclusions based solely on PET; however in combination with other imaging modalities (such as fMRI), a more reliable conclusion can be formed. Isotope production for PET is carried out in a cyclotron, near the scan site, as short half-life species used for imaging would lose potency if they needed to travel a considerable distance to the scanner. A cyclotron is a particle accelerator, which is able to produce isotopes for radiochemical coupling by collision of a stable atom with a proton (Spinks, 2000).

For an element's isotope to be compatible with PET, it must emit positrons during its half-life decay. Radioactive species with a short half-life decay period are used to minimise the harm to participants from the ionizing radiation. Table 5 summarises the most commonly used isotopes for PET imaging research (Paans et al., 2002). Protons are accelerated in the cyclotron before collision with a stable element. The bombardment forces a proton from the neutron of the atom, resulting in the production of an isotope with an unstable nucleus. The isotopes undergo annihilation, where a positron and neutron are emitted from the nucleus, leaving a stable atom in the ligand compound. For example, carbon-11 decays to form stable boron-11. The emitted positron combines with an electron and produces two anti-parallel gamma radiation photons with an energy of 511 keV (Badawi, 1998). This gamma radiation is detected by the PET camera and is subsequently used to determine the location of the bound isotope through coincidence detection, which will be discussed in due course.

| Isotope | Half life (mins) |
|---|---|
| $^{11}C$ | 20 |
| $^{13}N$ | 10 |
| $^{15}O$ | 2 |
| $^{18}F$ | 110 |

*Table 5. Common radioisotopes used in PET imaging experiments*

PET is an *in vivo* molecular imaging technique with a relatively high resolution with many benefits over post-mortem optical imaging techniques. The greatest of these advantages is that chemical and molecular changes relating to a specific context can be investigated temporally on both an acute timeframe, as well as chronically with a longitudinal study design.

## PET scanner

The detectors are arranged in a ring in the PET camera and detect the antiparallel waves of radiation (Turner and Jones, 2003). The subject lies in the scanner, with the target organ (in this case, the brain) centred in the field of view (FOV) (Figure 5).

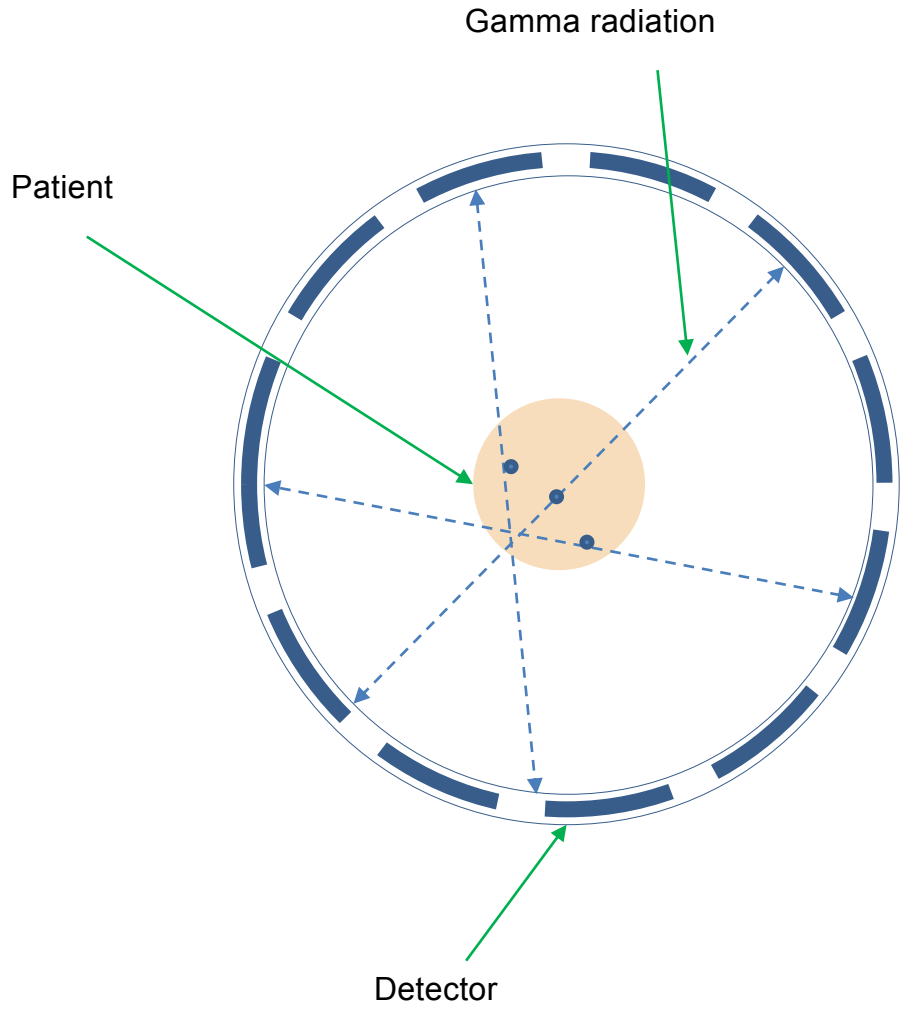


*Figure 5. PET scan schematic*

Schematic of the basic principal of gamma radiation detection in a PET scanner.

The detectors have a scintillator and Photo Multiplier Tubes (PMT) which record photon counts. When the photons reach the scintillator, a small flash of light is created and is amplified by the PMT, these flashes of light are recorded and used for the reconstruction of the dynamic image. Scintillator materials vary, however in the studies presented in this thesis a LSO (Lutetium orthosilicate) scintillator scanner is used (Spinks, 2000).

## Coincidence detection

Detection of the gamma rays occurs simultaneously on either side of the PET camera as an annihilation event produces two photon rays which will be detected on opposite sides of the detector ring (Spinks, 2000). Hence two events detected either side of the ring can be associated with the same annihilation event of the bound ligand. A time window for detection provides a coincidence detection threshold. If photons reach the detector outside of this temporal threshold they are no longer considered for detection.

## PET Image Reconstruction

These events of detection, also known as count rates, are used as the raw data for PET image reconstruction. The scan time is divided into varying groups of timed count rates called frames. The initial frames of the scan will cover a shorter period of time, where there is a vast amount of activity and a high number of detection events. As the injected activity decays, the frames lengthen to capture the less frequent events. The dynamic data from the frames are reconstructed into three-dimensional images through computed post processing. Filtered back projection or iterative reconstruction methods are used to reconstruct the PET image. The quantification of reconstructed images gives the distribution of the radiotracer in the tissue. Filtered back projection is standard for brain imaging studies. This is because it is very accurate from a quantitative point of view, although the visual image rendering is relatively poor. Clinical cancer imaging emphasizes visual quality over quantitative quality hence there is an emphasis on OSEM like techniques that, with a few iterations offer excellent visual rendering. However quantification with OSEM

and similar is still dependent on high iteration numbers where signal-to-noise degrades rapidly. Unlike the thorax, where areas with high signal are closer to cold areas, the brain has generally uniform uptake (ventricles excluded). Evaluation of iterative reconstruction and event detection bias (including image render quality, signal to noise ratios and image artefacts) is made by (Reilhac et al., 2008).

## Blood analysis

Whole blood (4 mL) was taken from patients before the PET scan, at the time of arterial cannulation. Blood was collected in an EDTA impregnated purple top blood tube and stored at -80oC until being sent for analysis. (Blood samples were analysed by ABS laboratories, UK. As the reagents and equipment needed for cytokine analysis were not available on site at the time of experiments). Cytokine analysis was conducted by ABS laboratories, Hertfordshire.

## *PET image analysis*

Analysis of the PET data obtained over the time course of the imaging experiment is complex. Accurate modelling of the *in vivo* kinetics largely influences the quality of data in this section, we will see the aspects of both tracer and tissue compartments which must be accounted for to provide high quality data.

### Tracer kinetics

The quantified distribution of tracer is a measure of the protein or receptor the tracer binds to, in this instance TSPO. The PET tracer is active in a state of equilibrium *in vivo*, where the bound ligand [L+R] and free ligand [L] are able to interact and dissociate from the receptors [R] where the net exchange is zero.

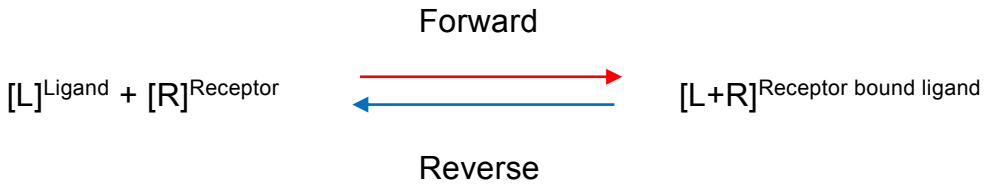


When the forward and reverse diffusion equilibrates, the dissociation constant ($K_D$, the rate of exchange at equilibrium) can be calculated.

$$K_D = \frac{\text{Concentration of reactants}}{\text{Concentration of products}}$$

This measure is a reciprocal representation of the ligand affinity. Hence a High KD reflects a low affinity and a low KD reflects a high affinity. The free and bound components related to the ligand used for imaging can be used to model tissue

distribution of the protein or receptor as we will see in the modelling paragraph, using [$^{11}$C]PBR28 (Rizzo et al., 2014).

## Quantification

Radio ligand activity is represented by signal from the tissue (in our case the brain) and the activity in the blood (the input function). We detect the tissue signal with the scintillator, however this does not account for activity in the blood stream. An arterial cannula can be placed to derive the input function, however for some tracers, a reference region, lacking target receptors, can be used to indirectly calculate the input function (Laruelle et al., 2002). In a region of interest model a time activity curve for that region is estimated, ultimately providing a representation of tracer dose in a volume of tissue (where volume of distribution is used, MBq/cm$^3$ is the unit of measure).

When quantifying the tissue component, factors such as blood flow, vascular binding, non-specific target binding and ability to cross the BBB contribute to the final tissue activity. Mathematical modelling of these components can make the tissue data more accurately reflect receptor distribution (see comparison of [$^{11}$C]PBR28 models, 2TCM and 2TCM-1K and (Turkheimer et al., 2015)).

## Tissue compartment modelling

This section is limited to ‘reversible’ tracers, with the KD profile discussed so far. Tracers such as [$^{11}$C]PBR28 have a reversible chemical equilibrium and reach this state rapidly after injection allowing for a relatively short scan duration (60-90 minutes), irreversible tracers have a much longer equilibrium time, hence a longer

scan duration. Compartmental modelling uses a theoretical model based on the known biology of a system to propose an activity cure to fit the data to, providing a mathematical representation to conduct analysis with. A tissue compartment is a biochemical dimension representing a pool of ligand, which is assumed to be homogenous within compartments, however separate compartments can exist in the same model with different dynamic properties (Laruelle et al., 2002). For receptor binding ligands, four compartments can be defined. The Model appropriate for this thesis is the two tissue compartmental model (Figure 6), where the plasma concentration of the ligand is one compartment (C1), free ligand and nonspecific binding is another compartment and the first tissue compartment (C2) and the receptor bound ligand is the third compartment and second tissue compartment (C3).

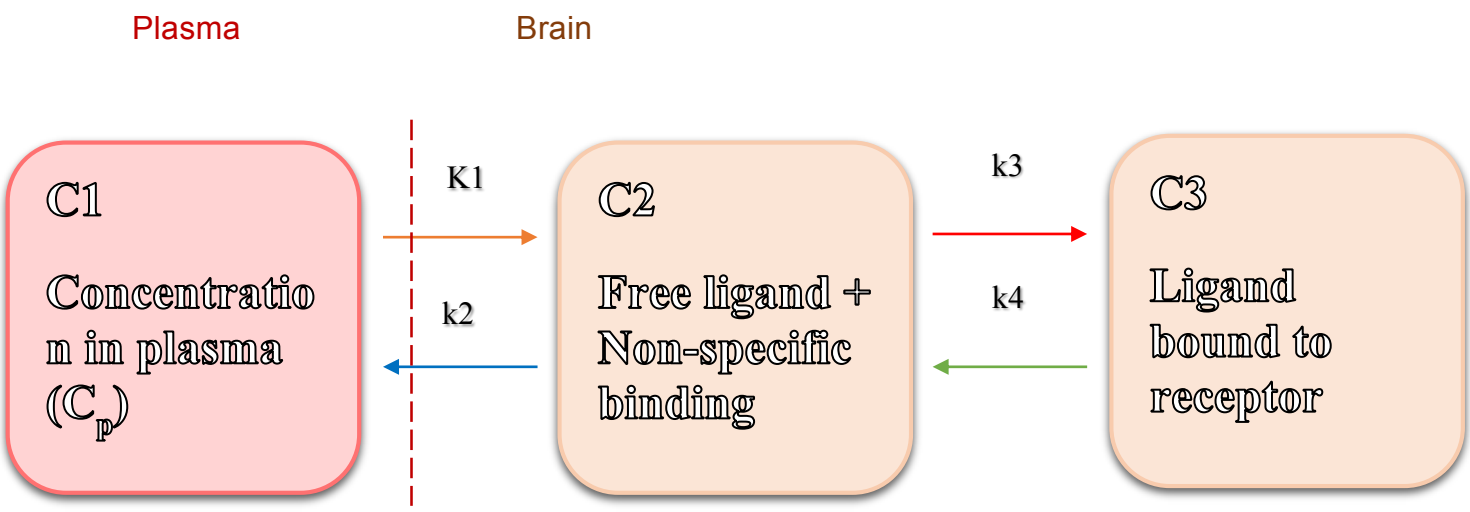


*Figure 6. Three compartment, Two tissue compartment model*

The diffusion rate constants K1 (influx), k2 (efflux), k3 (free to specific) and k4 (specific to free) represent the flow of ligand between compartments, it is possible

to have a third tissue compartment (four compartments total, C4 which models non-specific binding separately when the proportion is known), where k5 (free to non-specific) and k6 (non-specific to free) are the rate constants of transfer for that compartment.

In a reference tissue approach, the assumption that the concentrations of free and non-specific ligand are homogenous across regions.

Not all tracers are well enough understood for model fitting to be directly applied to PET data (Laruelle et al., 2002). Therefore it is often necessary to study the data that has been acquired to derive the correct kinetic components.

## Representations of PET data

Pet data analysis can be represented by different tissue distributions. Where the specific and non-specific components of tracers are known a non-displaceable binding potential ($BP_{ND}$) can be calculated. A volume of distribution ($V_T$) is the distribution of activity in a volume of tissue. Standardized uptake values (SUV) represent a $V_T$ normalized by body weight and injected activity. The distribution volume ratio (DVR) is a $V_T$ normalized by a reference region, this differs from the reference region analysis model as the arterial input is still calculated from blood data.

## *Neuroinflammation PET tracers*

PET tracers can be produced to bind to known receptors or replace a compound in a synthesis pathway. This could be the binding of a specific transmitter to a receptor, or the breakdown of a substrate by an enzyme. Similarly in certain situations, where a protein, receptor or biological compound is up-regulated, a PET tracer can be produced to image the process.

The focus of this thesis is neuroinflammation and a number of tracers exist with a primary purpose of imaging cortical inflammation. The majority of tracers used to image inflammation in the brain are based around the TSPO (Translocator protein). TSPO is a steroid synthesis protein found on the outer membrane of mitochondria. The functional significance of this protein is not widely understood. A single nucleotide polymorphism gene mutation affects TSPO in humans. There are three forms of the gene, distributed amongst the general population. There are high affinity binders with a G/G (Threonine/Threonine) copy, middle affinity binders with an A/G copy (Alanine/Threonine) and low affinity binders with an A/A copy (Alanine/Alanine); HABs, MABs and LABs respectively (Owen et al., 2011). While to some extent this phenomena affects all TSPO imaging, the different ligands in use have varying levels of binding, where in some instances low binders do not exhibit a decreased signal (Guo et al., 2012).

### PK11195

This tracer has widely been used for experimental investigation of neuroinflammation in a range of clinical disorders, including schizophrenia (Doorduin et al., 2009; van Berckel et al., 2008), Parkinson's (Gerhard et al., 2006),

multiple sclerosis (Giannetti et al., 2014; Rissanen et al., 2014), Huntington's (Politis et al., 2011) and Alzheimer's (Schuitemaker et al., 2013). A high nonspecific binding and poor signal-to-noise ratio of PK11195 lead to the development of a new generation of TSPO ligands, with an aim to address this issue (Guo et al., 2012).

## Second generation TSPO tracers

The second generation of TSPO binding radioligands (SGTs) are affected by the genetic polymorphism at the rs6971 allele. The development of this new generation of ligands aimed to address nonspecificity of PK11195. In an in silico modelling study, [$^{18}$F]PBR111, [$^{11}$C]PBR28, [$^{11}$C]DPA713 and [$^{11}$C]-(R)-PK11195 were compared across binding affinities. Within subject variability was reduced in the second generation tracers tested, when compared to PK11195 (0.9%-2.2% in SGTs, compared to 16%-36% with PK11195). Based on the data from this investigation, between-subject studies are predicted to require half the sample of those for PK11195 (Guo et al., 2012), Figure 7.

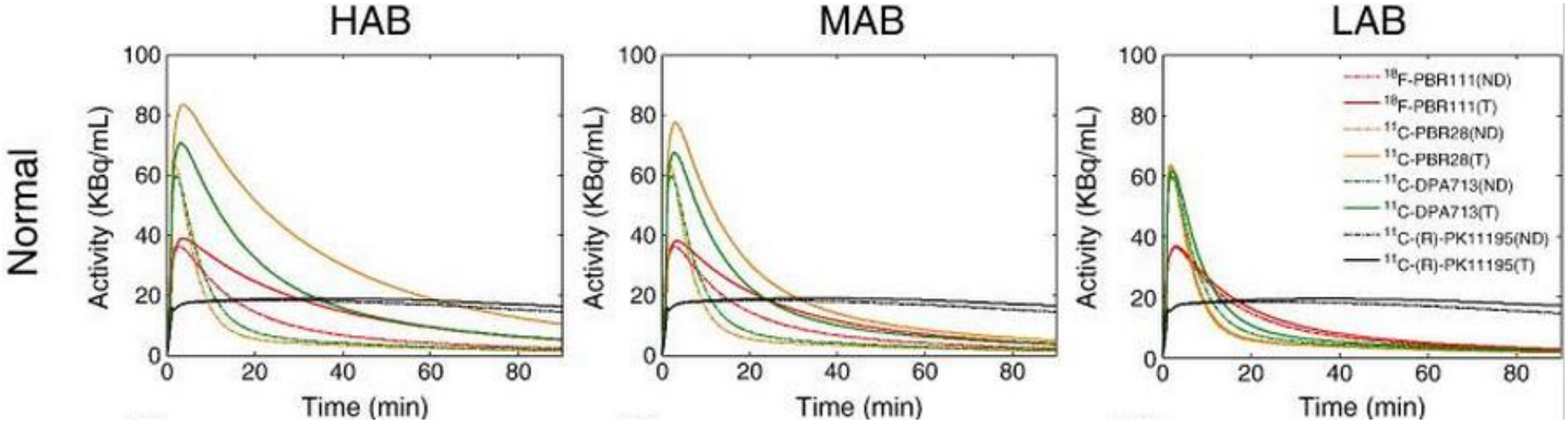


*Figure 7. Time-activity curves for TSPO tracers*

The three genotypes (HABs, MABs and LABs) across a number of TSPO tracers, including the first generation PK11195. Adapted from (Guo et al., 2012).

## Comparison of PK11195 and PBR28

[$^{11}$C]PBR28 is a second generation TSPO binding radioligand with a greater specificity than PK11195. A growing number of experimental studies have been published since its development in 2011 (Guo et al., 2014; Loggia et al., 2015; Owen et al., 2014). An *in vitro* kinetic comparison of PK11195 and PBR28 demonstrates how the two binding sites affect the signal of the tracers (Figure 8). PK11195 binding was not affected between HABs and LABs (26.4 and 22.3 nmol/L respectively), whereas PBR28 was significantly affected by the polymorphism between HABs and LABs (3.4 and 188 nmol/L respectively) (Owen et al., 2010). The variation in binding affinity is crucial for this [$^{11}$C]PBR28 study, as our in vivo signal would be dictated by the genotype of our subjects. For this reason, subjects undergoing the PBR28 experimental procedure were screened for binding affinity and LABs were excluded prior to experimental procedures.

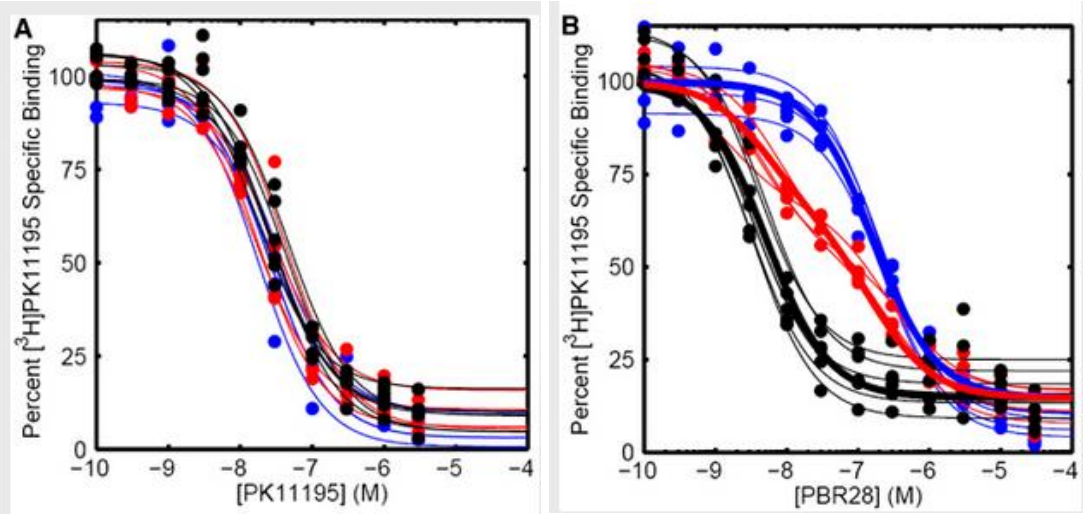


*Figure 8. In vitro binding for TSPO ligands*

HABs, MABs and LABs (blue red black respectively) for PK11195 (A) and PBR28 (B) *in vitro* Adapted from (Owen et al., 2010).

## *Experimental procedure for [$^{11}$C]PBR28 participants*

### PET scan Acquisition

All PET studies were conducted at Imanova, Hammersmith Hospital, London. Subjects arrived at least two hours before tracer injection, medical observations were performed by the study clinician and an arterial cannula was inserted to the radial artery and a contralateral antecubital venous cannula was inserted. All PET scans were performed on a Siemens Biograph™ TruePoint™ PET•CT scanner (Siemens Medical Systems, Germany). An initial CT scan was performed for attenuation and scatter correction (Lercher and Wienhard, 1994).

### [$^{11}$C]PBR28 synthesis

The radiotracer [$^{11}$C]PBR28 (Figure 9) was synthesized as previously described (Owen et al., 2014) by reaction of [$^{11}$C]Methyl Iodide with the desmethyl-PBR28 precursor.

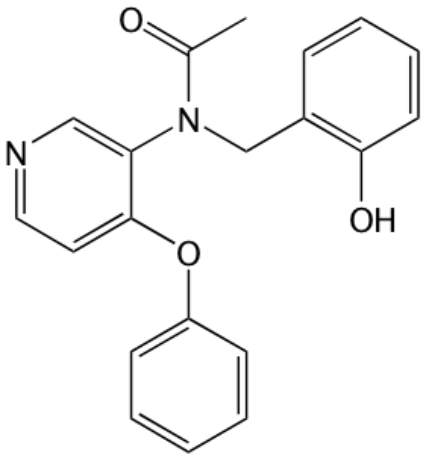


*Figure 9. PBR28 compound structure*

Chemical structure of PBR28 from synthesis, adapted from (Wang et al., 2009).

## [$^{11}$C]PBR28 injection

A bolus of [$^{11}$C]PBR28 was injected via the venous cannula over 30 seconds by the study physician (SS).

## Blood sampling for arterial input function

Discrete blood samples were manually withdrawn at 5, 10, 15, 20, 25, 30, 40, 50, 60, 70, 80, 90 minutes, centrifuged and used to determine the plasma over blood activity ratio (POB). Samples at 5, 10 and 15 minutes were used to calibrate the two sampling modalities. Samples taken at 5, 10, 20, 30, 50, 70 and 90 minutes were also analysed using HPLC to calculate the plasma fraction of authentic tracer free of metabolites (PPf). Both POB and PPf were fitted with an extended Hill model (Edison et al., 2009), while whole blood TACs were fitted using a multi-exponential (Tonietto, 2014). For each scan, a time delay was fitted and applied to the input functions (both parent and whole blood TACs) to account for any temporal delay between blood sample measurement and the target tissue data.

## MRI scans and Regions of Interest (ROI) Definition

Each subject underwent a T1 weighted MRI brain scan. MRI images were used for grey/white matter segmentation and region of interest (ROI) definition. A neuroanatomical atlas (Tziortzi et al., 2011) was co-registered on each subject's MRI scan and PET image using a combination of Statistical Parametric Mapping 8 (http://www.fil.ion.ucl.ac.uk/spm) and FSL (http://www.fsl.fmrib.ox.ac.uk/fsl) functions, implemented in MIAKAT$^{TM}$ (http://www.imanova.co.uk). The primary

region of interest was total grey matter. Secondary regions of interest were temporal and frontal lobe grey matter (Radewicz, 2000).

- *a priori* ROIs for TSPO assessment: Frontal cortex, temporal lobe and whole brain grey matter.
- Control ROIs for assessment of signal specificity: Cerebellum and brain stem

## *PET Image analysis*

### Image analysis

All PET images were corrected for head movement using nonattenuation-corrected images, as they include greater scalp signal, which improves re-alignment compared to attenuation-corrected images (Montgomery et al., 2006). Frames were realigned to a single 'reference' space identified by the individual T1 MRI scan. The transformation parameters were then applied to the corresponding attenuation-corrected PET frames, creating a movement-corrected dynamic image for analysis. Regional time-activity curves (TACs) were obtained by sampling the image with the coregistered atlas. Hence quantification of [$^{11}$C]PBR28 tissue distribution was performed using the two tissue compartmental model accounting for endothelial vascular TSPO binding (2TCM-1K) (Rizzo et al., 2014), as this has been shown to have improved performance compared with the two tissue compartmental model not accounting for endothelial binding (2TCM) (Rizzo et al., 2014). Nevertheless, for completeness, we analysed the data using the 2TCM as well (Table 11 & Table 12). Even after accounting for genotype, high inter-subject variability is seen in imaging with TSPO tracers. With PK11195 plasma protein binding is evident and may account for some levels of variability with TSPO imaging (Lockhart et al., 2003). Indeed TSPO ligand quantification approaches mostly use tissue reference methodologies (Turkheimer et al., 2007). Analysis of PK11195 is conducted using simplified reference tissue models (SRTM) and supervised cluster analysis (Yaqub et al., 2012). This method is not applicable to second generation TSPO tracers, including PBR28, as the higher ligand affinity leads to appreciable endothelial

binding in the blood brain barrier (BBB) (Rizzo et al., 2014). As a result, it is not possible to identify a supervised cluster for reference. Our outcome measure therefore was the distribution volume ratio (DVR, the ratio of the $V_T$ in the ROI to $V_T$ in the whole brain) as this accounts for inter-subject variability in the input function. In secondary analyses, we tested the regional specificity of group changes by comparing DVR between groups in regions (the cerebellum and brainstem) where we did not expect marked inflammatory changes based on the post-mortem studies and grey matter changes seen in people at risk of psychosis (Wood et al., 2008).

## Comparison of 2TCM and 2TCM-1K performances

Model fit performance analysis confirmed 2TCM-1K to be superior to 2TCM for describing [$^{11}$C]PBR28 PET data at region level. This finding is consistent with the results reported by Rizzo and colleagues applying [$^{11}$C]PBR28 imaging in a healthy population (Rizzo et al., 2014). 2TCM-1K provided a better fit of the tissue data for all the analysed ROIs, all the groups of subjects and all the affinities (Figure 10). The relative difference of the weighted residual sum of squares obtained with 2TCM-1K, compared to the 2TCM one, was -55%±25% while the relative difference of the residual sum of squares was -50%±30% (mean ± SD). Weighted residuals obtained with 2TCM-1K were consistent with the assumptions about the measurement error (random and uncorrelated). In terms of parsimony criteria (Akaike, 1974 ), 2TCM-1K Akaike Information Criterion (AIC)* was smaller than 2TCM AIC in 99.4% of the regions, thus confirming the identification of 2TCM-1K as the optimal model to describe [$^{11}$C]PBR28 brain data. In term of outliers the two models performed similarly (brain outlier fraction: 3% for 2TCM and 4% for 2TMC-1K). These were

concentrated particularly in small regions (average volume <3 $cm^3$), indicating they are very likely characterized by high noise data. After correction for outliers, individual $V_T$ estimate precisions were consistent for both models (for 2TCM CV $V_T$ = 4%±5%; for 2TCM-1K CV $V_T$ = 7%±5%).

*AIC is the Akaike Information criterion and it is defined as:

AIC = $nD \cdot \log(WRSS) + 2 \cdot nP$

where $nD$ represents the number of data fitted by the model, $WRSS$ the weighted residual sum of squares and $nP$ the number of model parameter.

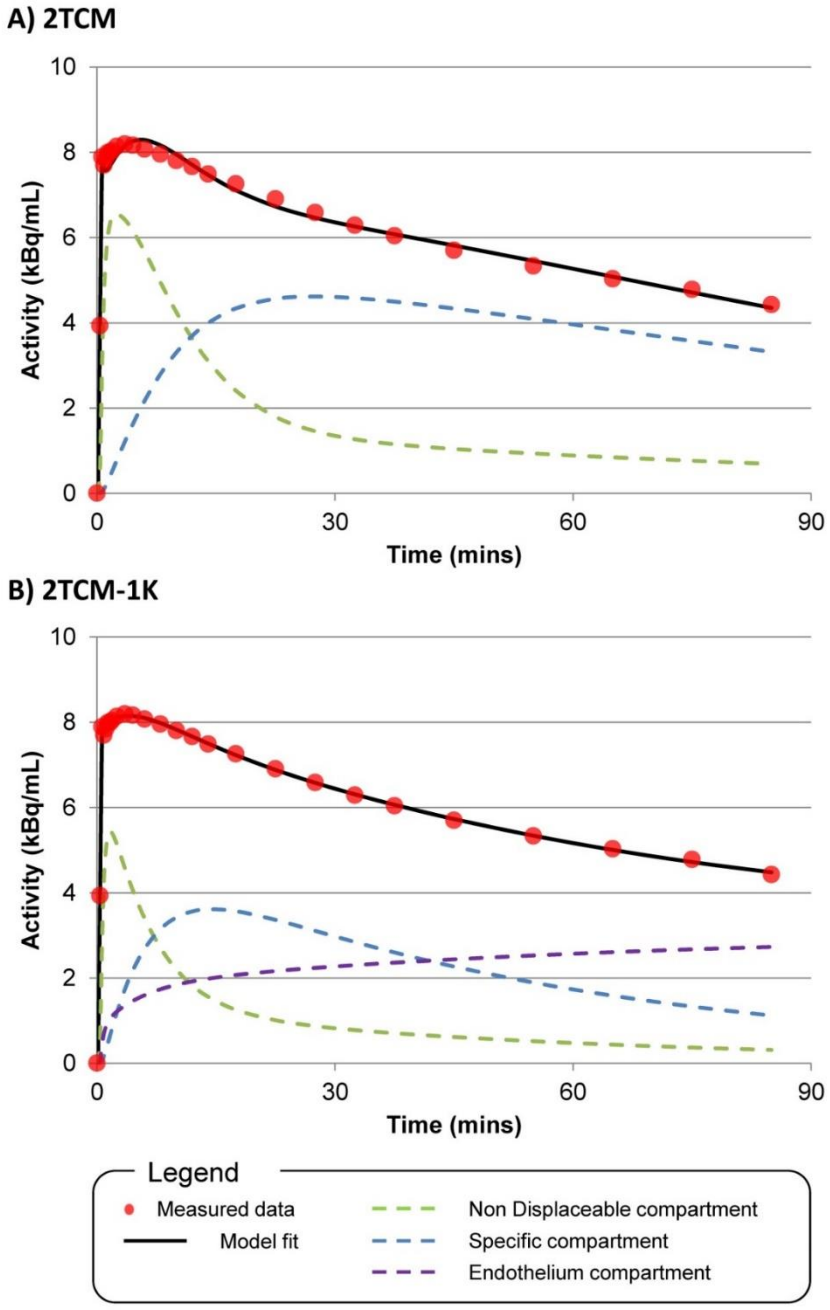


*Figure 10. 2TCM and 2TCM-1K fit comparison for [$^{11}$C]PBR28*

PET data in schizophrenia: application to cortical region in a representative HAB subject. The correspondence between the model fit (black line) and measured date (red circles) is closer in the 2TCM-1K than the 2TCM model.

## *General experimental methods for animal studies*

### Animals

For all *in vivo* experimentation, 250g male Sprague Dawley (SD) rats were used (Charles River, UK). Animals were randomized into cages, drug administration and subsequent post mortem analysis was conducted blindly. Animals were housed in individually ventilated cages with food and water ad libitum, with a 12 hour light/dark cycle. All experimental procedures were carried out in accordance with the animals (scientific procedures) act (ASPA) 1984 and home office regulations.

### Drug delivery Experimental drug administration

There are a number of techniques routinely used for administering drugs to animals, with varying ease of delivery and dose accuracy. In this section, the benefits and detriments of the available methods will be discussed.

#### Intra-peritoneal

The most commonly used method of delivery is intra-peritoneal (i.p.) injection. The drug is delivered to the peritoneal cavity, where it is absorbed into the bloodstream and systemically circulates. The ease of this method has made it the primary delivery method in rodent investigations. For single doses i.p. administration is certainly a valid and incredibly useful method, however with multiple dose of a drug, it is difficult to gain an accurate level of drug, especially if you are aiming to create a clinically comparable dose. The metabolism of rodents is far higher than that of a human and drugs are broken down at such a high rate that between doses, the drug compound is often fully removed from the system. In the past this has caused

investigators to used doses far higher than those applicable to the clinic (Kapur et al., 2003).

### Oral

It is possible to give animals drug doses orally, either in drinking water, food sources or by gavage. The first two methods are more likely to provide a continual dose of a drug, when compared to an i.p. injection, as animals will consume food and water throughout the day. However it is not an accurate way of delivering specific doses as food and water consumption varies greatly between animals and in cages of multiple animals dominance is a significant component in feeding patterns. As well as the uncertainty over dose delivery, there is often a chance that the taste of a drug will alter the amount of food or water consumed. Many pharmaceuticals have a distinctly bitter taste and result in avoidance in the drug dosed group. Gavage has similar issues as i.p. administration, where peaks and troughs of administration cause a problem for a chronic administration experimental design.

### Subcutaneous delivery

Subcutaneous delivery methods are relatively new for experimental setups, but provide an alternative method of delivery where a number of the issues previously mentioned are addressed. Delivery can be via pellets or osmotic mini-pumps. In the experiments presented here, animals were anaesthetized using volatile anaesthesia (isoflurane, VWR USA) prior to insertion of antipsychotic drug pellets. Animals received a low dose (0.05 mg/kg/day (Samaha et al., 2008)) of haloperidol via slow release drug pellets (Innovative Research of America, USA). Sterile drug pellets

were inserted subcutaneously above the right shoulder blade using a standard gauge trochar (Figure 11, Innovative Research of America, USA). The same method was implemented for control pellets .

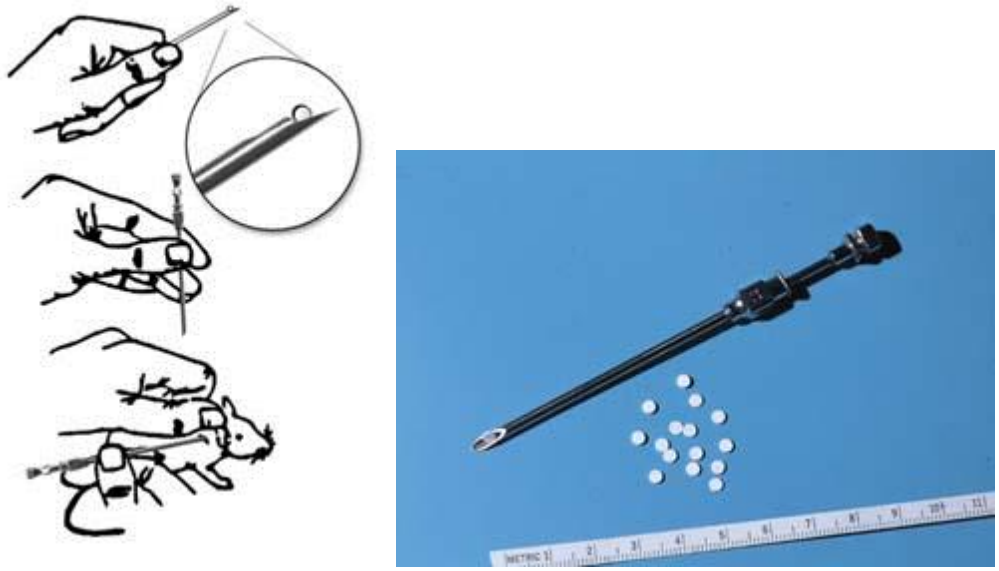

*Figure 11. Trochar implantation of pellets*

Subcutaneous drug pellet insertion technique (Images adapted from; Innovative Research of America (IRA, USA)).

## Immunohistochemistry

Animals were transcardially perfused with 4% paraformaldehyde (PFA) and postfixed over night at 4°C. Following post-dissection fixation, brains were transferred to sucrose solution for cryoprotection (30% sucrose made up in 0.1M PBS). Spinal cords were trimmed to cerebellar alignment and olfactory bulbs removed prior to weighing and volume calculation. Volumes were calculated using water displacement in a finely graduated cylinder (Dorph-Petersen et al., 2005). Brain weight was calculated using a top pan balance. Following volumetric and weight calculation, the left cerebral hemisphere was embedded in OCT mounting

media (CellPath, UK) and frozen using liquid nitrogen for cryosectioning and immunohistochemistry.

Samples were stored at -80$^{o}$C until cryosectioning (up to 48 hours). Sagittal brain slices (25 µm, cut on a Leica cryostat) were thaw mounted on glass superfrost slides (VWR, USA) and stored at -20$^{o}$C until immunohistochemical processing. A standard heat mediated antigen retrieval step was implemented prior to staining. Slides were outlines with liquid block (Dako, UK) and washed in PBS three times at 5 minute intervals. The primary antibody was then applied and incubated over night at 4$^{o}$C. Following incubation with the primary antibody, slides were then washed with the same regime of PBS before an hour of incubation with the secondary antibody at room temperature for one hour. Following secondary antibody incubation (see Table 6 for antibody details), slides were washed with PBS and cover slips were mounted using Hard-Set Vectorshield$^{TM}$ with an incorporated DAPI stain (Vector laboratories, USA). Slides were then stored at 4$^{o}$C for confocal Imaging.

| Antibody | Species | Concentration | Company | Catalogue number |
|---|---|---|---|---|
| Iba-1 | Goat | 1/1000 | Abcam | Ab5076 |
| Cleaved-Caspase-3 | Rabbit | 1/500 | Cell signalling technology | ASP175 |
| Cy3 | Donkey anti-Goat | 1/1000 | Jackson | 705-166-147 |
| AlexaFluor488 | Donkey anti-Rabbit | 1/1000 | Abcam | Ab150073 |

*Table 6. Antibody table*

Antibodies used in this thesis.

## Image acquisition

Images were acquired on a Leica SP5 confocal microscope (leica microsystems, USA). Sequential scanning was used to provide separation of channels. Z-stacks were acquired with a 20x lens to produce a volume made up of 11 planes (Kozlowski and Weimer, 2012). The prefrontal cortex was the primary ROI for analysis (Juckel et al., 2011). 3 channels were acquired, a low gain CY3, high gain CY3 and DAPI nuclear channel.

## Image analysis

Images were then analysed for cell density and volume density using two analysis paradigms. Cell density was calculated using colocalization of nuclear and cellular staining with Cell Profiler software (developed for this thesis, details of pipeline and modules are found in chapter 5). DAPI nuclei were identified and a 5 pixel proximity threshold was set for the colocalization count. The principals of detection were adapted from the literature ((Forero et al., 2010; Kozlowski and Weimer, 2012; Paolicelli et al., 2011) also see chapter 5).

## Blood analysis

Two samples of blood (2 mL each) were taken from the animals at the time of perfusion (or decapitation in the case of fresh frozen tissue collection). Blood was collected in an EDTA impregnated purple top blood tube. One sample was analysed for haloperidol levels and the other for peripheral levels of cytokines. (Blood samples were analysed by ABS laboratories, UK., as the reagents and equipment needed for cytokine and haloperidol analysis were not available on site at the time of experiments).

## Drug delivery analysis

Levels of haloperidol in the blood of animals were analysed to confirm pellet delivery. Haloperidol was quantified in whole rat blood using haloperidol d4 to internally standardise the procedure. Whole blood (100μL aliquot) was subjected to protein precipitation using acetonitrile containing the internal standard. The supernatant from the samples was evaporated to dryness under nitrogen and the residue reconstituted in 100 μL of 0.05% formic acid. Aliquots of 10 μL were injected for analysis and quantification using high performance liquid chromatography mass spectrometry with multiple reaction monitoring (MRM haloperidol m/z 376 to 165 and haloperidol d4 m/z 380 to 169). The LC-MS/MS system was a CTC DLW autosampler, Jasco LC and ABSciex API4000 tandem mass spectrometer. Calibration standards containing haloperidol in whole blood plasma were prepared in duplicate at 0 (blank), 0.1, 0.25, 0.5, 1.0, 5.0, 10.0, 50.0 and 100.0 ng/mL and the samples were analysed with duplicate quality control samples prepared at 0.3, 8 and 75 ng/mL. Standard FDA (FDA, 2001) and EMA (EMA, 2011) quality standards criteria were applied for the acceptance of the analysis batches.

## Cytokine analysis

For Human and rat whole blood samples, peripheral measures of cytokines (pro- and anti- inflammatory) were analysed using a V-PLEX$^{TM}$ multi-spot assay system (Mesoscale, USA, the full protocol for the system is available from www.mesoscale.com). A list of 10 possible cytokines were available for analysis including; IFN-ɣ, IL-1β, IL-2, IL-4, IL-6, IL-8, IL-10, IL-12p70, IL-13 and TNF--α. The figure below (Figure 12) demonstrates the principal of detection;

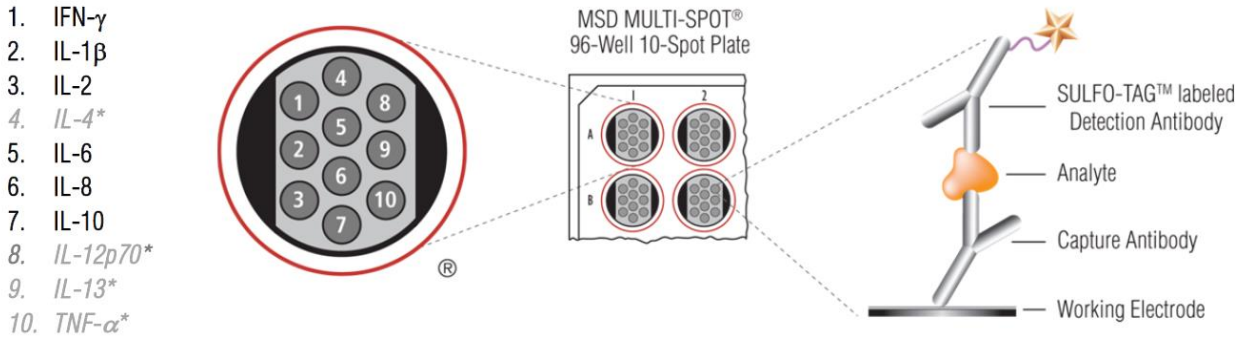


*Figure 12. Multiplex setup for cytokine detection*

Procedure in human blood (black text and *) and non-human primate blood (black text only) (cytokine detection range is the same as human blood for rat samples). Whole blood samples were applied to the 96-Well 10-Spot Plate, with two analysis runs per sample of blood. Prior to analysis, calibration solutions were run to provide detection ranges for the cytokines analysed.

Following collection, samples were frozen until required for the multiplex assay. Samples were diluted with a solution containing preservatives and enzyme blockers (Diluent 2). 50 µL of the samples, calibration solutions, or control solutions, were added to each well. Samples were run in duplicate and average values were calculated. Internal controls for human analysis were lyophilized human cytokines of known concentrations (3 controls, Mesoscale, USA, catalog # C4049-1). Similarly, rat samples were run with lyophilized rat cytokines of known concentrations (3 controls, Mesoscale, USA, Catalog # C4044-1). Concentration standard curves were produced for IFN-ɣ, IL-1β, IL-2, IL-4, IL-6, IL-8, IL-10, IL-12p70, IL-13 and TNF-α, alongside experimental samples to confirm detection. The plates were then

sealed and incubated at room temperature for 2 hours on an orbital shaker. The plate was washed three times using 150 µL of wash buffer per well. 25 µL of detection antibody was added to each well and incubated for 2 hours at room temperature on a shaker. The plate was washed three times with 150 µL of wash buffer per well. 150 µL of reading buffer was added per well before reading on the MSD instrument.

## *Statistics*

During experimental design, sample size and power were calculated to ensure cohort sizes in both clinical and animal experiments (Jones et al., 2003). Statistical analysis was performed using the Statistical Package for the Social Sciences (SPSS IBM, USA). For group analysis, an analysis of variance (ANOVA) was conducted, with appropriate post hoc tests to exclude type I errors (false positives). Correlation statistics were conducted using Pearson's correlation and a threshold for significance in statistical tests was defined at $p< 0.05$. Data were tested for homogeneity of variance using a Levene's test (Levene, 1960) and in multivariate analysis, Wilks Lambda was used to determine *F*-distribution fit (Wilks, 1938). Data are represented as the mean ± standard deviation, unless otherwise stated. Fisher's R-Z transformation was used to conduct group based comparisons of correlative analysis (Fisher, 1915).

# *Chapter 3 – Neuroinflammation in UHR and schizophrenia.*

## *Abstract*

Here we aim to determine whether microglial activity, measured using translocator-protein positron emission tomographic imaging (PET), is increased in unmedicated subjects presenting with pre-clinical symptoms indicating they are at ultra high risk of psychosis, and to determine if it is elevated in schizophrenia. We use the second generation radioligand [$^{11}$C]PBR28 and PET to image microglial activity in the brains of subjects at ultra high risk for psychosis. Subjects were recruited from early intervention centres. We also imaged a cohort of patients with schizophrenia and healthy controls for comparison. At screening, subjects were genotyped to account for the 18KD translocator-protein polymorphism. The main outcome measure was total grey matter [$^{11}$C]PBR28 binding ratio, representing microglial activity. [$^{11}$C]PBR28 binding ratio in grey matter was elevated in ultra high risk subjects, compared to matched controls, ($p$= 0.004, F= 10.3, Cohen's d >1.2), and was positively correlated with symptom severity ($r$= 0.730, $p$< 0.01). Patients with schizophrenia also demonstrated elevated microglial activity with respect to matched controls ($p$< 0.001, F= 20.8, Cohen's d >1.7). Microglial activity is elevated in schizophrenia and in subjects with pre-first episode symptoms who are at ultra high risk of psychosis. We also show how in the high risk subjects binding is related to high risk symptom severity. This indicates that neuroinflammation is linked to the risk of psychosis and related disorders, as well as the expression of sub-clinical symptoms. Follow up of ultra high risk subjects will determine whether this is specific to the later development of schizophrenia or risk factors in general.

## *Introduction*

Schizophrenia is a severe psychiatric disorder characterised by psychotic and cognitive symptoms, and is a leading cause of global disease burden (Howes and Murray, 2014). It is generally preceded by a prodromal phase of attenuated psychotic symptoms and functional impairment (Yung et al., 2005). Subjects meeting standardised criteria for this phase have an ultra high risk for developing a psychotic disorder, in most cases schizophrenia (Fusar-Poli et al., 2013a). Approximately ~35% of high risk subjects will develop a psychotic disorder within 24 months (Fusar-Poli et al., 2012).

Whilst the pathoaetiology of schizophrenia is not fully understood, there is increasing evidence for the involvement of neuroinflammatory processes. Microglia are the resident immune cells of the central nervous system and several lines of evidence indicate microglial involvement in the pathology of psychosis (Bayer et al., 1999; Doorduin et al., 2009; van Berckel et al., 2008). In ultra high risk subjects, there are elevations in the levels of pro-inflammatory cytokines (Perkins et al., 2014) which are also elevated in patients with schizophrenia (Miller et al., 2011). The levels of such peripheral markers have also been associated with the reductions in grey matter volume in both ultra high risk subjects (Cannon et al., 2014) and patients with schizophrenia (Meisenzahl EM, 2001). Post-mortem investigation of brain tissue has found elevated microglial cell density (with a hypertrophic morphology) in schizophrenia compared with controls (Bayer et al., 1999), particularly in the frontal

and temporal lobes (Radewicz, 2000), although some studies have found no differences (Steiner et al., 2006). However, as microglial activity is dynamic, post-mortem studies may miss alterations early in the development of the disease.

Elevations in microglial activity can be measured *in vivo* with positron emission tomography (PET) using radioligands specific for the 18kD translocator-protein (TSPO), which is expressed on microglia (Karlstetter et al., 2014). Investigations using the first generation radiotracer (R)-[$^{11}$C]PK11195 have revealed an increase in TSPO binding in medicated patients with schizophrenia when compared to healthy controls (Doorduin et al., 2009; van Berckel et al., 2008). The first investigation of microglia using PET in schizophrenia, in a cohort of 10 patients, revealed a total grey matter elevation of microglial activity in the five years following diagnosis (van Berckel et al., 2008). The most recent investigation in seven chronically medicated patients with schizophrenia using (R)-[$^{11}$C]PK11195 demonstrated an elevation in hippocampal binding potential and a non-significant 30% increase in total grey matter binding potential (Doorduin et al., 2009).

Whilst these studies indicate elevated microglial activity in schizophrenia, they included patients in whom the disorder was already established. It is therefore unknown whether this elevation predates the onset of, or becomes evident after, the first episode of frank psychosis.

Therefore in the present investigation we seek to determine whether microglial activity is elevated in ultra high risk subjects using the novel TSPO radioligand

[$^{11}$C]PBR28. Our *a priori* hypothesis was that microglial activity would be elevated in the total grey matter in ultra high risk individuals compared to matched controls. An additional prediction was that this elevation would be evident in frontal and temporal cortical regions, brain areas that have been particularly implicated in ultra high risk pathophysiology (Bose et al., 2008). [$^{11}$C]PBR28 is a second generation TSPO tracer with a higher affinity for TSPO than (R)-[$^{11}$C]PK11195 (Kreisl et al., 2010). Recent *in situ* binding evidence shows that a genetic polymorphism (a C/T substitution at rs6971) influences the binding of TSPO tracers, including [$^{11}$C]PBR28. This results in three TSPO binding profiles. High affinity binders (HABs, C/C) have the greatest tracer affinity, low affinity binders (LABs, T/T) have a 50 fold reduction in affinity, and mixed affinity binders (MABs, C/T) express both HAB and LAB TSPO in approximately equal proportion (Owen et al., 2011). In view of this we included a cohort of patients to test the hypothesis that TSPO binding is elevated in schizophrenia after adjusting for this polymorphism, as this has not been taken into account previously. We also tested the secondary hypothesis that there would be a positive relationship between total grey matter microglial activity and symptom severity.

## *Methods*

The study was approved by the local research ethics committee and was conducted in accordance with the Declaration of Helsinki. After complete description of the study to the subjects, written informed consent was obtained.

### Subjects

A total of 56 subjects were recruited and completed the study; 14 subjects meeting ultra high risk criteria, as assessed on the comprehensive assessment of the at risk mental state (CAARMS) (Yung et al., 2005), were recruited from OASIS (Outreach and Support in South London) (Fusar-Poli et al., 2013b) (Mean age ± SD: 24.3 ± 5.40; (M:F=7:7)). 14 age matched (± 5 years) control subjects were recruited through newspaper and poster adverts. 14 subjects with schizophrenia (Mean age ± SD: 47.0 ± 9.31; (M:F=12:3)) were recruited from London mental health centres (South London and Maudsley NHS Foundation Trust). A further 14 age matched (± 5 years) healthy control subjects were recruited for comparison with this second cohort (Table 7).

| | Control | Stdev | Ultra high risk | Stdev | p-value | Control | Stdev | Schizophrenia | Stdev | p |
|---|---|---|---|---|---|---|---|---|---|---|
| | N = 14 | | N = 14 | | - | N=14 | | N = 14 | | - |
| Age in years | 28.14 | 7.99 | 24.29 | 5.40 | 0.133[a] | 46.21 | 13.62 | 47.00 | 9.31 | 0.982[a] |
| Years of education | 14.8 | 3.0 | 14.3 | 1.6 | 0.344[a] | 12.3 | 3.0 | 12.2 | 2.0 | 0.374[a] |
| Gender (M:F) | 10:4 | | 7:7 | | 0.352 [b] | 12:3 | | 12:3 | | 1.000[b] |
| TSPO genotype (HAB) | 10 | | 7 | | 0.352 [b] | 14 | | 13 | | 0.541[b] |
| Smoking (cigarettes/day) | <1 | 0.41 | 3.43 | 5.56 | 0.009[a] | 2.15 | 4.90 | 12.50 | 13.69 | 0.006[a] |
| Alcohol (units/week) | 10.78 | 8.79 | 6.64 | 12.89 | 0.833[a] | 7.13 | 6.24 | 9.29 | 22.22 | 0.297[a] |
| Drugs of abuse (no. tried) | <1 | 1.05 | 3.75 | 2.90 | 0.003 | 1.00 | 1.00 | 1.29 | 1.07 | 0.671[a] |
| ***CAARMS/ PANSS*** | | | | | | | | | | |
| Positive | - | - | 11.2 | 4.5 | - | - | - | 17.0 | 6.1 | - |
| Negative | - | - | 6.1 | 4.3 | - | - | - | 14.1 | 4.0 | - |
| General | - | - | 19.1 | 12.3 | - | - | - | 32.6 | 8.7 | - |
| Total | - | - | 49.5 | 21.6 | - | - | - | 63.7 | 18.1 | - |

*Table 7. Demographic characteristics of experimental and control subjects*

[a]independent samples t-test. [b]Mann-Whitney U test. Symptom scales measured in high risk subjects on the CAARMS (comprehensive assessment of the 'at risk mental state') and in schizophrenia on the PANSS (positive and negative syndrome scale).

Healthy control subjects with a personal history of a psychiatric disorder or a first degree relative with schizophrenia or a psychotic illness were excluded.

## Clinical and neuropsychological measures

At screening all subjects were assessed using the SCID (Spitzer et al., 1992). Ultra high risk subjects were assessed on the CAARMS (Yung et al., 2005) by a trained investigator and patients with a diagnosis of schizophrenia were assessed on the positive and negative syndrome scale (PANSS) (Kay et al., 1987) by a clinician on the day of the PET scan. Depressive symptoms were assessed using the Beck Depression Inventory (BDI) (Beck et al., 1961).

## PET imaging

An initial computer tomography (CT) scan was acquired for attenuation and scatter correction using a Siemens Biograph™ TruePoint™ PET•CT scanner (Siemens Medical Systems, Germany). Subjects then received a bolus injection of [$^{11}$C]PBR28 (mean Mbq activity ±SD: 325.31 ± 27.03) followed by a 90-minute emission scan. PET data were co-registered with whole brain structural images acquired with a 3T magnetic resonance imaging (MRI) scanner (Trio, Siemens Medical Systems, Germany). A 32 channel coil was used for all but one scan, where a 12 channel coil was used instead.

## PET acquisition

PET data were acquired dynamically over a 90-minute time window and binned into 26 frames (durations: 8 x 15 s, 3 x 1 min, 5 x 2 min, 5 x 5 min, 5 x 10 min). Images were reconstructed using filtered back projection, which provides better data quality and signal-to-noise ratio over iterative methods (Reilhac et al., 2008), and corrected for attenuation and scatter. During the PET acquisition, arterial blood data were sampled via the radial artery using a combined automatic-manual approach. A continuous (one sample per second) sampling system (ABSS Allogg, Mariefred, Sweden) measured whole blood activity for the first 15 minutes of each scan.

## Structural MRI

Each subject underwent a T1 weighted MRI brain scan. MRI images were used for grey/white matter segmentation and region of interest (ROI) definition. A neuroanatomical atlas (Tziortzi et al., 2011) was co-registered on each subject's MRI scan and PET image using a combination of Statistical Parametric Mapping 8 (http://www.fil.ion.ucl.ac.uk/spm) and FSL (http://www.fsl.fmrib.ox.ac.uk/fsl) functions, implemented in MIAKAT$^{TM}$ (http://www.imanova.co.uk). The primary region of interest was total grey matter. Secondary regions of interest were temporal and frontal lobe grey matter (Radewicz, 2000).

## Statistical analysis

Data, other than for gender and genotype, were shown to have a normal distribution following a Shapiro-Wilk test (Shapiro, 1965). Hence parametric tests were implemented for all but gender and affinity analyses, where a Mann-Whitney U test

was used. Demographic data and tracer activity data were analysed using independent-samples *t*-tests. Multiple analysis of covariance (ANCOVA) with Bonferroni correction (Dunn, 1961) was used to determine whether there was an effect of group on [$^{11}$C]PBR28 binding associated microglial activity in the total grey matter, frontal lobe, and temporal lobe. There is data to suggest that cortical microglial density, hence TSPO binding, is elevated with aging (Schuitemaker et al., 2012), which is also evident in our data (Table 8). For this reason, we performed group level analysis using age as a covariate. TSPO genotype was also included as a co-variate in analysis as there is a significantly higher binding of tracer in HABs than MABs (Owen et al., 2011). For all statistical comparisons alpha was set at a 0.05 threshold (two-tailed) for significance. Statistical analysis was performed using SPSS 21 (IBM, USA). Partial correlation analysis was used to test the association of microglial activity with symptom severity and total grey matter volumes, with age and affinity as covariates of no interest.

| Measure | r statistic | *p* value |
|---|---|---|
| Total grey matter Vt | 0.336 | 0.016* |
| Frontal lobe Vt | 0.368 | 0.008** |
| Temporal lobe Vt | 0.329 | 0.018* |
| Frontal lobe DVR | 0.307 | 0.032* |

*Table 8. Age correlations*

(Pearson's two-way product moment correlation coefficient) with volume of distribution (Vt) and distribution volume ratios (DVR) *Pearson's correlation (two-way, *p<0.05; **p<0.01).*

## *Results*

### Demographic Comparisons and Tracer Dosing

No significant demographic differences between the two groups of controls and respective patient groups were observed (Table 7). There were no differences in the injected dose, injected mass, specific activity, parent plasma fraction or plasma over blood ratio between ultra high risk subjects or patients with schizophrenia and their respective controls (Table 9).

| | Control (SD) | Ultra high risk (SD) | p[a] | Control (SD) | Schizophrenia (SD) | p[a] |
|---|---|---|---|---|---|---|
| Injected dose (MBq) | 326.6 (26.6) | 327.6 (26.7) | 0.982 | 326.3 (25.5) | 318.9 (33.8) | 0.910 |
| Injected mass (μg) | 2.8 (1.3) | 3.4 (2.1) | 0.390 | 2.5 (0.8) | 2.5 (1.1) | 0.905 |
| Specific activity (GBq/μmol) | 49.3 (22.1) | 43.4 (21.4) | 0.418 | 50.0 (18.4) | 52.7 (20.9) | 0.981 |
| Parent plasma fraction (%) | 8.5 (2.1) | 9.9 (3.5) | 0.376 | 12.0 (3.6) | 12.7 (3.0) | 0.635 |
| POB (ratio) | 0.0034 (0.0017) | 0.0033 (0.0013) | 0.667 | 0.0039 (0.001) | 0.0044 (0.002) | 0.511 |

*Table 9. Scan Parameters for [$^{11}$C]PBR28*

[a]independent samples t-tests.

## [$^{11}$C]PBR28 distribution in total grey matter regions

The [$^{11}$C]PBR28 distribution volume ratios in total grey matter, frontal lobe and temporal lobe grey matter were significantly increased in ultra high risk when compared with matched control subjects (Figure 13 A and Table 10). Similarly, patients with a diagnosis of schizophrenia had elevated [$^{11}$C]PBR28 DVRs in total, frontal lobe and temporal lobe grey matter with respect to matched control subjects (Figure 13 B and Table 10). Secondary analysis to investigate regional specificity revealed no difference between ultra high risk or schizophrenia and respective controls in cerebellar or brainstem DVR (Table 10). Representative PET images of control, ultra high risk and patients with schizophrenia are presented in Figure 13 C. When comparing regions using $V_t$, with either 2TCM or 2TCM-1K, no significant group difference was observed (Table 11 & Table 12).

| Mean Regional DVR of [11C]PBR28 | Control | SD | Ultra high risk | SD | F | P | Cohen's d | Control | SD | Schizophrenia | SD | F | p | Cohen's d |
|---|---|---|---|---|---|---|---|---|---|---|---|---|---|---|
| Total grey Matter | 2.032 | 0.017 | 2.088 | 0.021 | 10.332 | 0.004 | 1.244 | 2.465 | 0.020 | 2.557 | 0.014 | 20.802 | <0.001 | 1.769 |
| Frontal lobe | 2.000 | 0.038 | 2.087 | 0.026 | 5.339 | 0.030 | 0.894 | 2.489 | 0.037 | 2.606 | 0.025 | 9.883 | 0.005 | 1.245 |
| Temporal lobe | 1.914 | 0.041 | 2.001 | 0.028 | 4.417 | 0.047 | 0.829 | 2.282 | 0.065 | 2.518 | 0.044 | 13.089 | 0.001 | 1.430 |
| Cerebellum | 2.307 | 0.055 | 2.287 | 0.081 | 0.062 | 0.805 | - | 2.863 | 0.060 | 2.873 | 0.063 | 0.015 | 0.905 | - |
| Brain stem | 2.291 | 0.191 | 2.489 | 0.28 | 0.500 | 0.487 | - | 2.514 | 0.154 | 2.097 | 0.234 | 3.194 | 0.088 | - |

*Table 10. Microglial activity in UHR and schizophrenia*

Microglial activity, as measured by PBR28 distribution volume ratio, is elevated in subjects at ultra high risk of psychosis (df=21 $p$=0.004) and patients with schizophrenia (df=21 $p$<0.001) in the total grey matter, frontal and temporal cortical regions of interest but not in control regions (the cerebellum and brainstem). The mean regional distribution volume ratios are shown for each group together with those for matched controls. The results of the ANCOVA covarying for age and translocator-protein genotype are shown for each case-matched control comparison.

| Regional DVR of [11C]PBR28 | Control (SD) | UHR (SD) | p | Control (SD) | Schizophrenia (SD) | p |
|---|---|---|---|---|---|---|
| Total grey Matter | 4.169 (0.010) | 4.204 (0.015) | 0.031* | 4.676 (0.015) | 4.738 (0.011) | 0.001# |
| Frontal lobe | 4.093 (0.029) | 4.140 (0.043) | 0.290 | 4.623 (0.050) | 4.682 (0.034) | 0.024* |
| Temporal lobe | 4.230 (0.041) | 4.225 (0.061) | 0.940 | 4.807 (0.047) | 4.693 (0.033) | 0.256 |

*Table 11. [$^{11}$C]PBR28 Distribution volume ratios (DVR)*

Microglial activity, as measured by PBR28 distribution volume ratio with a 2TCM analysis, is elevated in subjects at ultra high risk of psychosis (df=21 $p$=0.031) and patients with schizophrenia (df=21 $p$=0.001). The mean regional distribution volume ratios are shown for each group together with those for matched controls. The results of the ANCOVA covarying for age and translocator-protein genotype are shown for each case-matched control comparison (*p<0.05; #p<0.01).

| Regional VT of [11C]PBR28 (2TCM) | Control (SD) | UHR (SD) | P | Control (SD) | Schizophrenia (SD) | p |
|---|---|---|---|---|---|---|
| Total grey Matter | 4.444 (0.245) | 3.929 (0.357) | 0.162 | 4.925 (0.348) | 4.488 (0.502) | 0.393 |
| Frontal lobe | 4.362 (0.242) | 3.870 (0.352) | 0.175 | 4.867 (0.342) | 4.437 (0.494) | 0.762 |
| Temporal lobe | 4.493 (0.238) | 3.962 (0.346) | 0.138 | 5.055 (0.404) | 4.445 (0.501) | 0.691 |
| Regional VT of [$^{11}$C]PBR28 (2TCM-1K) | | | | | | |
| Total grey Matter | 2.145 (0.157) | 1.975 (0.228) | 0.461 | 2.740 (0.210) | 2.361 (0.306) | 0.228 |
| Frontal lobe | 2.113 (0.158) | 1.974 (0.230) | 0.551 | 2.764 (0.212) | 2.406 (0.310) | 0.260 |
| Temporal lobe | 2.019 (0.148) | 1.896 (0.215) | 0.569 | 2.543 (0.207) | 2.322 (0.302) | 0.471 |

*Table 12. [$^{11}$C]PBR28 Distribution volumes ($V_T$)*

Microglial activity, here measured by PBR28 $V_T$ with a 2TCM and 2TCM-1K analysis, did not differ between groups (UHR df=21 $p$>0.05; Schizophrenia df=21 $p$>0.05). The mean regional VTs are shown for each group together with those for matched controls. The results of the ANCOVA covarying for age and translocator-protein genotype are shown for each case-matched control comparison.

## Antipsychotic medication

Two subjects in the ultra high risk group had taken citalopram in the past. However only one was using the medication at the time of scan, and no other UHR subjects had taken psychotropic drugs. Re-analysis excluding the two subjects who had taken citalopram did not alter the significant elevation in [$^{11}$C]PBR28 DVR in the high risk group in the total ($F=6.601$, $p=0.018$) and frontal lobe ($F=5.392$, $p=0.030$) grey matter but the finding in the temporal cortex was no longer significant ($p=0.149$). All but one Patient with schizophrenia were taking medication at the time of scan.

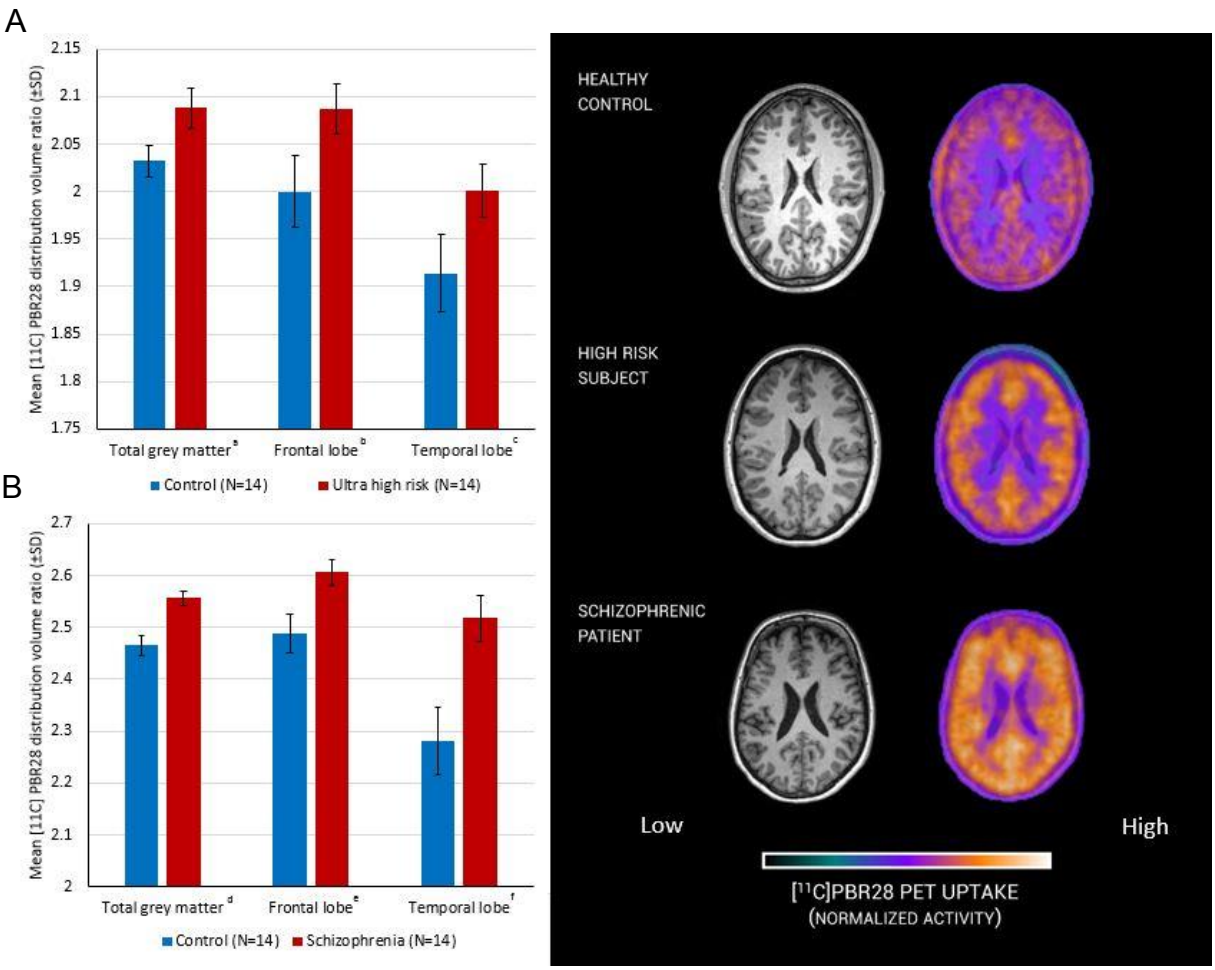


*Figure 13. Microglial activity measured with PET*

Data and representative scans from ultra high risk subjects, patients with schizophrenia and matched controls Significant difference between experimental (red) and control (blue) groups, ANCOVA (covarying for age and genotype). A, a (df=21 p=0.004). b (df=21 p=0.030). c (df=21 p=0.047). B, d (df=21 p<0.001). e (df=21 p=0.005). f (df=21 p=0.001). C, representative [$^{11}$C]PBR28 PET images from subject groups.

## Relationship between [$^{11}$C]PBR28 distribution and symptom severity

In ultra high risk subjects, there was a positive correlation between the total CAARMS symptom severity score and [$^{11}$C]PBR28 DVR in total grey matter ($r = 0.730$, $p = 0.011$, Figure 14). No correlation was observed between [$^{11}$C]PBR28 DVR in total grey matter and duration of ultra high risk symptoms ($r= -0.086$, $p= 0.802$). In patients with schizophrenia, there was no significant correlation between total grey matter DVR and total PANSS score (Figure 15). There was no relationship between depressive symptom severity (Beck Depression Inventory score) and total grey matter DVR in either patients with schizophrenia ($r= 0.478$ $p= 0.162$) or ultra high risk subjects ($r=-0.339$ $p= 0.506$).

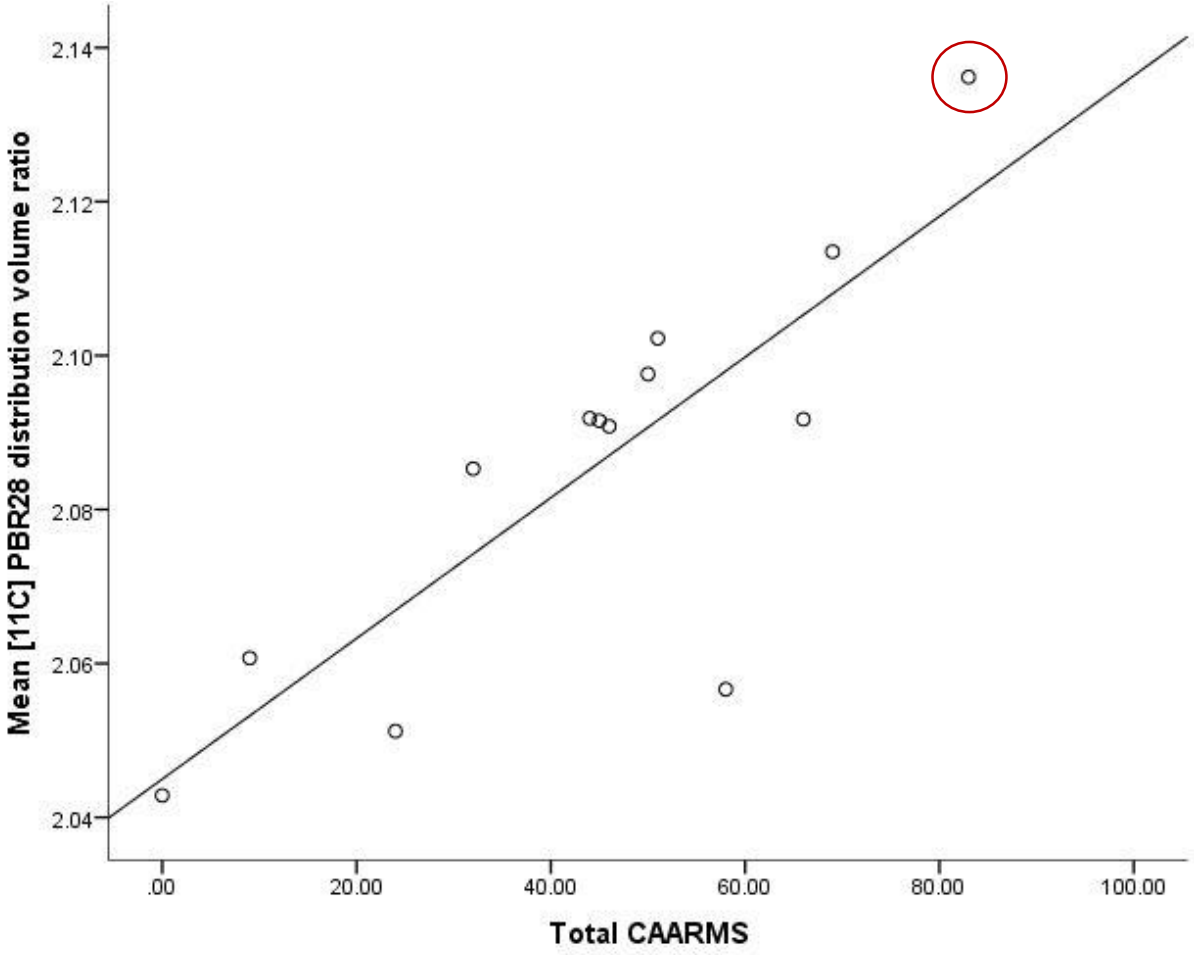


*Figure 14. Microglial activity and symptoms in UHR subjects*

Significant correlation between measures. Partial correlation including age and genotype as covariates (N=13, data were missing for 1 subject r= 0.730, *p*= 0.011). Highlighted subject, transition case.

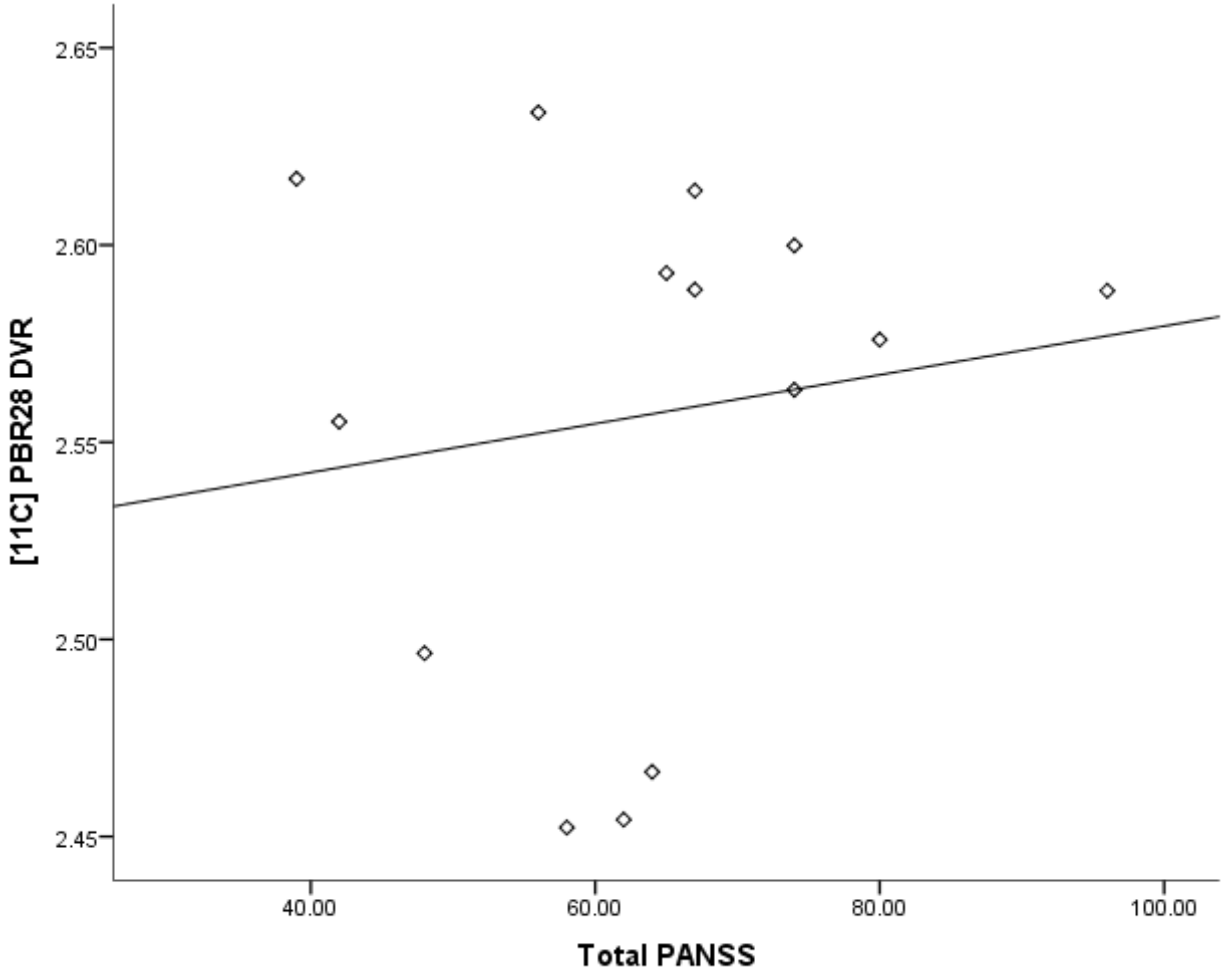


*Figure 15. Microglial activity and symptoms in schizophrenia*

Total grey matter [11C]PBR28 distribution volume ratios were not significantly correlated with symptoms in patients with schizophrenia (r= 0.538, p= 0.071), measured on the positive and negative syndrome scale (PANSS).

## Exploratory analysis of DVR normalization

To evaluate whether our findings were influenced by the signal used for normalization, we conducted exploratory analyses using the cerebellum and white matter as alternative normalization regions. Cerebellar normalization did not alter the major regional findings (frontal lobe $p$=0.001; temporal lobe $p$=0.006). White matter normalization performed similarly to the cerebellum (Table 13).

| Region of interest | Normalization region | Control (SD) | Schizophrenia (SD) | p |
|---|---|---|---|---|
| Frontal lobe- grey matter | | | | |
| | Cerebellum | 2.345 (0.100) | 2.710 (0.070) | 0.001# |
| | White matter | 2.400 (0.111) | 2.695 (0.074) | 0.014* |
| Temporal lobe- grey matter | | | | |
| | Cerebellum | 2.232 (0.120) | 2.599 (0.084) | 0.006# |
| | White matter | 2.208 (0.145) | 2.592 (0.096) | 0.015* |

*Table 13. Exploratory analysis of the region used for normalization*

[$^{11}$C]PBR28 DVR in frontal and temporal grey matter regions for varying normalisation regions. The results of the ANCOVA covarying for age and translocator-protein genotype are shown for each case-control comparison (*p<0.05; #p<0.01). Significant regional elevations of microglial activity, as measured by PBR28 distribution volume ratio, are seen in patients with schizophrenia when using cerebellar and white matter normalization approaches, consistent with the findings with the whole brain normalization.

## *Discussion*

Our main finding is that [$^{11}$C]PBR28 binding ratio, a marker of microglial activity, is elevated in people at ultra high risk of psychosis, with a large effect size (Cohen's *d* >1.2). Furthermore [$^{11}$C]PBR28 binding ratio was associated with the severity of symptoms in ultra high risk subjects, linking elevated microglial activity to the expression of sub-clinical psychotic symptoms. Importantly we found no relationship with depressive symptoms, suggesting elevated microglial activity is specific to the development of psychotic-like symptoms, rather than psychiatric symptoms in general. It would be valuable to examine change in [$^{11}$C]PBR28 signal during the course of the prodromal period to determine if there is a change during the prodromal phase. As the ultra high risk subjects, who had recently presented to psychiatric services, were medication naïve and had no history of psychotic disorder, these findings cannot be attributed to effects of previous illness or its treatment. Interestingly, at the time of writing, one ultra high risk subject has transitioned to first episode psychosis. This subject had the highest total grey matter [$^{11}$C]PBR28 signal in the cohort (DVR=2.14). Follow up of the remaining subjects is required to determine the role of elevated TSPO availability in the onset of psychosis.

The present findings are consistent with recent evidence of elevated peripheral inflammatory markers in people at high risk of psychosis (Cannon et al., 2014; Perkins et al., 2014), and suggest that elevated microglial activity predates the onset of frank psychosis. We also found evidence of elevated microglia activity in people with schizophrenia relative to controls with a large effect size (Cohen's *d* >1.7). This

extends previous PET studies which have not controlled for TSPO genotype (Takano et al., 2010), a potential confound as genotype influences binding, by showing that TSPO binding is elevated after controlling for TSPO genotype. Our findings are also consistent with the findings of a post-mortem study in schizophrenia, which also used PBR28. However, because it was *in vitro*, was able to use a two-point assay to quantify specific PBR28 binding to show elevated PBR28 binding in schizophrenia (Kreisl et al., 2013). We did not find the same symptom correlation in schizophrenia as we did in ultra high risk subjects. This may be due to the fact that these patients were not acutely unwell.

## Limitations

Antipsychotic treatment is a potential confound in the schizophrenia group but not the ultra high risk group. There is growing evidence to suggest an influence of antipsychotic medication on microglial cell dynamics, including evidence that antipsychotics may reduce microglial activity (Kato et al., 2007; Seki et al., 2013; Zhu et al., 2014). Hence in future studies it would be preferable to investigate patients with schizophrenia who were medication naïve.

In this investigation, we have used an approach to analysis (accounting for endothelial and vascular binding), which has been shown to be more reliable than alternative approaches (Rizzo et al., 2014). This was applied in a standardized automated manner across groups, and also applied to control regions (brain stem and cerebellum) to examine the specificity for our findings. A limitation of all current approaches to imaging microglia, including with [$^{11}$C]PBR28, is that the outcome measure is Vt. Thus the elevation in grey matter could reflect increased non-specific

tracer binding as well as biological signal. However, blocking studies have shown that a substantial proportion of Vt for [$^{11}$C]PBR28 is specific binding to the TSPO (Owen et al., 2014), although the proportion in schizophrenia remains to be determined. We used the distribution volume ratio (DVR), in this case with whole brain signal as our normalization region, as our outcome measure. We also showed that the main findings remained significant when other regions were used, suggesting that the findings are robust to the method of normalization. The use of DVR analysis is a standard approach in PET imaging that has recently been applied to second generation TSPO tracers (Coughlin et al., 2014; Dimber et al., 2014), including using whole brain normalization (Loggia et al., 2015), as well as to the first generation TSPO tracer PK11195 (Arias, 2014; Rissanen et al., 2014). Preclinical studies have demonstrated that the DVR approach is able to detect microglial changes due to inflammatory stimuli and confirmed that elevated DVR signal corresponds to elevated levels of TSPO and other markers of microglia measured *ex vivo* using immunohistochemistry and/or autoradiography (Converse et al., 2011; Imaizumi et al., 2007; Maeda et al., 2011; Martín et al., 2010). These preclinical studies thus indicate the functional significance of elevated [$^{11}$C]PBR28 DVR and support further *in vivo* investigation in patients.

Large regions of analysis were used as the primary outcome measure in this chapter. The choice of whole brain grey matter was based on the changes reported in the literature with the first generation ligand PK11195. Further to this we selected the frontal and temporal lobes for analysis as these are regions which demonstrate the greatest volume changes through the course of the disease. At the time if writing, analysis methods, including voxelwise analysis of PBR28 are still in development.

Hence while sub regions were calculated in analysis, large regions were chosen for this thesis, where signal could be more reliably quantified, over smaller voxels which are more susceptible to noise and artefacts.

Interpretation of the DVR using the whole brain signal for normalization is complicated as it includes grey matter signal as well. The exploratory analysis using white matter signal for normalization showed an elevation in total grey matter signal, which was greater in absolute terms than that seen when whole brain signal was used for normalization. This suggests that there may be a relative reduction in white matter TSPO signal in schizophrenia. Taken with our regionally specific elevations in frontal and temporal cortices, these findings are consistent with a re-distribution of microglia from white matter and other brain regions to grey matter in frontal and temporal cortices, in line with findings after cortical injury (Lloyd-Burton et al., 2013). However, a longitudinal study is required to determine whether this interpretation is correct.

The normalization approach would likely account for global group differences in non-specific binding but we cannot exclude a grey matter selective increase in non-specific binding contributing to the elevations seen. Whilst the signal-to-noise ratio of [$^{11}$C]PBR28 PET imaging is better relative to first generation tracers, it remains relatively low. However this noise would obscure a difference between groups, so is unlikely to account for our findings. In this study we did not correct for possible partial volume effects. Given that brain volume is generally reduced in schizophrenia, these would tend to underestimate the elevations observed here and not account for our group differences. There is a relatively higher binding in control subjects matched to patients with schizophrenia over those matched to the ultra

high risk group. This can be explained in part by age associated increases in TSPO but also by an increased number of MABs in the ultra high risk matched controls. Finally, it is important to note that not all the ultra high risk subjects will go on to develop a psychotic disorder and we will conduct clinical follow-up to determine whether the elevated microglial activity is specific to the development of the disorder or risk factors for psychosis.

## Implications

Whilst TSPO may be expressed on astrocytes (Martin et al., 2009) and some neuronal sub-types (Varga et al., 2009), it is predominantly expressed on microglia (Taylor and Sansing, 2013). The direct biological relationship between microglia and TSPO binding *in vivo* is not fully understood. However, in non-human primates inflammation induced increases in microglial activity cause marked increases in [$^{11}$C]PBR28 signal, confirmed post mortem to be largely due to microglial binding (Hannestad et al., 2012). Microglia perform immune surveillance roles, mount inflammatory response to injury (Kettenmann et al., 2011) and are involved in synaptic modulation in experience dependent plasticity (Tremblay et al., 2010). Interpretation of elevated activity is therefore complex and not defined by 'activated' or 'resting'. The elevations presented here might reflect a protective response triggered by associated pathology, such as glutamatergic excitotoxicity (Howes et al., 2015) or indicate a primary neuroinflammatory process linked to risk factors for psychosis and the development of sub-clinical symptoms. When biological data (e.g. PET) and symptoms (e.g. CAARMS or PANSS) are being assessed, longitudinal investigation is particularly useful for interpreting the relationship of the measures.

If the two demonstrate corresponding fluctuations over time it provides further evidence for inter-related processes. TSPO PET has been demonstrated to vary quite considerably in healthy volunteers, with PBR28 test retest variation being between 13-26% with a 2-5 day interval (Collste et al., 2015). Similarly, psychotic symptoms change over time with transition rates being the highest in the first 2 years from presentation to psychiatric services, with symptoms reaching threshold for psychosis in 25% of individuals at 1 year and 35% at the 2 year time point (Cannon et al., 2008). To date there has not been a comprehensive investigation of symptom variability during this prodromal stage.

When our findings are interpreted with evidence that anti-inflammatory drugs are effective in schizophrenia (Müller, 2002), particularly in addressing early negative symptoms (Chaudhry et al., 2012), they suggest a neuroinflammatory process is involved in the development of psychotic disorders. Whilst this indicates that anti-inflammatory treatment may be effective in preventing the onset of the disorder, further studies are required to determine the clinical significance of elevated microglial activity.

## *Conclusions*

Here we provide, to our knowledge, the first evidence of elevated brain microglial activity in people at ultra high risk of psychosis, and show that greater microglial activity is associated with greater symptom severity. We also demonstrate the first *in vivo* elevations of TSPO binding in schizophrenia with a second generation tracer after adjusting for TSPO genotyping. These findings are consistent with increasing

evidence that that there is a neuroinflammatory component in the development of psychotic disorders, raising the possibility that it plays a role in its pathogenesis.

# *Chapter 4 – TSPO, cytokines and MRI*

## *Abstract*

Patients with schizophrenia and subjects at ultra-high risk for psychosis (UHR) have reduced cortical grey matter volumes, UHR subjects who transition to psychosis also have a more rapid rate of grey matter volume reduction. Patients and UHR subjects also demonstrate higher concentrations of pro-inflammatory cytokines in peripheral blood. In the previous chapter we have seen how patients and UHR subjects have elevated levels of microglial activity. It is unclear how peripheral cytokine levels, volumetric brain changes and microglial activity relate, if at all. In this study we investigate patients, UHR subjects and matched controls to determine whether cytokine levels, cortical volumes and cortical microglial activity are associated.

Subjects received an [$^{11}$C]PBR28 PET scan and a structural MRI scan. Peripheral blood, from the time of the PET scan, was analysed for levels of pro-inflammatory cytokines. Correlation analysis was performed to determine whether relationships between measures were apparent.

Patients and UHR subjects consistently exhibited higher levels of inflammatory cytokines, however these levels only reached significance with TNF--α ($p$= 0.018 and $p$= 0.013 for UHR and schizophrenia respectively). Patients with schizophrenia had a reduced cortical volume compared to both control and UHR subjects ($p$= 0.004 & $p$= 0.025, respectively). Peripheral levels of TNF--α, IL-6, IL-1β, IL-10 and IFNɣ did not correlate with cortical volumes or [$^{11}$C]PBR28 signal in matched regions of interest. Cortical volumes were not correlated with [$^{11}$C]PBR28 binding in UHR, schizophrenia or control groups.

## *Introduction*

Cortical grey matter loss is associated with a conversion from high clinical risk to first episode psychosis (Pantelis et al., 2003b; Wood et al., 2008). Progressive grey matter detriments are also seen following the first episode of psychosis (Bose et al., 2009; McGlashan and Hoffman, 2000; Ortiz-Gil et al., 2011; Sandu et al., 2008). In schizophrenia, a reduction in grey matter volume is associated with antipsychotic administration (Fusar-Poli et al., 2013c; Radua et al., 2012), which is also seen in animals treated with antipsychotics ((Dorph-Petersen et al., 2005; Vernon et al., 2011) See chapter 6). The exact cause of this reduction is unclear.

Peripheral inflammatory cytokine levels (including IFNɣ, TNF--α, IL-1β, IL-2, IL-6 and IL-10) are also associated with the progressive loss of grey matter in UHR subjects and the onset of first episode psychosis, where higher levels of pro-inflammatory cytokines relate to a higher probability of transition (Cannon et al., 2014; Perkins et al., 2014). Patients with schizophrenia have elevated levels of peripheral cytokines, independent of medication status (Miller et al., 2011). In particular, peripheral levels of the inflammatory cytokine interleukin 6 (IL-6) were found to be elevated in patients with schizophrenia when compared to control subjects (Nunes et al., 2006). Recent investigations of inflammatory markers IL-6 and c-reactive protein have revealed an association between childhood serum levels and the incidence of depression and psychosis in young adult life (Khandaker et al., 2014). Pro-inflammatory cytokines are released by microglial cells in states of inflammatory stress and in response to tissue damage (Kettenmann et al., 2011). A severe state of systemic inflammation in animals produces reactive microglia centrally, alongside elevated levels of peripheral cytokines (Cunningham, 2013).

Microglia are also known to be responsive to signalling proteins when involved in plasticity events involving synaptic reorganisation (Parkhurst et al., 2013; Tremblay et al., 2010).

Schizophrenia is associated with greater binding of TSPO radiotracers, thought to reflect elevated levels of microglial activity (Doorduin et al., 2009; van Berckel et al., 2008). In the previous chapter, we have seen how this is evident with the novel PET tracer [$^{11}$C]PBR28 in patients with schizophrenia, as well as UHR subjects compared to matched controls.

It is currently unclear whether cortical volume changes, peripheral cytokine levels and cortical microglial activity are associated in patients with schizophrenia or UHR subjects. In the previous chapter we have seen how symptoms associate with [$^{11}$C]PBR28 binding in UHR, here we analyse peripheral cytokine levels as well as cortical grey matter volumes alongside TSPO PET signal ([$^{11}$C]PBR28) to determine whether these peripheral and cortical parameters are related to psychosis.

## *Methods*

The study was approved by the local research ethics committee and was conducted in accordance with the Declaration of Helsinki. After complete description of the study to the subjects, written informed consent was obtained.

## Participants

A total of 35 subjects were recruited and completed this multimodal imaging study; 13 subjects meeting UHR criteria, as assessed on the comprehensive assessment of the at risk mental state (CAARMS) (Yung et al., 2005), were recruited from OASIS (Outreach and Support in South London) (Fusar-Poli et al., 2013b) (Mean age ± SD: 24.38 ± 5.61; (M:F=6:7)). 11 subjects with schizophrenia (Mean age ± SD: 43.64 ± 10.8; (M:F=9:2)) were recruited from London mental health centres (South London and Maudsley NHS Foundation Trust). 8 healthy control subjects were recruited for comparison (Table 14).

| | Control | Ultra high risk | Schizophrenia | *p* |
|---|---|---|---|---|
| N= | 8 | 13 | 11 | |
| Age (mean(±sd)) | 27.00 (7.73) | 24.38 (5.61) | 43.64 (10.82) | <0.001 |
| Genotype (MAB:HAB) | 2:6 | 7:6 | 2:9 | 0.279 |
| Sex (M:F) | 4:4 | 6:7 | 2:9 | 0.162 |
| Total symptoms (mean (±sd)) | - | 46.18 (20.02) | 64.36 (15.46) | - |

*Table 14. Demographic characteristics of subjects*

Patients with schizophrenia were significantly older than both control subjects and UHR subjects (Symptom measures for UHR and schizophrenia are measured on the CAARMS and PANSS respectively).

## Correlations between total grey matter volume & TSPO signal

Brain volumes, [$^{11}$C]PBR28 signal and peripheral inflammatory measures were analysed for correlation. Regions of interest were defined by the results from chapter 3, where whole brain grey matter, frontal and temporal lobe regions were found to be elevated in case groups. Respective MRI volumes were extracted as structural data for correlative analysis.

## MRI and PET registration

Each subject underwent a T1 weighted MRI brain scan. MRI images were used for grey/white matter segmentation and region of interest (ROI) definition. A neuroanatomical atlas (Tziortzi et al., 2011) was co-registered on each subject's MRI scan and PET image using a combination of Statistical Parametric Mapping 8 (http://www.fil.ion.ucl.ac.uk/spm) and FSL (http://www.fsl.fmrib.ox.ac.uk/fsl) functions, implemented in MIAKAT$^{TM}$ (http://www.imanova.co.uk). The primary region of interest was whole brain grey matter. Secondary regions of interest were temporal and frontal lobe grey matter (Radewicz, 2000).

## MRI analysis methods

MRI volumes were analysed using the "FreeSurfer image analysis suite", which is an open source analysis suite available for download online (http://surfer.nmr.mgh.harvard.edu/). The methods of analysis are previously published and have been used extensively (Reuter et al. 2012). Images were processed in the FreeSurfer longitudinal stream to produce volume estimates (Reuter et al., 2012). Skull stripping, Talairach transformations, atlas registration as

well as spherical surface maps and parcellations are applied after a within-subject template.

## PET acquisition and analysis

PET acquisition and analysis was performed as outlined in chapters 2 & 3 of this thesis.

## Cytokine analysis

Cytokine analysis was performed using a multiplex system (Mesoscale Discovery, USA), as described in the general methods in chapter 2.

## Statistical analysis

DVRs were created using the methods described in chapters 2 & 3, where whole brain PET signal was used to provide a normalization for regional signal. Group differences were assessed using an ANOVA with a Tukey's post hoc comparison. Spearman's rho correlation (two-way) was implemented for correlation of PET, MRI and blood data. We used Spearman's over Pearson's here as it is less influenced by outliers (Kornbrot, 2005), which may present an issue with the smaller cohort sizes in this chapter. Data were analysed using SPSS 21 (IBM, USA).

## *Results*

### Demographic variations

There is an age difference between the three groups ($p< 0.001$), where the patients with schizophrenia are significantly older than both controls and UHR subjects. Unfortunately we were unable to obtain peripheral inflammatory measures and both scan types for all subjects, which prevented us from having two individually matched control cohorts as in chapter 3. Hence age was factored in as a covariate of analysis. The demographics of the groups are outlined in Table 14.

### Cortical volume analysis

Consistent with the literature, there were significant total grey matter volume reductions in patients with schizophrenia when compared to control subjects as well as UHR subjects ($p= 0.004$, $p= 0.025$ respectively, Figure 16). There was no difference between UHR and control subjects ($p> 0.05$). Temporal and frontal lobe volumes were not significantly different between groups.

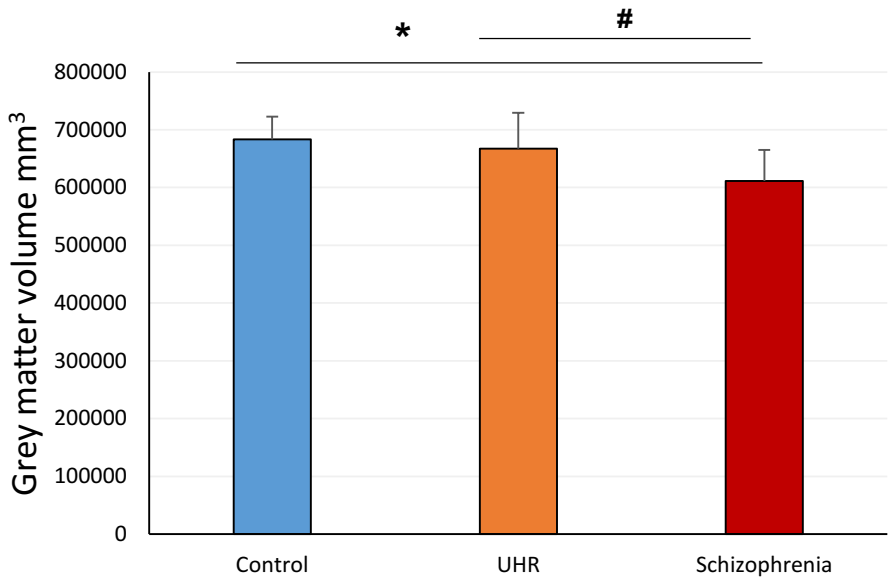


*Figure 16. Total grey matter volumes*

Total grey matter volume reductions were present in patients with schizophrenia when compared with both control and UHR subjects. Volumes did not differ between UHR and control subjects.

## Symptoms and Volume

There was no correlation between symptom score and cortical volumes in UHR or patients with schizophrenia (rho= 0.305 *p*= 0.310; rho= -0.142 *p*= 0.677, respectively). Total grey matter volume and symptom correlations are presented in Figure 17.

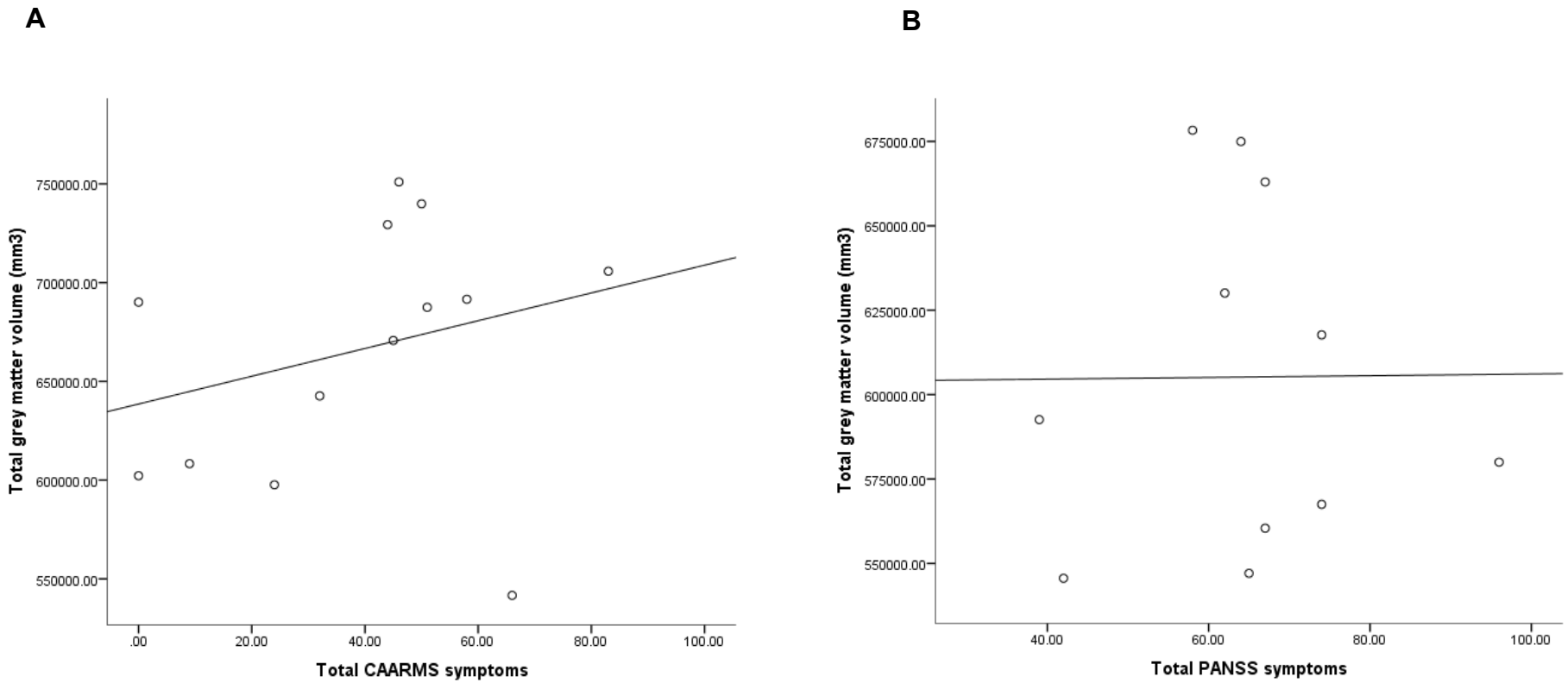


*Figure 17. Total grey matter volumes and symptom correlations*

There was no correlation between the volumes of total grey matter and symptom scores on the CAARMS or PANSS in UHR (A) and patients with schizophrenia (B) respectively.

## Medication and volume

The literature suggests medication impacts cortical volume. In patients with schizophrenia, we see a correlation between the chlorpromazine equivalent dose of medication and total grey matter volume (rho= -0.674 *p*= 0.023, Figure 18).

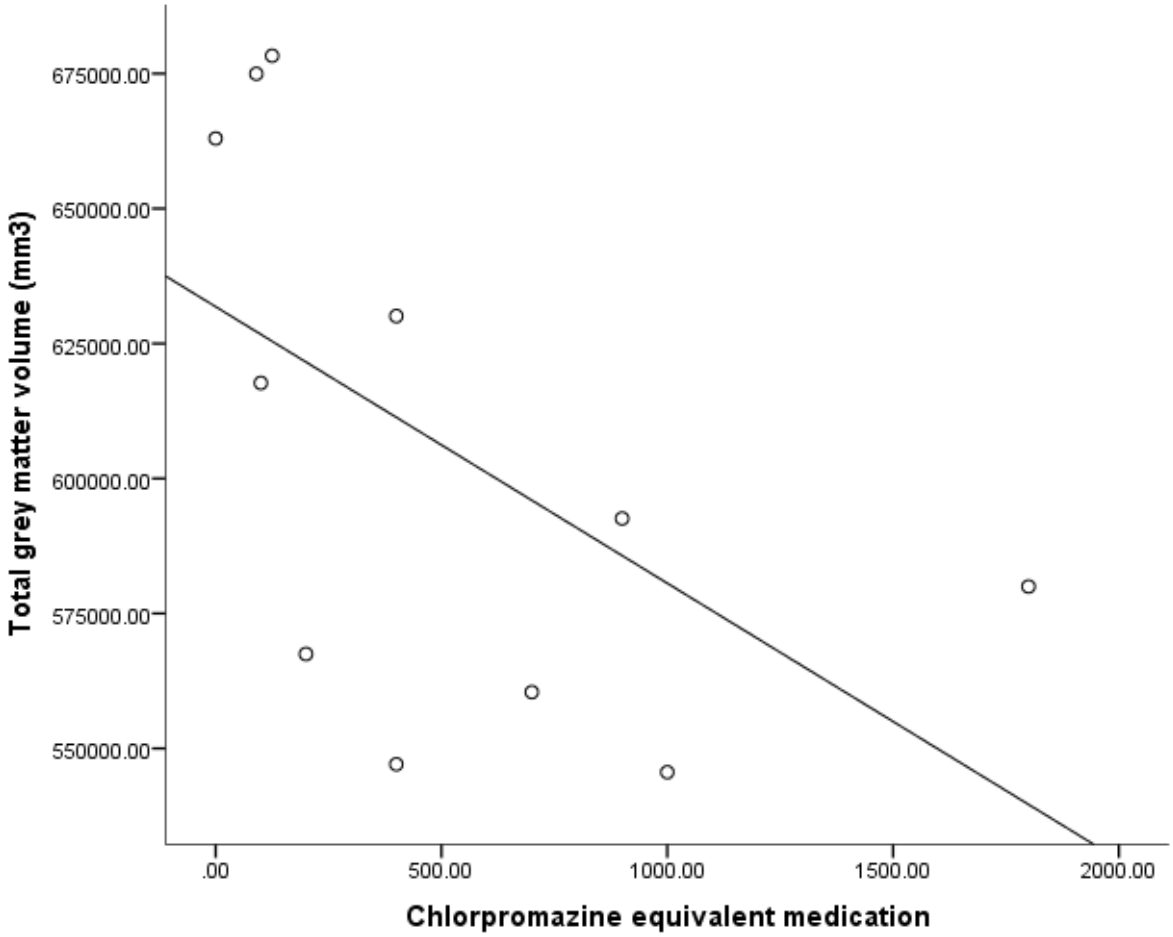


*Figure 18. Medication doses and volume correlation in schizophrenia*

The volume of total grey matter in the brains of patients with schizophrenia was negatively correlated with the level of chlorpromazine equivalent doses of medication.

## Correlations between total grey matter volume & TSPO signal

There was no correlation between the levels of [$^{11}$C]PBR28 binding in whole brain grey matter and the volume of total grey matter across any of the groups ($p$> 0.05, Figure 19). There was no correlation between temporal or frontal lobe [$^{11}$C]PBR28 binding and respective volumes in any of the participant groups (data not shown).

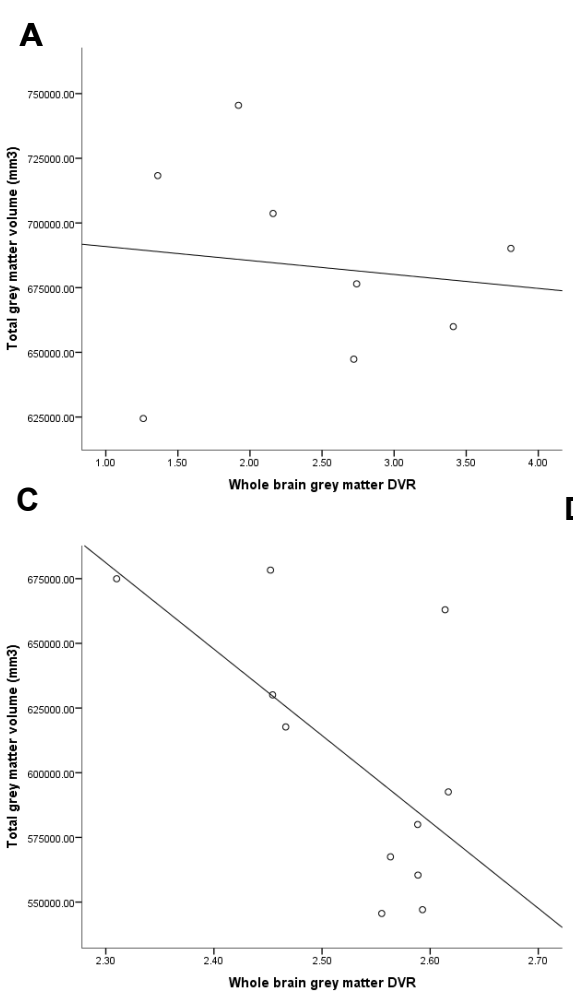


D

| Group | Total grey matter volume/Whole brain grey matter DVR correlation |
|---|---|
| Control | Rho=-0.095 p=0.823 |
| UHR | Rho=0.181 p=0.553 |
| Schizophrenia | Rho=-0.455 p=0.160 |

*Figure 19. Correlation plots for total grey volume and whole brain grey DVR*

Volumes and [$^{11}$C]PBR28 DVR were not correlated in control subjects (A), UHR subjects (B) or patients with schizophrenia (C). With statistical summary table (D).

## Cytokine analysis

Here we were not able to perform analysis of cytokines for all subjects that we had imaging data from (a number of subjects did not produce adequate amounts of blood for analysis). When the full cohort of subjects with blood data were included, 11 control, 11 UHR and 13 patients with schizophrenia could be analysed for peripheral blood markers. In this instance, both the UHR and schizophrenia groups demonstrated elevated levels of TNF--α when compared to control ($p$= 0.018 and $p$= 0.013 respectively, Figure 20). All other cytokines were numerically elevated in experimental groups, however TNF--α was the only statistically significant elevation. Of the peripheral cytokines only IL-10 correlated with the level of cortical inflammation using a DVR but not $V_T$ approach (Table 15). Cytokines did not correlate with total grey matter volumes.

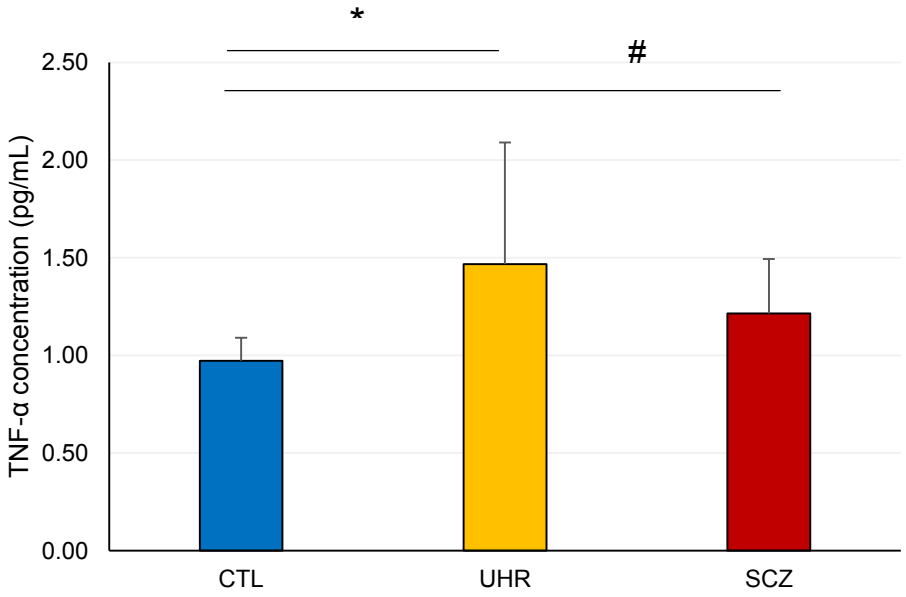


*Figure 20. Whole blood TNF-α levels in patients and controls*

Peripheral levels of TNF-α were elevated in both UHR subjects and patients with schizophrenia when compared to healthy control subjects.

| Cytokine | Grey matter DVR | Grey matter $V_T$ | Total grey matter volume |
|---|---|---|---|
| TNF--α | Rho=-0.277 p=0.191 | Rho= -0.364 p=0.081 | Rho=-0.292 p=0.166 |
| IL-6 | Rho=-0.067 p=0.749 | Rho=0.136 p=0.518 | Rho=0.000 p=0.998 |
| IL-1β | Rho=-0.104 p=0.621 | Rho=0.020 p=0.926 | Rho=0.128 p=0.543 |
| IL-10 | Rho=0.396 p=0.05 | Rho=0.345 p=0.091 | Rho=-0.276 p=0.197 |
| IFNɣ | Rho=-0.114 p=0.588 | Rho=-0.012 p=0.953 | Rho=0.048 p=0.819 |

*Table 15. Microglial and inflammatory marker correlation analysis*

Correlation statistic and *p* values for all subject analysis of [$^{11}$C]PBR28 signal (DVR, $V_T$ & MRI volume) and peripheral blood cytokine concentration. Of the cytokines tested only IL-10 was associated with central measures of inflammation.

## *Discussion*

In this study, we have demonstrated a reduction in total grey matter volume in patients with schizophrenia compared to control and UHR subjects. Interestingly, while numerically lower, the total grey matter volumes of UHR subjects was not significantly lower than control subjects. Patients with schizophrenia exhibited a reduction in total grey matter volume when compared to control and UHR, however no correlation between volume and [$^{11}$C]PBR28 binding was present. Average levels of peripheral cytokines were higher in UHR subjects and patients with schizophrenia, however only TNF--α reached statistical significance. The anti-inflammatory cytokine IL-10 was negatively correlated with the level of whole brain grey matter [$^{11}$C]PBR28 binding, however it is unclear how this relates as it is an association present when all subjects are combined.

As discussed in the previous chapter, partial volume correction should be implemented for accuracy in PET data. However, in this instance partial volume correction has not yet been applied to [$^{11}$C]PBR28 data, due to the methodological complexities with this novel tracer.

There is a significant reduction in total grey matter volume in patients with schizophrenia compared to control and UHR subjects. While age is a confound in this context, the patients in this investigation were also taking antipsychotic medication. When we compared equivalent medication dose with cortical volume, we saw a relationship in patients with schizophrenia. This correlation may be a consequence of disease duration and severity, as subjects at a later stage of disease exhibit greater reductions in volume (Fusar-Poli et al., 2013c; van Haren et al., 2008), however literature on this topic suggests medication alone produces

cortical volume reductions (Dorph-Petersen et al., 2005; Fusar-Poli et al., 2013c; Radua et al., 2012; Vernon et al., 2011). We included age as a covariate of analysis to help minimise the effect of age on brain volume. Chapter 6 will further address the implications of antipsychotic medication on brain volume, as well as the presence of microglia in the cortex.

## Implications

This investigation is, to our knowledge, the first dual cohort multi-modality study of cortical inflammation (TSPO), peripheral inflammation (cytokine levels) and cortical volume in schizophrenia and UHR subjects.

Follow up of UHR subjects will be useful to determine whether cortical changes progress as in patients with schizophrenia. The results in this section suggest medication is a greater influence than psychotic-like symptoms for cortical volume loss. The animal literature suggests volumetric loss is influenced strongly by medication (Dorph-Petersen et al., 2005; Vernon et al., 2014; Vernon et al., 2011), however longitudinal study shows withdrawal of medication allows recovery of volumetric deficits in animals (Vernon et al., 2011). It would be interesting to know whether antipsychotic withdrawal in patients would have a similar effect on brain volume recovery. It would also be interesting to determine whether subjects discharged from psychiatric services return to a control subject level of TNF--α in the blood stream.

While we have investigated volume and [$^{11}$C]PBR28 correlations it would also be useful to analyse cognitive function to see how activity of cortical microglia may

associate with cognition. This could be done using fMRI, with tasks relating to executive function or working memory.

## Limitations

This investigation is limited by the number of subjects we managed to obtain all measures for, subsequently the statistical power for analysis is low and does not provide a comprehensive assessment of relationships between parameters. Where the number of subjects is low, as in this experiment, data analysis is affected greatly by Type I & II statistical errors, where falsely positive or negative results occur due to insufficient statistical power (Banerjee et al., 2009). These correlation analyses were exploratory in nature and will form the basis of future experiments on this topic. In the previous chapter, we discussed the influence of age on TSPO and [$^{11}$C]PBR28 binding. The literature suggests that age is associated with cortical volume reductions and ventricular enlargement (Ge et al., 2002). In our cohorts, the subjects with the lowest cortical volumes are the patients with schizophrenia. The patients are also older than the control and UHR populations. Unfortunately we were not able to analyse all the control subjects analysed in chapter 3 for brain volumes and cytokines to provide the same two evenly matched control groups as used for analysis in the previous chapter. In the future we will be able to assess the structural MRI from these participants for appropriately age matched cohorts.

## *Conclusion*

In this investigation we have determined that the cortical volume reduction seen in patients with schizophrenia is not correlated with levels of microglial activity. Further to this we see elevated levels of the peripheral inflammatory marker TNF--α, in both UHR subjects and patients with schizophrenia. Elevated TNF-α levels are not associated with elevated TSPO tracer binding or cortical volume alteration.

# *Chapter 5 – Haloperidol LPS microglia.*

## *Abstract*

Microglia are restricted to the central nervous system, they provide innate immunity and are also involved in synaptic turnover. In chapter 3 we have seen how microglial activity is elevated in association with the early stages of psychosis, as well as in patients with chronic schizophrenia receiving antipsychotic medication. In chapter 4 we have seen reductions in cortical volume in chronically medicated patients with schizophrenia. At present it is unclear how psychosis and antipsychotic medication interact in terms of microglia density or morphology and cortical volumes. Here we administer haloperidol, a first generation antipsychotic with a predominantly Dopamine receptor D2 (DRD2) occupancy, to naïve and lipopolysaccharide (LPS)/saline control treated groups of Sprague Dawley rats to test the effects on animals exposed to no stimulus and an inflammatory stimulus respectively. We aim to discover potential alterations in cortical volume and microglial cell density and morphology *in vivo*. We demonstrate that in naïve and LPS dosed animals microglial cell density and morphology is not altered by haloperidol administration. In naïve animals, haloperidol treatment resulted in a reduction in whole brain volume, which was absent in LPS/saline treated groups. These findings suggest haloperidol is not associated with microglial cell changes.

## *Introduction*

Clinical imaging modalities provide an insight to the ways in which neurochemistry is altered in patients, as demonstrated with positron emission tomography (PET). Cognitive changes in patients cohorts can be investigated using fMRI (functional Magnetic Resonance Imaging) and structural deficits can be revealed with MRI. Cortical structure and chemistry in patients can be investigated both with respect to healthy controls (cross sectional) and over time against a baseline scan (longitudinal). While the progression of disease symptoms can be followed over time, it is not possible to determine which changes in patients are medication related and which are purely a consequence of disease progression (Cannon et al., 2015; Dorph-Petersen et al., 2005; van Haren et al., 2008). In chapter 3 we saw how medicated patients with schizophrenia had an elevated level of microglial activity compared to matched healthy controls. We also saw elevated microglial activity in un-medicated subjects at ultra high-risk for psychosis (UHR). The level of microglial associated signal was relatively higher in medicated patients, but it is unclear how medication influences this. While progression of disease and age effects (Schuitemaker et al., 2012) may be the cause of this elevation, medication may serve to exacerbate or attenuate these levels.

Animal models of schizophrenia are commonly investigated experimentally (Jones et al., 2011; Juckel et al., 2011; Taylor, 2009) and the efficacies of antipsychotic drugs are assessed with behavioural (Zhu et al., 2014), electrophysiological (Kato et al., 2008) and histological techniques (Juckel et al., 2011). Reduction of disease model associated behavioural deficits are often the primary outcome measure. Until

relatively recently, drug effects had not been investigated *in vivo* without the influence a disease model.

A number of studies investigating the influence of antipsychotic medication on cortical volumes have demonstrated drug associated reductions in both whole brain and regional analysis (Dorph-Petersen et al., 2005; Vernon et al., 2014; Vernon et al., 2011). Similarly, investigation of antipsychotic effects using PET have been conducted to look at the effects of antipsychotic treatment on post-synaptic enzyme activity (Natesan et al., 2014). There is a growing body of literature investigating the effects of antipsychotic drugs on different brain cells, including microglia. A range of experiments have been conducted by the Kanba laboratory in Japan to investigate the effects of antipsychotic medication on microglial cells (Bian et al., 2008; Kato et al., 2008; Kato et al., 2007). We saw in chapter 1 that the findings of these experiments demonstrate decreases in inflammatory action of microglial cells in many contexts. A number of studies observed changes with second generation antipsychotics, but not first generation drugs. These results come from isolated microglial populations *in vitro* (see introductory chapter 1) and often use a high dose of antipsychotic drug, when compared to a clinical context. The doses of haloperidol in the literature can be over 2mg/kg, inducing catalepsy and leading to a receptor occupancy far higher than applicable to the clinic (Kapur et al., 2003). *In vivo* models of traumatic brain injury (TBI) and multiple sclerosis have investigated antipsychotic medication for the attenuation of functional impairment. Functional improvements and reduced numbers of CNS macrophages and microglia were observed with risperidone in a mouse model of MS (O'Sullivan et al., 2014). However in the TBI

study a functional deficit was exacerbated by the highest dose of haloperidol (0.3mg/kg), no immunohistochemistry was performed (Wilson, 2003).

A single investigation of risperidone in an inflammatory lesion model of schizophrenia has been conducted *in vivo*. The study demonstrated a reduction in the density of microglial cells, however quantification of cellular morphology (soma size, branch length, stain intensity) were not included (Zhu et al., 2014).

Microglial cell morphology and density can be diverse. The mechanisms and functions related to these cellular morphologies are largely uncharacterised. Changes in cell density are believed to occur through the proliferation or apoptosis of quiescent cells (Gómez-Nicola et al., 2013). The interruption of the cell cycle can inhibit proliferation and reduce production of proinflammatory cytokines (Koguchi et al., 2003; Zhang et al., 2009).

In this investigation we administered haloperidol continuously to naïve and systemically inflamed rats to address the following hypotheses, using the software cell profiler software (see appendix 1);

*Main hypothesis:*

Haloperidol reduces microglial density and morphological complexity.

*Secondary hypotheses:*

Reduction in cell numbers associated with haloperidol is due to increased amounts of microglial apoptosis.

## *Methods*

### Animals

Male Sprague Dawley (SD) rats were randomised into cages and acclimatised for 1 week prior to the start of drug dosing. Animals were housed in a 12h light/dark cycle at 21$^{o}$C, with food and water ad libitum and in accordance of the home office regulations outlined in the animals in scientific procedures act (A(SP)A, 1964). *Experiments were conducted by PSB, with blinding of drug administration conducted by Federico Grillo, Graham Little, Lucien West and Katerina Popadopoulou. After tissue processing and slide preparation, PSB was further blinded to slide number by the previous individuals.*

### *Drug dosing*

Haloperidol was administered using chronic slow release subcutaneous drug pellets (0.05 mg/kg for 2 weeks, Innovative Research of America, USA). Two experiments were conducted, in experiment 1 we sought to determine whether haloperidol treatment (n=11) had brain (volume mass or density) or microglial associated effects when compared to placebo controls (n=18).The dose of haloperidol was calculated to provide a ~40-50% receptor occupancy to make findings more applicable to a clinical context (Kapur et al., 2003). Continuous delivery is preferable to i.p. administration as it removes peak and trough doses, which are not comparable to the metabolic profile of patient medication (Bédard et al., 2011; Kapur et al., 2003). In experiment 2, LPS was administered i.p. over two weeks with four doses (1mg/kg n=13 LPS+placebo, n=7 LPS+haloperidol) LPS, sigma Aldrich, USA) this was to

provide a chronic state of systemic and cortical inflammation. Acute LPS produces a robust inflammatory response peaking between 8 and 24 hours (Buttini et al., 1996). However we were seeking a more chronic regime producing the hypertrophic chronically inflamed morphology seen in post-mortem schizophrenia (Bayer et al., 1999; Steiner et al., 2006). We selected the 4x doses at 1 mg/kg regime based on (Chen et al., 2012), producing a reactive morphology (Figure 21), over 2 weeks.

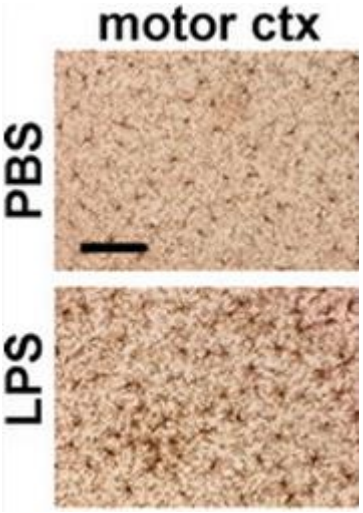


*Figure 21. Chronic LPS regimen cortical microglial morphology*
Adapted from (Chen et al., 2012), scale bar = 60 μm.

Control animals were dosed with saline (i.p. 4x over 2 weeks, Saline/placebo n=5, Saline/haloperidol n=4) and placebo pellets were inserted. Haloperidol was measured in the bloodstream of animals as outlined in the general methods (chapter 2).

## Cerebral morphology

Cerebral mass and volume were assessed using a top pan balance and fine graduated cylinder, where water displacement was used to determine cerebral volume (Dorph-Petersen et al., 2005). Density was calculated using the equation;

$$density = \frac{mass}{volume}$$

## Immunohistochemistry

Tissue was processed as described in the general methods for histological assessment.

## Confocal image acquisition

Images were acquired on a Leica SP5 confocal microscope as described in chapter 2.

## Generation of maximum projections

Maximum intensity projections (MIPs) were created from image stacks for automated analysis. These were processed using a batch script implemented in Fiji (Fiji Is Just ImageJ, NIH, USA) for each image set. Following generation of MIPs, image folders were imported to Cell Profiler for automated quantification.

## Confocal image acquisition

For acquisition see Appendix 1.

## Image analysis

Microglial cell analysis was conducted using the cell profiler and Fiji skeleton analysis (Morrison and Filosa, 2013) as outlined in Appendix 1, Figure 22 shows the acquisition and analysis as a schematic. For apoptosis analysis, DAPI nuclei were substituted with a caspase-3 channel.

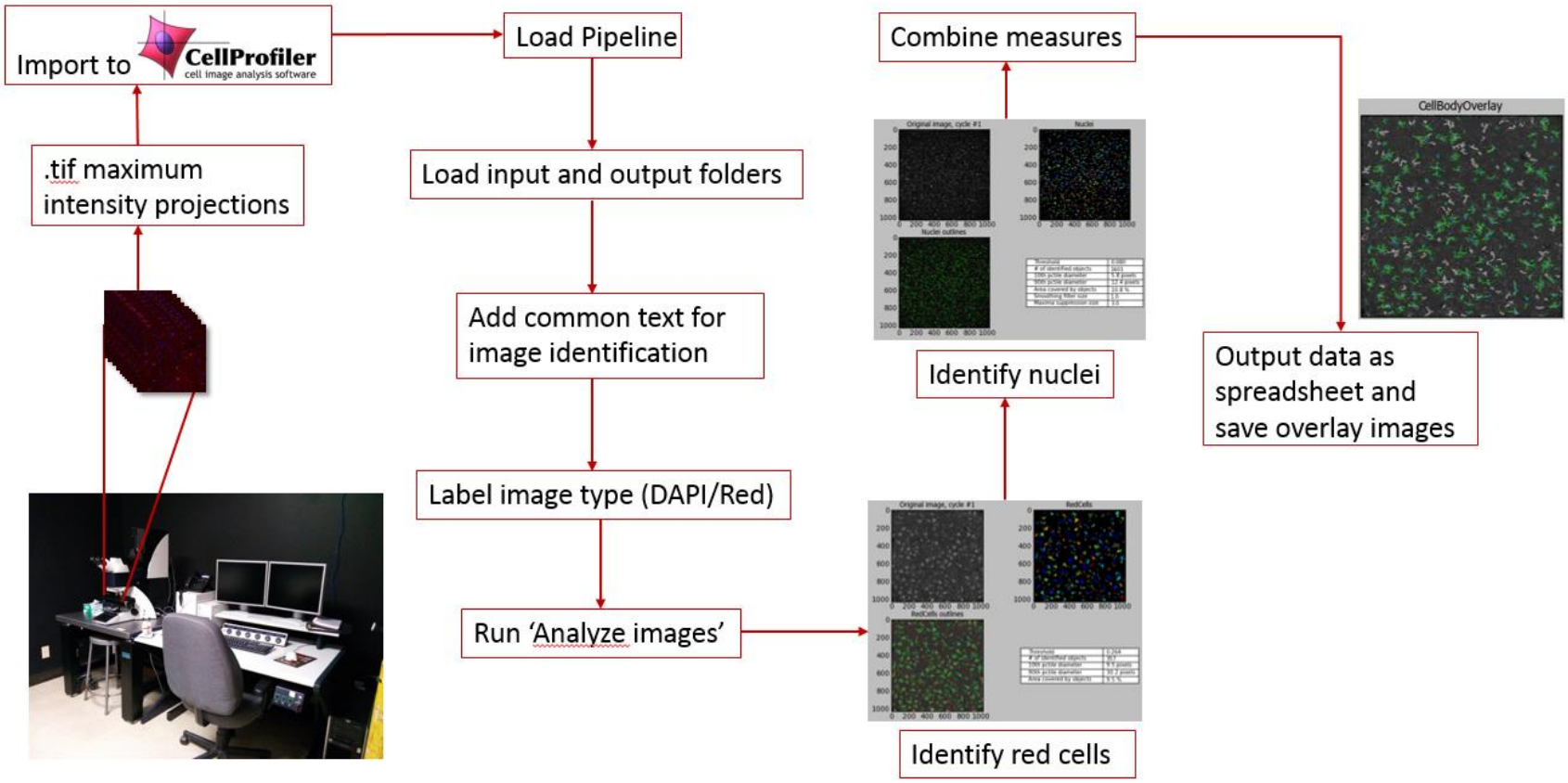


*Figure 22. Pipeline summary schematic*

Schematic flow diagram with a simplified sequence of analysis steps.

## Statistical analysis

Data were analysed in SPSS, for group statistics an ANOVA with a Tukey's posthoc test was performed. Alpha was set as a $p < 0.05$ threshold for significance.

## *Results*

Due to the two experimental contexts in this section, results figures with be presented as part A (placebo vs haloperidol pellets) and part B (saline/placebo vs LPS/placebo vs LPS/haloperidol, vs saline/haloperidol).

Administration of antipsychotic medication via subcutaneous drug pellets resulted in a low level of plasma haloperidol in pellet treated animals (mean ± SD 0.23 ng/mL ± 0.12). No haloperidol was detected in placebo pellet dosed animals. Body weight was not different across experimental conditions (see Table 16). LPS dosed animals exhibited piloerection and nasal/ocular discharge. No severe adverse side effects were observed in any groups.

| Group | Mean body weight | SD |
|---|---:|---:|
| Placebo | 379.61 | 24.85 |
| Haloperidol | 369.30 | 23.14 |
| Saline/placebo | 348.20 | 26.45 |
| LPS/placebo | 347.92 | 22.21 |
| LPS/haloperidol | 345.38 | 21.26 |
| Saline/haloperidol | 345.00 | 1.95 |

*Table 16. Animal body weight*

Endpoint body weights for experimentally dosed animals (mean ± SD), placebo n=18, haloperidol n= 11, saline/placebo n=5, LPS/placebo n=13, LPS/haloperidol, n=7, saline/haloperidol n=4. P>0.05 ANOVA).

The dose regime used was relatively low, hence was not expected to cause extrapyramidal side effects or catalepsy. For this reason, vacuous chewing movements were not assessed.

## Brain morphology

In animals treated with haloperidol there was a reduction in brain volume compared to placebo (placebo, mean ± SD 1.931 $cm^3$ ± *0.210;* haloperidol, 1.546$cm^3$ ± 0.292 **p* = 0.014, effect size= 0.226, -19.9%, 24A). In LPS, saline and haloperidol treatment groups there was no change in brain volume (p> 0.05 figure 24B). Total brain mass was not altered in any treatment conditions (*p*> 0.05). When mass and volume were combined to provide density, haloperidol treated animals exhibited a relative elevation in cerebral density compared to control (placebo compared to haloperidol p= 0.022).

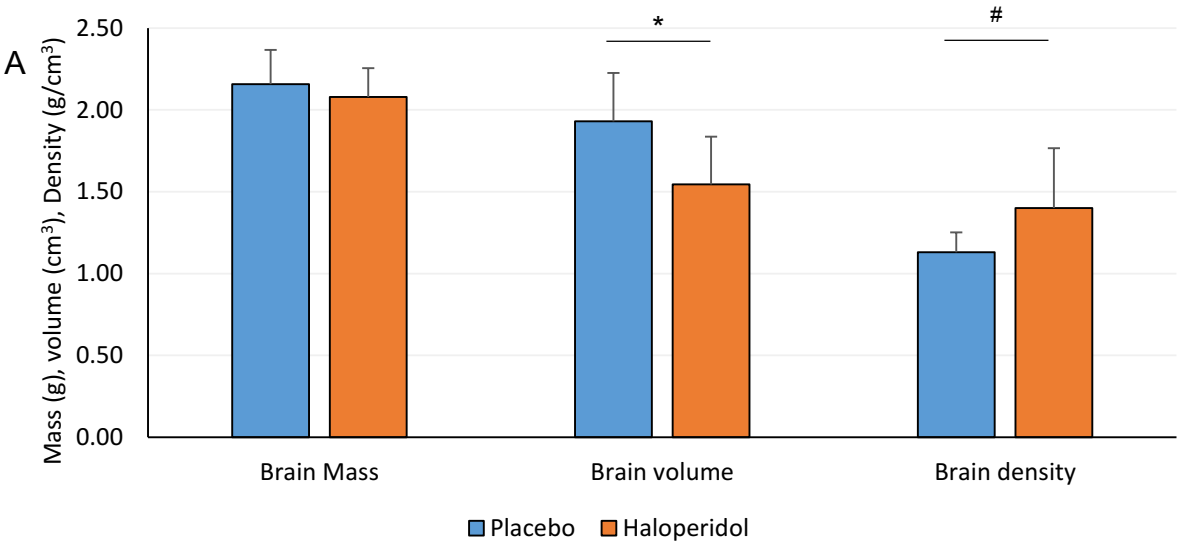

B

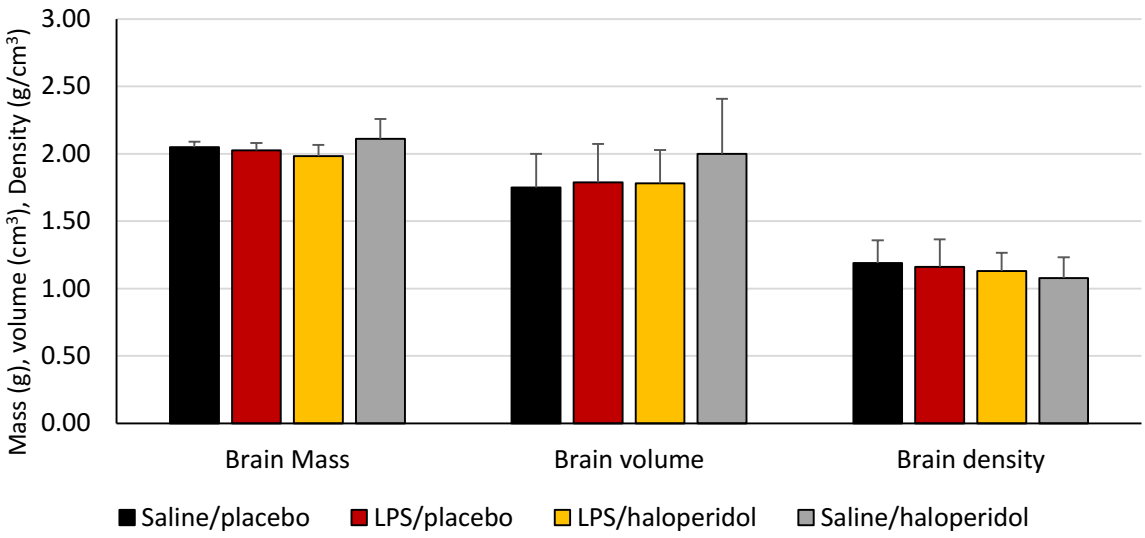


*Figure 23. Brain mass, volume and density*

(**A**) Brain mass was not altered with haloperidol treatment, brain volume was reduced (p= 0.014) and cerebral density was elevated (p= 0.022) in animals treated with haloperidol (n=11) when compared with placebo dosed counterparts (n=18) mean values ± SD. (**B**) In saline/placebo n=5, LPS/placebo n=13, LPS/haloperidol, n=7 and saline/haloperidol n=4 dosed animals, there were no differences in brain volume mass nor density (p> 0.05). Mean values ± SD.

## Microglial cell measures

The parameters of assessment developed in Appendix 1 were used for microscopy analysis in this chapter.

### Cell density

Haloperidol treatment did not alter microglial density when compared with placebo controls (mean ± SD; 106.57 ± 35.38, 107.56 ± 19.65; n= 11, 18 respectively, p> 0.05, Figure 25A). Administration of LPS did not result in an elevation of microglial cell density compared to saline controls (mean ± SD for saline/placebo = 90.53 ± 31.41, LPS = 98.96 ± 31.82 *p*> 0.05 figure 25B), haloperidol treatment did not alter the density of cells in any experimental condition (*p*> 0.05).

A

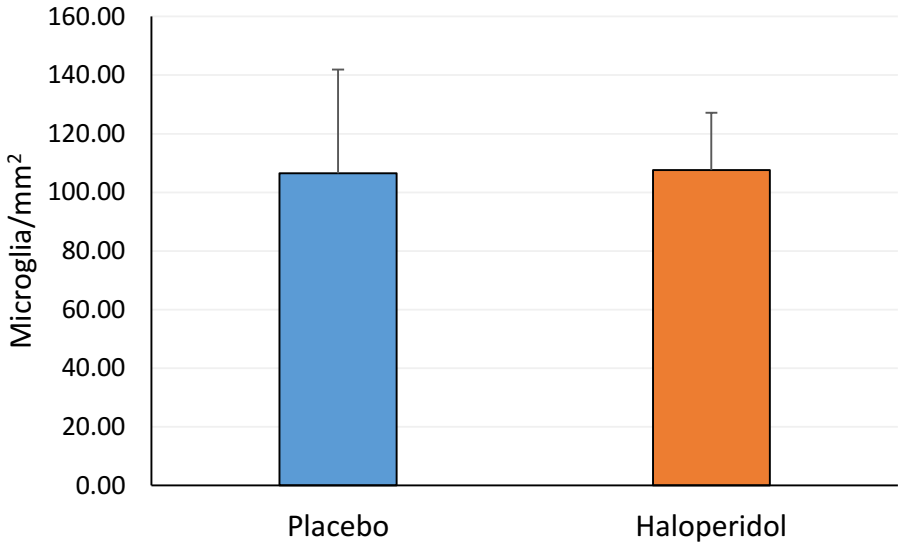

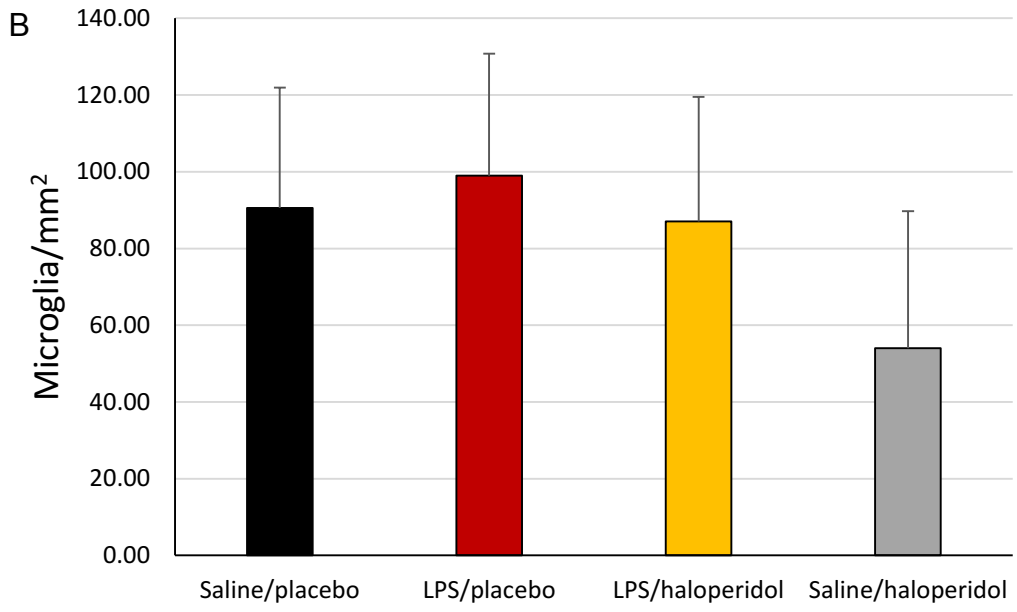


*Figure 24. Microglial cell density quantification*

(**A**) Microglial cell densities were not altered with haloperidol (n=11) treatment compared to placebo (n=18) (p= >0.05 ANOVA). Mean values ± SD. (**B**) In saline/placebo n=5, LPS/placebo n=13, LPS/haloperidol, n=7 and saline/haloperidol n=4 dosed animals, there was no difference in microglial cell densities (p> 0.05 ANOVA). Mean values ± SD.

## Soma area

Soma size was not altered in either naïve (Figure 25A, p> 0.05) or LPS/Saline (Figure 25B, p> 0.05) conditions.

A

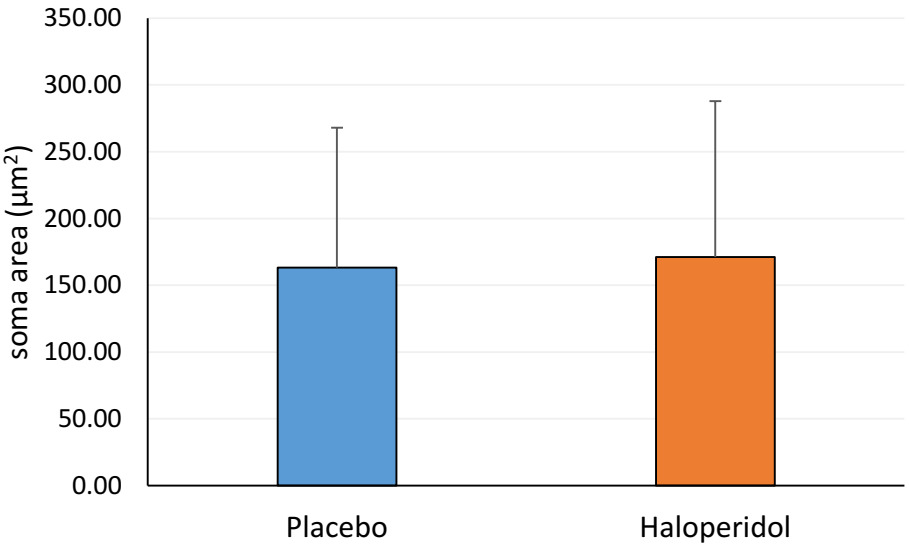

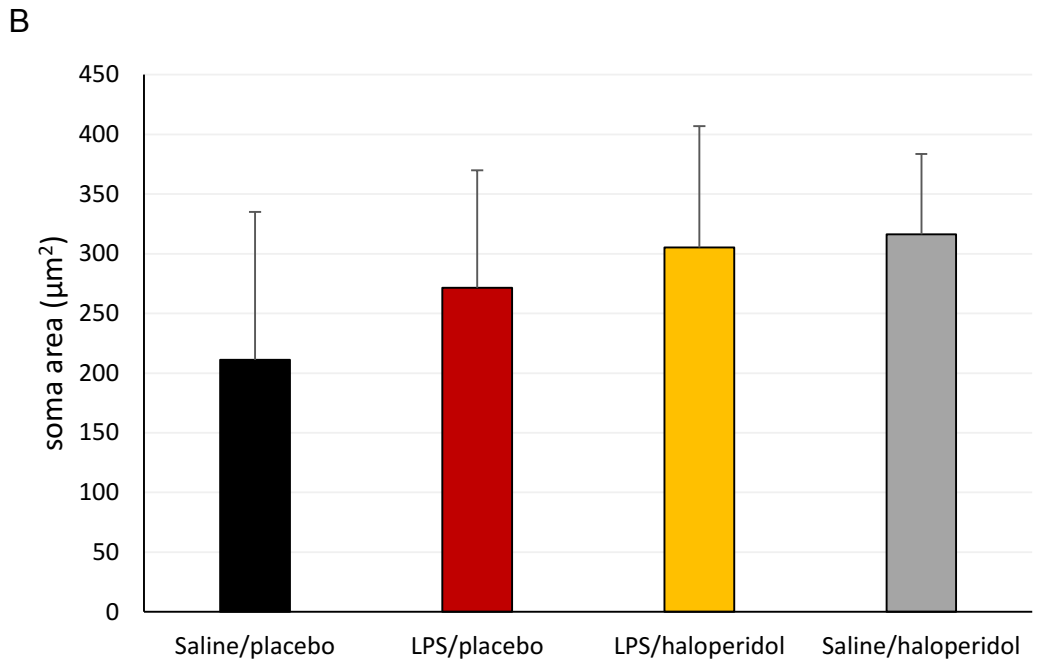


*Figure 25. Microglial soma size quantification*

(**A**) Microglial soma sizes were not altered with haloperidol (n=11) treatment compared to placebo (n=18) ($p > 0.05$) mean values ± SD. (**B**) In saline/placebo n=5, LPS/placebo n=13, LPS/haloperidol, n=7 and saline/haloperidol n=4 dosed animals, there was no difference in microglial cell densities ($p > 0.05$). Mean values ± SD.

## Soma intensity

Haloperidol treatment did not alter microglial density when compared with placebo controls (Figure 26A, n= 11, 18 respectively, p> 0.05). Administration of LPS did not result in an elevation of microglial cell density compared to saline controls (*p*> 0.05), haloperidol treatment did not alter the density of cells in any experimental condition (*p*> 0.05 Figure 26B).

A

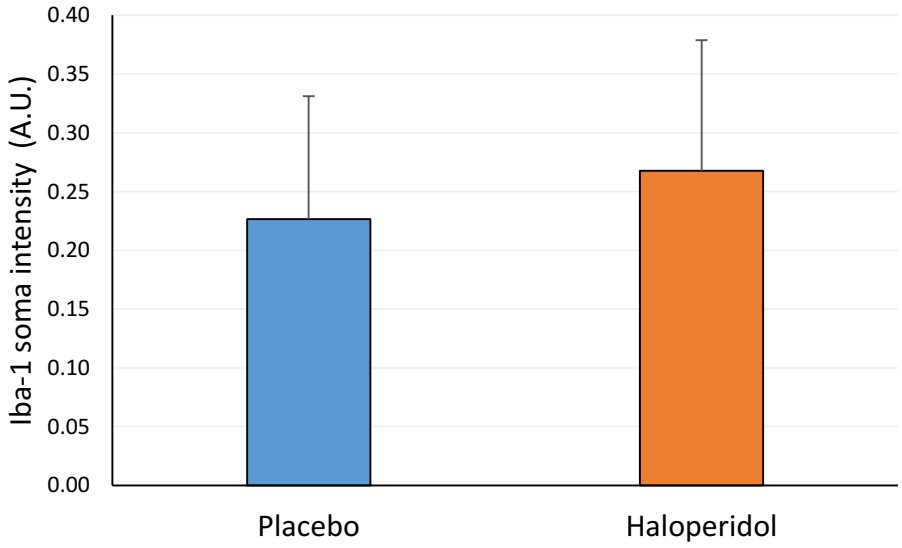

B

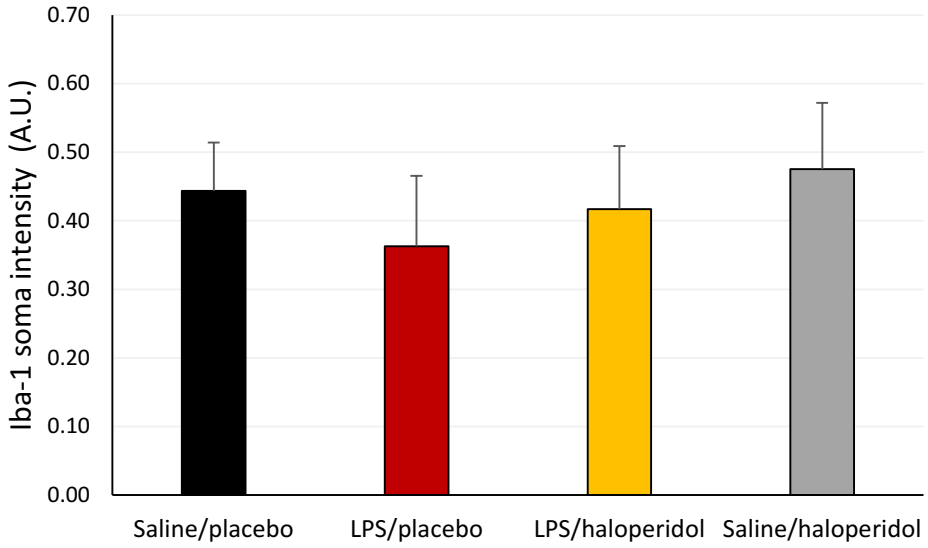


*Figure 26*. Microglial soma stain intensity

(**A**) The average Iba-1 intensity (AU) of the cell body was not altered with haloperidol (n=11) treatment compared to placebo (n=18) ($p > 0.05$) mean values ± SD. (**B**) In saline/placebo n=5, LPS/placebo n=13, LPS/haloperidol, n=7 and saline/haloperidol n=4 dosed animals, there was no difference in soma intensity ($p > 0.05$). Mean values ± SD.

## Skeleton morphology

Haloperidol did not alter average branch lengths compared to placebo dosed animals ($p$> 0.05,). LPS did not alter branch morphology compared to Saline controls (p> 0.05) **Error! Reference source not found.**, C-F, demonstrates a epresentative field of view from each experimental group, due to age of tissue, background intensity of staining obscured processes for quantification with this approach, subsequently n= is lower than in previous analysis approaches where bacground was less of a problem for quantification.

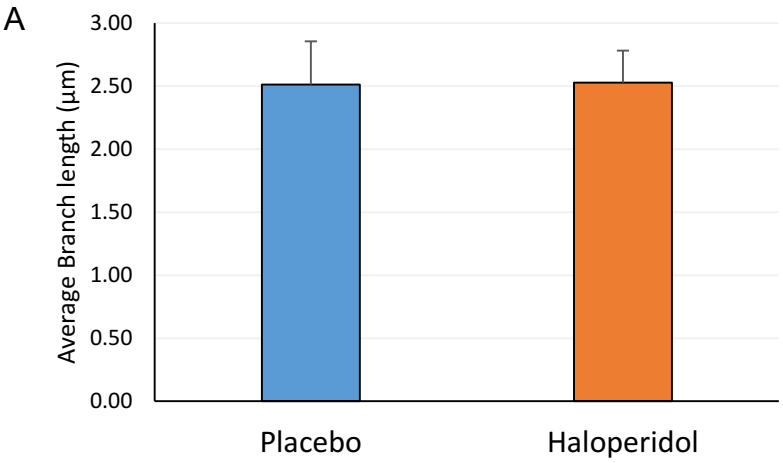


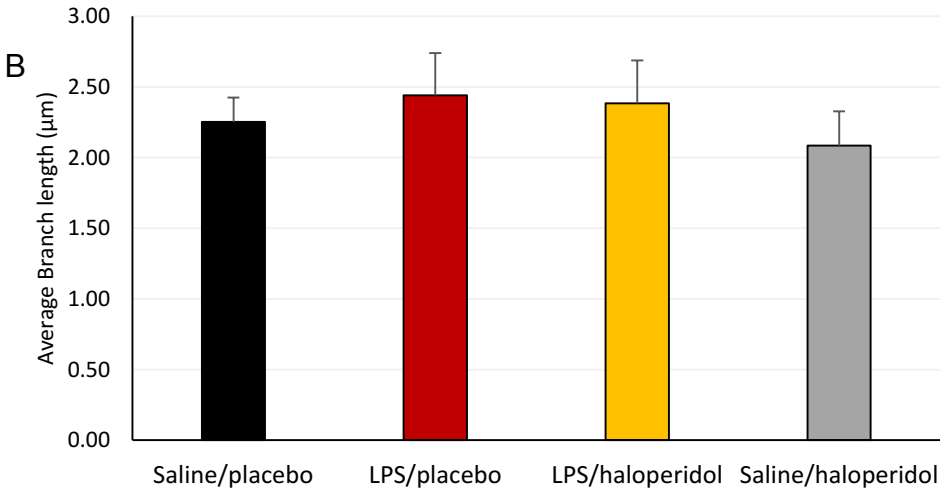

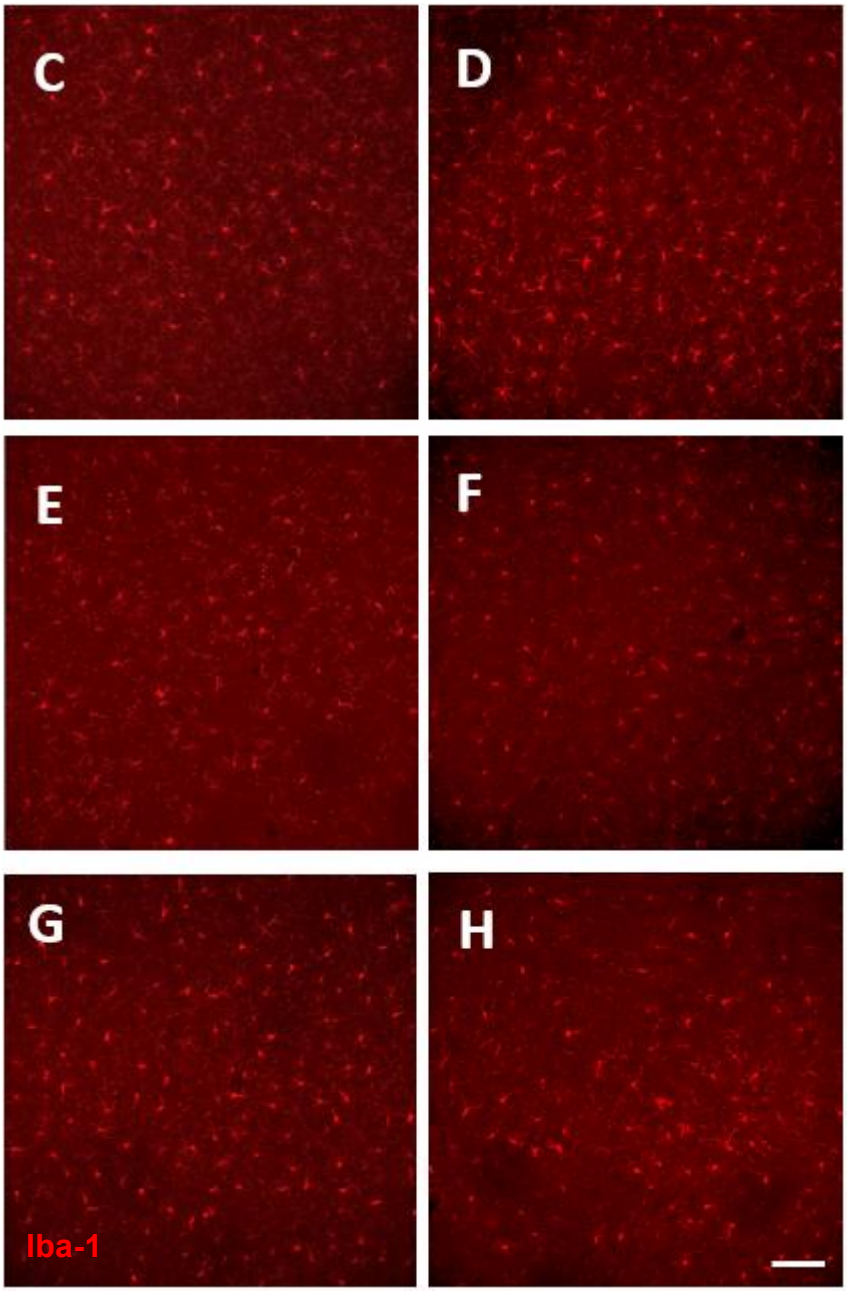


*Figure 27. Process morphology analysis*

(**A**) Branch lengths were not altered with haloperidol (n=3) treatment compared to placebo (n=8) ($p > 0.05$) mean values ± SD. (**B**) In saline/placebo n=5, LPS/placebo n=13, LPS/haloperidol, n=7 and saline/haloperidol n=4 dosed animals, there was no difference in microglial branch morphology ($p > 0.05$). Mean values ± error bars

= SD. Microglial staining from the groups: placebo (**C**) haloperidol (**D**) saline/placebo (**E**) LPS/placebo (**F**) LPS/haloperidol (**G**) saline/haloperidol (**H**) scale bar = 100μm.

## Nuclear counts

The numbers of total cell nuclei were not altered in haloperidol (n=11) treated animals compared to placebo (n=18, p> 0.05). Similarly in LPS/Saline dosed groups there was no difference in cortical nuclei (saline/placebo n=5, LPS/placebo n=13, LPS/haloperidol, n=7 and saline/haloperidol n=4, p> 0.05, figure 28B).

A

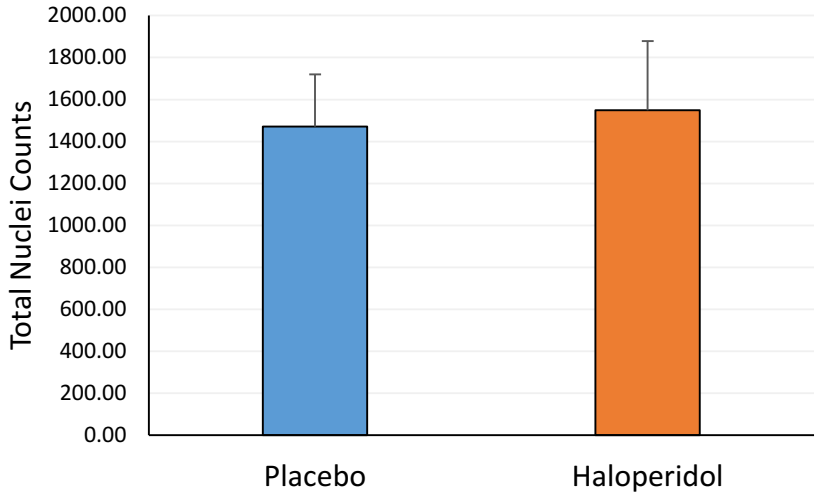

B

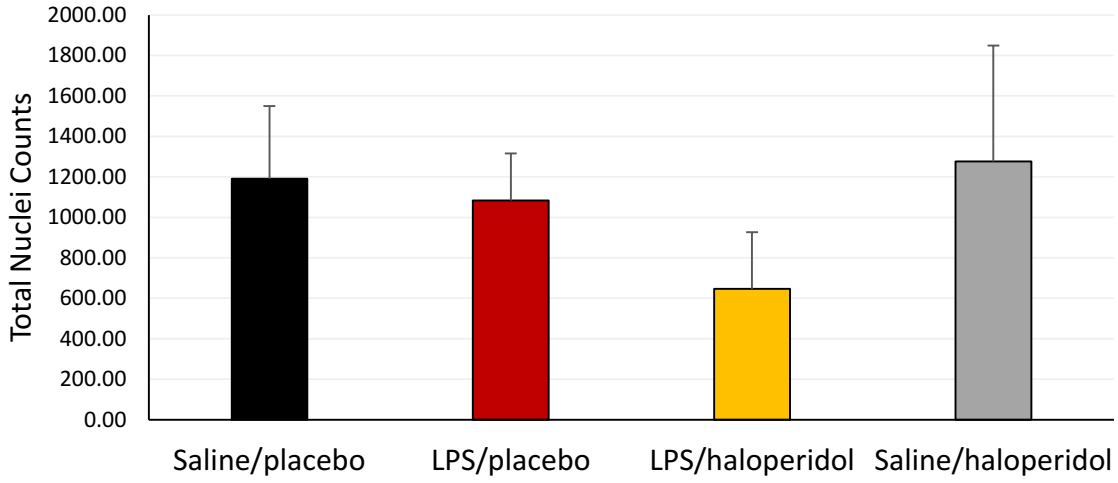


Figure 28. Total nuclear counts

(**A**) The average number of DAPI stained nuclei was not altered with haloperidol (n=11) treatment compared to placebo (n=18) ($p > 0.05$) mean values ± SD. (**B**) In saline/placebo n=5, LPS/placebo n=13, LPS/haloperidol, n=7 and saline/haloperidol n=4 dosed animals, there was no difference in numbers of nuclei ($p > 0.05$). Mean values ± SD.

## Apoptotic cells

Analysis of caspase-3 a marker of apoptotic cell death (Burguillos et al., 2011) was used to determine whether numbers of microglia in the different groups were sustained with different rates of turnover. There was no difference between total numbers of caspase-3 positive cells or caspase-3 positive microglial cells between groups ($p$>0.05 figure 29).

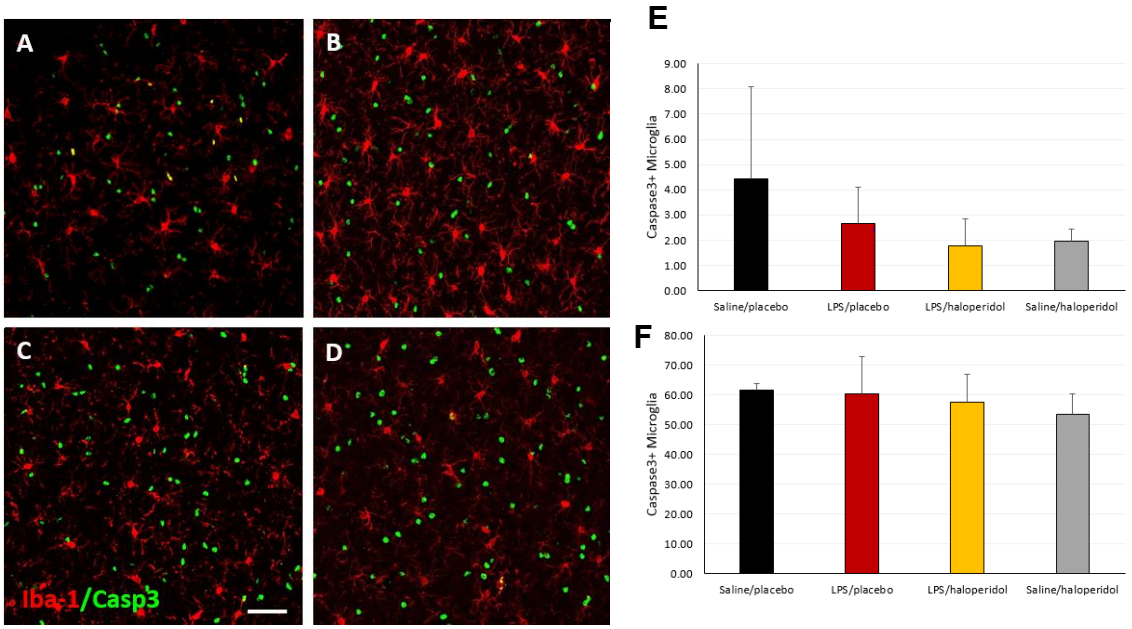


*Figure 29. Apoptotic cell and nuclear counts*

Numbers of apoptotic nuclei and apoptotic microglia were not altered by either LPS or haloperidol treatments ($p>0.05$). Representative images of microglia and apoptotic nuclei (Iba-1 (red) and caspase3 (green) respectively. Scale bar = 50 μm) for saline/placebo (n=5) ***A***, LPS/placebo (n=7) ***B***, LPS/haloperidol (n=6) ***C*** and saline/haloperidol (n=6) ***D*** treated groups. Graphical representation of numbers of apoptotic microglia ***E*** and total apoptotic cells ***F***.

## *Discussion*

In this chapter we have seen that haloperidol does not alter microglial cell densities across a range of treatments. We saw a reduction in cerebral volume with haloperidol treatment when compared to placebo dosed controls. Our LPS regimen did not produce the desired response seen in (Chen et al., 2012).

In this investigation, we see a cerebral volume reduction in our haloperidol treated animals compared to placebo controls (~20%). This reduction is not apparent with the LPS and saline treatments. This reduction is comparable to that seen in patients with early onset schizophrenia after the first five years of treatment (Thompson et al., 2001), as well as previous animal experiments using a high dose and different time courses of regime (Dorph-Petersen et al., 2005; Vernon et al., 2014; Vernon et al., 2011). The percentage difference in volume is greater in our investigation than in the Dorph-Petersen and Vernon studies. This may be a result of the low resolution of discrimination we have in our modality compared to the use of larger primate brains (Dorph-Petersen et al., 2005) and MRI (Vernon et al., 2011).

Further clinical studies expanding on this have demonstrated cortical loss in schizophrenia and UHR subjects (Bose et al., 2009; Ortiz-Gil et al., 2011; Pantelis et al., 2003a; Sandu et al., 2008; Walterfang et al., 2008). This raises the possibility that cortical reductions may be attributed, at least in part, to the medication used to treat the disorder. Indeed in chapter 4 we demonstrate cortical volume reductions in medicated patients with schizophrenia, but not the unmedicated UHR subjects. The present replication of previous findings is reassuring in terms of drug delivery and cortical consequences of administration. We did not see a reduction in the total

number of cells present across the groups. With a reduced volume, but a preserved cell number, it is unclear where the volume reduction is taking place. It is speculated that psychotropic medication associated volume loss may arise due to a reduction in synapse number (Moorhead et al., 2007; Tost et al., 2010) however further investigation is needed to determine the cause of the loss we see.

Previous research has demonstrated how, antipsychotic medication is able to reduce a range of inflammatory actions of microglial cells *in vitro* (Bian et al., 2008; Kato et al., 2008; Kato et al., 2007; Kato et al., 2011; Kowalski et al., 2003; Labuzek et al., 2005; Seki et al., 2013). However, a number of these studies report conflicting results and it is not clear how the *in vitro* models relate to the whole brain. A recent study using a neonatal lesion model of schizophrenia revealed a reduction in microglial cell density *in vivo* (Zhu et al., 2014). The analysis in this investigation was limited to manual cell counting and had a primary focus on behavioural deficits, as well as using a relatively high dose of medication. A recent investigation of haloperidol in rats, using a high continuous dose of haloperidol demonstrated an elevation in numbers of activated microglial cells (Cotel et al., 2015). The inconsistencies in findings across the varying studies from *in vivo* to *in vitro* suggest that there are subtleties to the interaction of microglial cells and antipsychotic medication. For example, the (Cotel et al., 2015) study uses higher doses of medication and in vitro studies have different time courses in isolated microglial preparations, where cell-cell type interactions existing *in vivo* are not present.

The staining of apoptosis using caspase3 does not correspond with reports in the literature (Burguillos et al., 2011). Staining was initially tested in control and LPS

treated tissue and a secondary antibody only staining was performed to determine specificity of stain signal. In a control condition few apoptotic cells should be present, whereas we see many positive nuclei (50-60 positive nuclei per ROI). This suggests that the antibody is not specific for activated caspase-3 and binding to both active and inactive forms. To determine how accurate the staining is, it would be useful to confirm these stainings using TUNEL (Kyrylkova et al., 2012) and Fluoro jade B (Schmued and Hopkins, 2000) approaches.

## Future investigation

There are 2 largely open questions at the end of this chapter;

1. What underlies the reduction in brain volume following haloperidol administration?

Psychotropic medication is hypothesised to reduce brain volume through synaptic remodelling (Tost et al., 2010). To address this I will perform western blots to quantify the amount of synaptic proteins following haloperidol.

2. Why did LPS not result in the same changes in cell density reported by (Chen et al., 2012)?

The Chen study delivered LPS on consecutive days, whereas our doses were spread over two weeks. This may be responsible for a lack of visible response in our experiments. Animals were lightly anaesthetised for i.p. injections in my study, which may have an anti-inflammatory influence (Hofstetter, 2007). An alternative approach that would provide a positive control for future studies is to administer LPS in a single acute dose, where the peak of the inflammatory response is thought to be between 8 and 24 hours post administration (Buttini et al., 1996). We would be

able to compare these results to previous experiments demonstrating acute LPS induced responses (Kozlowski and Weimer, 2012; Zhu et al., 2014).

## Limitations

A limitation of the Cell Profiler analysis is that quantification was conducted on 2D images rather than in 3D. This is a potential confound as the entire cell may not be contained in the ROI and overlapping cells may be less accurately quantified. The use of a DAPI channel reduces this problem to an extent, however full 3D analysis would be ideal. The dose of Haloperidol is relatively low, which was chosen to provide a striatal D2 occupancy similar to that achieved in the clinic (Kapur et al., 2003). While this provides a better clinical interpretation, it is significantly lower than that used in the animal and *in vitro* literature to date (Hou et al., 2006). This makes interpretation of our findings more difficult. However the blood doses of haloperidol we see in our animals is comparable to the lower end of the clinical literature (Coryell et al., 1998).

The drug delivery in this study was via subcutaneous drug pellets. These pellets use a matrix driven delivery (MDD, Innovative research of America, Florida USA) system (Singh et al., 2008), where the contents are released over a period of time when inserted subcutaneously. The use of continuous delivery is not ubiquitous in antipsychotic literature and is, in some cases, considered to be less effective and more subject to tolerance effects (Samaha et al., 2008). In this context we were looking for a paradigm which would approximate the medication dynamics in patient cohorts. Through to the end of the experiment blood levels of haloperidol were detectable, at a consistent low level. As with the general antipsychotic literature, the

literature using IRA pellets implements a range of doses of haloperidol (Adán et al., 2013; Liskowsky and Potter, 1987), the one used here is low in comparison but seems effective. For many of the animals pellets were recovered post dissection. In some animals the pellet may have fully dissolved or merely was not distinguishable during dissection. The study presented here investigates the effects of haloperidol at a single time point, it would however be useful to have a longitudinal design of study to determine when the brain and potential glial changes first occur. Previous investigations of brain volume using haloperidol and MRI in rats demonstrated a return to baseline volume after drug withdrawal (Vernon et al., 2011). It would be interesting to see how microglial cells would respond in this paradigm of administration-withdrawal.

## *Conclusions*

Here we demonstrate how microglial cell densities or soma sizes are not altered with haloperidol treatment. Interestingly there were brain volume reductions associated with haloperidol treatment, which may explain some of the cortical loss seen in medicated patients. The results suggest clinical investigation of cortical microglial cells may not be influenced by antipsychotics but brain volumes may well be reduced.

# *Chapter 6 – Summary discussion conclusion*

## *Summary of findings*

In this thesis, our main experimental questions were addressed. The three aims are presented below with a summary of the findings from the associated chapters;

Aim 1: To determine whether neuroinflammation is present in subjects with subthreshold psychotic symptoms, using PET imaging with the 2nd generation TSPO ligand [$^{11}$C]PBR28.

Results: Relative to age and genotype matched healthy controls, [$^{11}$C]PBR28 signal was significantly elevated in UHR subjects. Whole brain normalized $V_T$ was used to provide a DVR of [$^{11}$C]PBR28 with 2TCM-1k analysis. Significant elevations of [$^{11}$C]PBR28 signal were observed in total grey matter, frontal lobe and temporal lobe regions of interest. No cerebellar difference was observed, suggesting elevations are of a specific origin. Similarly, medicated patients with schizophrenia demonstrated elevations of [$^{11}$C]PBR28 in the same regions of interest when compared with a second cohort of matched control subjects.

Aim 2: To assess the relationship between [$^{11}$C]PBR28 signal and symptom severity, cortical structure alterations and peripheral inflammatory measures in patients and UHR subjects.

Results: There were elevations in peripheral TNF-α in UHR and patients with schizophrenia. Patients with schizophrenia demonstrated significant cortical volume reduction in whole grey matter. This correlation was not present in control of

schizophrenia groups. Peripheral measures didn't correlate with volume or PET signal.

Aim 3: To determine the effects of haloperidol treatment on microglial cells and cerebral volume in naïve and inflamed rat brain tissue.

Results: Haloperidol reduced brain volume in naïve rats, of a magnitude similar to findings in the literature (~20%). We designed Cell Profiler software pipelines to provide accurate quantification of cell density, cell body area and cell body stain intensity. This provided an accurate and precise workflow for the assessment of haloperidol treated tissue. Haloperidol did not alter microglial cell density, soma size or stain intensity in the prefrontal cortex in naïve or LPS inflamed tissue. There was no reduction in total number of nuclei in haloperidol animals, suggesting volume loss is not through a reduction in total number of cells. Further investigation is required to determine the mechanism of reduction of brain volume.

## *Discussion*

The research questions within this thesis cover a number of research themes, from the basic function of specific cell types to cortical alterations in a complex psychiatric illness. The discussion of these topics will be addressed in the order presented in the body of work and then combined to produce a more integrative perspective.

## *Clinical study discussion*

In the clinical study we have demonstrate how microglial activity is elevated in subjects prior to the onset of first episode psychosis, as measured through PET imaging of TSPO. Here we discuss the implications of this finding and future investigations which could be conducted on the topic.

## Neuroinflammation in psychosis

As we saw in the introductory chapter, there is considerable evidence that neuroinflammation is a component of schizophrenia, from post mortem (Bayer et al., 1999; Steiner et al., 2006) and *in vivo* PET imaging studies (Doorduin et al., 2009; van Berckel et al., 2008). Peripheral inflammatory markers are also elevated in patients with schizophrenia and those with prodromal psychotic symptoms (Cannon et al., 2015). TSPO is used as the PET imaging target for microglial activity and has been used to demonstrate neuroinflammation in a range of disorders. To date, psychosis has not been investigated in pre-first episode subjects. The present thesis investigates the role of neuroinflammation in association with the TSPO binding ligand [$^{11}$C]PBR28 in UHR subjects and patients with schizophrenia.

The findings indicate that both patients with schizophrenia and UHR subjects have elevated whole brain grey matter, frontal lobe and temporal lobe binding compared to matched healthy controls. There are a number of caveats which will be discussed, however the greatest limitation for interpreting our finding is that UHR subjects will not all develop a psychotic disorder, hence cannot be viewed as a prodrome. In this investigation, the transition rate to psychosis to date is 7%, which is far lower than the rates reported in the literature (20-35%) (Wood et al., 2008; Yung et al., 2005).

The low transition rates we see may be a consequence of our subjects being recruited from an early intervention service, where various forms of medication and cognitive treatment are used to prevent first episode transition. In the interval from scanning a number of UHR subjects started on antipsychotics. In the UHR group, symptom severity was positively correlated with [$^{11}$C]PBR28 signal, however this relationship was not present in patients with schizophrenia. There is a possibility that this is related to medication, as UHR subjects were antipsychotic naïve and patients were on a range of medication. The literature suggests an anti-inflammatory role of antipsychotics *in vitro* (Kato et al., 2007), the latter chapters of this thesis confirm this *in vivo* for haloperidol. The patients with schizophrenia and UHR subjects investigated ultimately are heterogeneous groups, where none were acutely psychotic, hence may not be truly reflective of psychosis. Beyond psychosis, there is evidence that microglia are involved with depression (Setiawan et al., 2015) and may prove to be a feature of general psychiatric illness.

## Future directions

The evidence for the involvement of microglia in psychosis is compelling and demonstrates, for the first time, that microglial activity is associated with psychotic-like symptoms presenting before an episode of frank psychosis. While this is an interesting finding, it is crucial to determine how this is related to outcome. We have had 1 subject transition to first episode psychosis, and interestingly, this subject had the highest [$^{11}$C]PBR28 binding. A possible future investigation would be to perform longitudinal follow up to determine whether subjects transitioning continue to

develop elevations in microglial activity, as well as seeing whether those discharged from psychiatric services have levels which return to those of controls.

[$^{11}$C]PBR28 is still a relatively novel ligand for PET imaging, hence the precise details of tracer specificity and signal to noise ratio are unclear. A small study has been conducted to determine the ratio of specific to non-specific ratio of binding (Owen et al., 2014). However it is not known whether this level of specific and non-specific binding is consistent across clinical cohorts. Hence it would be valuable to conduct a similar blocking study with [$^{11}$C]PBR28 in our cohorts to determine these signal components.

As TSPO is elevated prior to the onset of first psychotic episode, it is therefore a potential therapeutic target. TSPO is involved in steroidal transport, however acts as a marker of inflammation in the brain. Hence it is possible to investigate whether anti-inflammatories may be able to prevent transition or ameliorate symptoms in UHR subjects, or maybe be applied to patients with schizophrenia. The latter investigation has been performed in a small cohort, using minocycline, and proved successful in treating symptoms assessed on the PANSS (Miyaoka, 2008).

## Limitations

### PET methodology issues

Second generation TSPO ligands have proven difficult to analyse. A larger affinity has produced profound difficulties when assessing signal to noise ratios and specificity of signal. Indeed many studies conducted using second generations ligands have not demonstrated differences with $V_T$ as the outcome measure (Hannestad et al., 2013; Kenk et al., 2015; Park et al., 2015a; Takano et al., 2010).

This has raised concern over the use of such ligands, however there has been progress in addressing the issue of noise by using normalization approaches, such as the DVR approach used in this thesis. Two recently published studies have demonstrated the use of the cerebellum (Lyoo et al., 2015) and, as we have here, the whole brain signal (Loggia et al., 2015).

## TSPO Genotyping

The brain TSPO that [$^{11}$C]PBR28 binds to is affected by an SNP in the general population, 10% being LABs, 40% being MABs and 50% being HABs (Owen et al., 2011). The results of our investigation demonstrated a very close proportional representation here (7% LAB, 37%MAB & 56% HAB). We scanned mid and high binders and co-varied in analysis rather than stratifying groups. This decision was made to provide a more representative sample for the clinical population, the analysis of a stratified UHR group did not differ to those of the combined analysis and data from differing genotypes overlapped considerably.

## TSPO & microglial distribution

A major limitation of TSPO imaging studies is the relationship between microglia at the cellular level and the signal from scanning. Preclinical investigation has demonstrated TSPO presence on a range of cell types. With expression detected on astrocytes, microglia and neural progenitor cells. TSPO is also expressed in relatively low concentrations in the brain, tissues with higher expression include adrenal glands and testes (steroid synthetic tissues) (Banati et al., 2014).

## Comorbidity and cohort validity

Patient cohorts are variable and patients with schizophrenia are particularly heterogenous. In the investigations here, we have controlled for or minimized variability where possible, however there are inevitably caveats and variables which cannot be controlled. Larger cohorts of participants could be stratified, however it is not a simple objective task.

When using a clinical cohort for a study such as this, it is very often patients that are high functioning and at experiencing less severe stages of the disorder that are able to participate. This is partly a consequence of ease of investigation, but also an ethical consideration. The patients that are potentially the most interesting in terms of function and psychopathology are often not of consenting capacity. Hence such individuals are not able to take part in research.

Schizophrenia as a disease is affected by a number of comorbid health risks, some of which arise as a consequence of medication, however many are closely related to features of disease.

A small number of subjects in our patient cohort were taking medication for diabetes. Comorbidity of diabetes and schizophrenia is relatively common, indeed there is an association between antipsychotic medication and diabetic status in patients with schizophrenia (Llorente and Urrutia, 2006). As with diabetes, obesity is present in higher proportions in patients with schizophrenia, there is evidence that obesity and inflammation are associated (Lim and Marsland, 2013; Thaler et al., 2013; Vgontzas et al., 1997), however the literature is somewhat conflicting in the role of TSPO in this context (Lassance et al., 2015). Similar to obesity, there are age associated changes in inflammatory status, with a greater level of cortical inflammation in later

life, which has been studied with PET using [$^{11}$C]-(R)-PK11195 (Schuitemaker et al., 2012).

A number of patients and UHR subjects reported use of recreational substances, where the control cohorts did not. Cocaine use and cannabis use were the two most frequently reported drugs. The former has been shown to have no relationship with [$^{11}$C]PBR28 (Narendran et al., 2014). However cannabinoids are potentially inhibitory to reactive gliosis (Gomes et al., 2015), PET evidence is yet to be published on this topic. While use of cannabis may influence microglial activity, the effects would reduce levels and would serve to reduce the margin between control and experimental groups.

## PBR28 ligand and analysis methods

The use of TSPO as a marker has raised a number of issues in assessing microglial activity. PK11195 was not optimum for in vivo investigation, hence the development of a second generation of TSPO tracers. Unfortunately, the second generation has not delivered in the ways expected, particularly PBR28. The affinity of PBR28 is higher than PK11195, however this results in considerable noise and non-specific binding. Further than this, the SNP affecting affinity binding makes PBR28 a tedious ligand to work with, as genotyping subjects prior to scanning can prove troublesome, particularly in patient cohorts, where attendance is unpredictable. We have discussed these methods in (Turkheimer et al., 2015).

### *Animal study discussion*

In these experiments we have investigated microglia following antipsychotic administration in inflammatory and naïve contexts. The role of microglia in the healthy and diseased brain has received a lot of attention recently. New discoveries regarding microglia in synapse organisation (Parkhurst et al., 2013) has revealed how crucial microglia are to brain function. The clinical investigations in this thesis demonstrate a change in microglial activity prior to the onset of psychosis, however the role of antipsychotic mediation was an uncontrollable variable in the patient cohort. We administered haloperidol at a low, clinically comparable (Kapur et al., 2003), dose for two weeks. Our inflammatory setting was not intended to be a model of psychosis or schizophrenia, however was designed to produce a cellular morphology which has been described in post mortem schizophrenia tissue examination (Bayer et al., 1999; Steiner et al., 2008; Steiner et al., 2006). Unfortunately the LPS administration did not produce the desired effect reported in (Chen et al., 2012) The primary aim of the animal investigations was to determine the *in vivo* effects of a low dose of antipsychotic medication on microglia. We also demonstrated how haloperidol administration is associated with cortical volume reduction.

## Mechanistic considerations

Haloperidol is associated with reduced brain volume, however the mechanism of this alteration is unclear. Nuclear counting did not reveal a difference between treatment groups, suggesting reductions are not a result of a lower overall number of brain cells.

## Neuron glial interaction

Microglia-neuron interactions are able to modulate neuronal signalling, particularly in the spinal cord where peripheral signals relay sensory inputs (Staniland et al., 2010). Work in the field of pain signal transduction has revealed immune cell mediated modulation in the CNS (Sheridan and Murphy, 2013; Sheridan et al., 2014). It is not only the interaction between neurons and microglia to consider, as there is potential for astrocytic and oligodendrocytic consequences as well.

## Future directions

The major outstanding question of the animal investigations is how the changes in brain volume occur with haloperidol treatment. In translating the findings from the animal experiments to the clinical setting, it is also essential to determine how medication and brain volume directly relate in patients. Additionally it is unclear how cortical volume changes with age or disease phenotype.

## Limitations

Beyond the direct translation of biological information, there are a number of considerations when interpreting clinical and animal findings together. The animals are 2-3 months old (250g), which corresponds to a young adult or late adolescent period (Sengupta, 2013). The patients receiving medication were on average 45 years old. Age matching is a major consideration for clinical investigation, particularly when investigating volumetric changes and inflammation, as there are large age effects on both features. Animal equivalent years are difficult to translate, however it would be desirable to use animals of a greater age as it has recently

been demonstrated that the same age-microglial association is present in rats (Walker et al., 2015).

As with our imaging experiments, the animal investigation was of a cross sectional design. The changes we see are from a single time point following chronic administration of medication. It would be useful to determine the time point where volume changes or microglial reductions first occur. For this we would need to implement the non-invasive methods used in the clinical studies. While this gains temporal resolution, our spatial resolution for brain volume/microglial cell assessment would be hindered. However we would be able to perform direct comparisons at the endpoint between animal PET of TSPO and tissue staining for microglia.

The patients with schizophrenia in the clinical study were receiving a myriad of medication, many of which were second generation antipsychotics with diverse receptor antagonism profiles. In our investigation we administered haloperidol, which is more specific in its action at DRD2 than second generation counterparts (Miyamoto et al., 2012). It would be useful to conduct the investigation with multiple first and second generation antipsychotics, over a range of doses to apply more directly to the nature of clinical administration.

## *Translational discussion*

Implementing research in a translational manner is open to interpretation and criticism as comparing human findings directly to animals is not trivial. Modelling diseases, particularly of a psychiatric nature, are highly controversial, as the pathology and symptomatic expression are particularly unique to a human condition. It is unreasonable to say an animal model of schizophrenia is valid, as the complex symptoms that are features of psychosis are not assessable in animals.

However, assessing pharmacology and consequences of medication, as in the investigations here, is less of a stretch. We will come to discuss the limitations of translation of our findings, however we can begin to interpret the two findings together. The clinical investigations demonstrate how microglial activity would appear to be associated with psychosis. In the UHR group this is associated with symptom severity, indeed the only subject to transition at this point had the highest [$^{11}$C]PBR28 binding. This symptom relationship was not apparent in the patients with schizophrenia, where medication was a major caveat. To address this issue and determine the *in vivo* consequences of antipsychotic medication, we designed the animal experiments to determine the effects of the typical DRD2 antagonist haloperidol on microglia. We do not see haloperidol associated microglial changes, but do see a reduction in brain volume. If we take the clinical and animal findings together, antipsychotics would not appear to alter microglial activity in medicated patients. It would be useful to investigate different doses and receptor profile antipsychotics to investigate this to a greater extent.

## *Conclusion*

In conclusion my studies have shown that sub-threshold psychotic symptoms are related to the levels of neuroinflammation/microglial cell activity as measured by TSPO PET imaging. Haloperidol administration demonstrated a reduction in brain volume in animals, however microglial cells did not appear to be altered after treatment. Based on the present findings, prior to the onset of first episode psychosis cortical inflammation may provide a novel therapeutic target.

# References

Abi-Dargham, A., Mawlawi, O., Lombardo, I., Gil, R., Martinez, D., Huang, Y., Hwang, D.-R., Keilp, J., Kochan, L., Van Heertum, R., *et al.* (2002). Prefrontal Dopamine D1 Receptors and Working Memory in Schizophrenia. The Journal of Neuroscience *22*, 3708-3719.

Adán, N., Guzmán-Morales, J., Ledesma-Colunga, M.G., Perales-Canales, S.I., Quintanar-Stéphano, A., López-Barrera, F., Méndez, I., Moreno-Carranza, B., Triebel, J., Binart, N., *et al.* (2013). Prolactin promotes cartilage survival and attenuates inflammation in inflammatory arthritis. The Journal of Clinical Investigation *123*, 3902-3913.

Akaike, H. (1974 ). A new look at the statistical model identification. IEEE Transactions on Automatic Control, *19,* , 716-723.

American Psychiatric, A., American Psychiatric, A., and Force, D.S.M.T. (2013). Diagnostic and statistical manual of mental disorders : DSM-5.

Arias, R., Tuisku, Dickens, Anthony, Rinne (2014). In Vivo PET Imaging of Activated Microglial Cells Can Be Used to Differentiate Between Inactive and Active Chronic Lesions in Progressive Multiple Sclerosis. Neurology *82 no. 10 Supplement S44.003*.

Badawi, R.D. (1998). Aspects of Optimisation and Quantification in Three-Dimensional Positron Emission Tomography. . Unliversity of London, London.

Banati, R.B., Middleton, R.J., Chan, R., Hatty, C.R., Wai-Ying Kam, W., Quin, C., Graeber, M.B., Parmar, A., Zahra, D., Callaghan, P., *et al.* (2014). Positron emission tomography and functional characterization of a complete PBR/TSPO knockout. Nat Commun *5*.

Banerjee, A., Chitnis, U.B., Jadhav, S.L., Bhawalkar, J.S., and Chaudhury, S. (2009). Hypothesis testing, type I and type II errors. Industrial Psychiatry Journal *18*, 127-131.

Bayer, T.A., Buslei, R., Havas, L., and Falkai, P. (1999). Evidence for activation of microglia in patients with psychiatric illnesses. Neuroscience Letters *271*, 126-128.

Beck, A.T., Ward, C.H., Mendelson, M.M., Mock, J.J., and Erbaugh, J.J. (1961). AN inventory for measuring depression. Archives of General Psychiatry *4*, 561-571.

Bédard, A.-M., Maheux, J., Lévesque, D., and Samaha, A.-N. (2011). Continuous, but not Intermittent, Antipsychotic Drug Delivery Intensifies the Pursuit of Reward Cues. Neuropsychopharmacology *36*, 1248-1259.

Bell, C.C. (2001). Diagnostic and Statistical Manual of Mental Disorders, Fourth Edition, Text Revision: DSM-IV-TRQuick Reference to the Diagnostic Criteria from DSM-IV-TR. JAMA: The Journal of the American Medical Association *285*, 811-812.

Bian, Q., Kato, T., Monji, A., Hashioka, S., Mizoguchi, Y., Horikawa, H., and Kanba, S. (2008). The effect of atypical antipsychotics, perospirone, ziprasidone and quetiapine on

microglial activation induced by interferon-Î³. Progress in Neuro-Psychopharmacology and Biological Psychiatry *32*, 42-48.

Boizeau, M.-L., Fons, P., Cousseins, L., Desjobert, J., Sibrac, D., Michaux, C., Nestor, A.-L., Gautret, B., Neil, K., Herbert, C.*, et al.* (2013). Automated Image Analysis of In Vitro Angiogenesis Assay. Journal of Laboratory Automation *18*, 411-415.

Bose, S.K., Mackinnon, T., Mehta, M.A., Turkheimer, F.E., Howes, O.D., Selvaraj, S., Kempton, M.J., and Grasby, P.M. (2009). The effect of ageing on grey and white matter reductions in schizophrenia. Schizophrenia Research *112*, 7-13.

Bose, S.K., Turkheimer, F.E., Howes, O.D., Mehta, M.A., Cunliffe, R., Stokes, P.R., and Grasby, P.M. (2008). Classification of schizophrenic patients and healthy controls using [18F] fluorodopa PET imaging. Schizophrenia Research *106*, 148-155.

Burguillos, M.A., Deierborg, T., Kavanagh, E., Persson, A., Hajji, N., Garcia-Quintanilla, A., Cano, J., Brundin, P., Englund, E., Venero, J.L.*, et al.* (2011). Caspase signalling controls microglia activation and neurotoxicity. Nature *472*, 319-324.

Buttini, M., Limonta, S., and Boddeke, H.W.G.M. (1996). PERIPHERAL ADMINISTRATION OF LIPOPOLYSACCHARIDE INDUCES ACTIVATION OF MICROGLIAL CELLS IN RAT BRAIN*. Neurochemistry International *29*, 25-35.

Cajal, S.R.y. ((1913) ). Estudios sobre la Degeneración y Regeneración del Sistema Nervioso. . *2 vols. Moya: Madrid.*

Cannon, T.D., Cadenhead, K., Cornblatt, B., Woods, S.W., Addington, J., Walker, E., Seidman, L.J., Perkins, D., Tsuang, M., McGlashan, T.*, et al.* (2008). Prediction of Psychosis in Youth at High Clinical Risk: A Multisite Longitudinal Study in North America. Archives of general psychiatry *65*, 28-37.

Cannon, T.D., Chung, Y., He, G., Sun, D., Jacobson, A., van Erp, T.G., McEwen, S., Addington, J., Bearden, C.E., Cadenhead, K.*, et al.* (2015). Progressive reduction in cortical thickness as psychosis develops: a multisite longitudinal neuroimaging study of youth at elevated clinical risk. Biol Psychiatry *77*, 147-157.

Cannon, T.D., Chung, Y., He, G., Sun, D., Jacobson, A., van Erp, T.G.M., McEwen, S., Addington, J., Bearden, C.E., Cadenhead, K.*, et al.* (2014). Progressive Reduction in Cortical Thickness as Psychosis Develops: A Multisite Longitudinal Neuroimaging Study of Youth at Elevated Clinical Risk. Biological Psychiatry.

Chaudhry, I.B., Hallak, J., Husain, N., Minhas, F., Stirling, J., Richardson, P., Dursun, S., Dunn, G., and Deakin, B. (2012). Minocycline benefits negative symptoms in early schizophrenia: a randomised double-blind placebo-controlled clinical trial in patients on standard treatment. Journal of psychopharmacology *26*, 1185-1193.

Chen, Z., Jalabi, W., Shpargel, K.B., Farabaugh, K.T., Dutta, R., Yin, X., Kidd, G.J., Bergmann, C.C., Stohlman, S.A., and Trapp, B.D. (2012). Lipopolysaccharide-Induced

Microglial Activation and Neuroprotection against Experimental Brain Injury Is Independent of Hematogenous TLR4. The Journal of Neuroscience *32*, 11706-11715.

Clayton, J., Collins FS. (2014). Policy: NIH to balance sex in cell and animal studies. Nature *509:282–310.1038/509282a*.

Collste, K., Forsberg, A., Varrone, A., Amini, N., Aeinehband, S., Yakushev, I., Halldin, C., Farde, L., and Cervenka, S. (2015). Test–retest reproducibility of [11C]PBR28 binding to TSPO in healthy control subjects. European Journal of Nuclear Medicine and Molecular Imaging *43*, 173-183.

Consortium, T.N.P.A.S.o.t.P.G. (2015). Psychiatric genome-wide association study analyses implicate neuronal, immune and histone pathways. Nat Neurosci *18*, 199-209.

Converse, A.K., Larsen, E.C., Engle, J.W., Barnhart, T.E., Nickles, R.J., and Duncan, I.D. (2011). 11C-(R)-PK11195 PET Imaging of Microglial Activation and Response to Minocycline in Zymosan-Treated Rats. Journal of Nuclear Medicine *52*, 257-262.

Coryell, W., Miller, D.D., and Perry, P.J. (1998). Haloperidol Plasma Levels and Dose Optimization. American Journal of Psychiatry *155*, 48-53.

Cotel, M.-C., Lenartowicz, E.M., Natesan, S., Modo, M.M., Cooper, J.D., Williams, S.C.R., Kapur, S., and Vernon, A.C. (2015). Microglial activation in the rat brain following chronic antipsychotic treatment at clinically relevant doses. European Neuropsychopharmacology *25*, 2098-2107.

Coughlin, J.M., Wang, Y., Ma, S., Yue, C., Kim, P.K., Adams, A.V., Roosa, H.V., Gage, K.L., Stathis, M., Rais, R.*, et al.* (2014). Regional brain distribution of translocator protein using [(11)C]DPA-713 PET in individuals infected with HIV. Journal of neurovirology *20*, 219-232.

Cuijpers, P., and Smit, F. (2004). Subthreshold depression as a risk indicator for major depressive disorder: a systematic review of prospective studies. Acta Psychiatrica Scandinavica *109*, 325-331.

Cunningham, C. (2013). Microglia and neurodegeneration: The role of systemic inflammation. Glia *61*, 71-90.

Davalos, D., Grutzendler, J., Yang, G., Kim, J.V., Zuo, Y., Jung, S., Littman, D.R., Dustin, M.L., and Gan, W.-B. (2005). ATP mediates rapid microglial response to local brain injury in vivo. Nat Neurosci *8*, 752-758.

del Río-Hortega, P. (1918). Microglia in Cytology and Cellular Pathology of the Nervous System (edPenfield, W) 481–534 (Hoeber, 1932).

Dieset, I., Haukvik, U.K., Melle, I., Røssberg, J.I., Ueland, T., Hope, S., Dale, A.M., Djurovic, S., Aukrust, P., Agartz, I.*, et al.* (2015). Association between altered brain morphology and elevated peripheral endothelial markers — Implications for psychotic disorders. Schizophrenia Research *161*, 222-228.

Dimber, R., Vera Rojas, J., Guo, Q., Adonis, A., Bishop, C., Newbould, R., Winston, A., Gunn, R., Taylor, G., and Rabiner, E. (2014). Imaging brain TSPO availability with [11C]PBR28 PET in patients with retroviral (HTLV1 and HIV-1) infection. J NUCL MED MEETING ABSTRACTS *55*, 376-.

Domercq, M., Vázquez-Villoldo, N., and Matute, C. (2013). Neurotransmitter signaling in the pathophysiology of microglia. Frontiers in Cellular Neuroscience *7*, 49.

Doorduin, J., de Vries, E.F.J., Willemsen, A.T.M., de Groot, J.C., Dierckx, R.A., and Klein, H.C. (2009). Neuroinflammation in Schizophrenia-Related Psychosis: A PET Study. Journal of Nuclear Medicine *50*, 1801-1807.

Dorph-Petersen, K.-A., Pierri, J.N., Perel, J.M., Sun, Z., Sampson, A.R., and Lewis, D.A. (2005). The Influence of Chronic Exposure to Antipsychotic Medications on Brain Size before and after Tissue Fixation: A Comparison of Haloperidol and Olanzapine in Macaque Monkeys. Neuropsychopharmacology *30*, 1649-1661.

Dunn, O.J. (1961). Multiple Comparisons among Means. Journal of the American Statistical Association *56*, 52-64.

Edison, P., Brooks, D.J., Turkheimer, F.E., Archer, H.A., and Hinz, R. (2009). Strategies for the generation of parametric images of [11C]PIB with plasma input functions considering discriminations and reproducibility. NeuroImage *48*, 329-338.

Elovic, E., Jasey, Neil; Eisenberg, Michal (2008). The Use of Atypical Antipsychotics After Traumatic Brain Injury. Journal of Head Trauma Rehabilitation, The Wolters Kluwer Health.

EMA (2011). Guideline on Bioanalytical Method Validation. Committee for Medical Products for Human Use (CHMP). . *EMEA/CHMP/EWP/ 192217/2009.* .

FDA (2001). Guidance for Industry. Bioanalytical Method Validation issued by the U.S. Department of Health and Human Services Food and Drug Administration (FDA). .

Fisher, R.A. (1915). Frequency Distribution of the Values of the Correlation Coefficient in Samples from an Indefinitely Large Population. Biometrika *10*, 507-521.

Forero, M.G., Learte, A.R., Cartwright, S., and Hidalgo, A. (2010). DeadEasy Mito-Glia: Automatic Counting of Mitotic Cells and Glial Cells in <italic>Drosophila</italic>. PLoS ONE *5*, e10557.

Fusar-Poli, P., Bechdolf, A., Taylor, M.J., Bonoldi, I., Carpenter, W.T., Yung, A.R., and McGuire, P. (2013a). At Risk for Schizophrenic or Affective Psychoses? A Meta-Analysis of DSM/ICD Diagnostic Outcomes in Individuals at High Clinical Risk. Schizophrenia Bulletin *39*, 923-932.

Fusar-Poli, P., Bonoldi, I., Yung, A.R., and et al. (2012). Predicting psychosis: Meta-analysis of transition outcomes in individuals at high clinical risk. Archives of General Psychiatry *69*, 220-229.

Fusar-Poli, P., Byrne, M., Badger, S., Valmaggia, L.R., and McGuire, P.K. (2013b). Outreach and support in south London (OASIS), 2001-2011: ten years of early diagnosis and treatment for young individuals at high clinical risk for psychosis. European psychiatry : the journal of the Association of European Psychiatrists *28*, 315-326.

Fusar-Poli, P., Smieskova, R., Kempton, M.J., Ho, B.C., Andreasen, N.C., and Borgwardt, S. (2013c). Progressive brain changes in schizophrenia related to antipsychotic treatment? A meta-analysis of longitudinal MRI studies. Neuroscience and Biobehavioral Reviews *37*, 1680-1691.

Fusar-Poli, P.P., Stone, J.M., Broome, M.R., and et al. (2011). THalamic glutamate levels as a predictor of cortical response during executive functioning in subjects at high risk for psychosis. Archives of General Psychiatry *68*, 881-890.

Ge, Y., Grossman, R.I., Babb, J.S., Rabin, M.L., Mannon, L.J., and Kolson, D.L. (2002). Age-Related Total Gray Matter and White Matter Changes in Normal Adult Brain. Part I: Volumetric MR Imaging Analysis. American Journal of Neuroradiology *23*, 1327-1333.

Gerhard, A., Pavese, N., Hotton, G., Turkheimer, F., Es, M., Hammers, A., Eggert, K., Oertel, W., Banati, R.B., and Brooks, D.J. (2006). In vivo imaging of microglial activation with [11C](R)-PK11195 PET in idiopathic Parkinson's disease. Neurobiology of Disease *21*, 404-412.

Giannetti, P., Politis, M., Su, P., Turkheimer, F., Malik, O., Keihaninejad, S., Wu, K., Reynolds, R., Nicholas, R., and Piccini, P. (2014). Microglia activation in multiple sclerosis black holes predicts outcome in progressive patients: An in vivo [(11)C](R)-PK11195-PET pilot study. NEUROBIOLOGY OF DISEASE *65*, 203-210.

Ginhoux, F., Greter, M., Leboeuf, M., Nandi, S., See, P., Gokhan, S., Mehler, M.F., Conway, S.J., Ng, L.G., Stanley, E.R., *et al.* (2010). Fate Mapping Analysis Reveals That Adult Microglia Derive from Primitive Macrophages. Science *330*, 841-845.

Gomes, F.V., Llorente, R., Del Bel, E.A., Viveros, M.-P., López-Gallardo, M., and Guimarães, F.S. (2015). Decreased glial reactivity could be involved in the antipsychotic-like effect of cannabidiol. Schizophrenia Research *164*, 155-163.

Gómez-Nicola, D., Fransen, N.L., Suzzi, S., and Perry, V.H. (2013). Regulation of Microglial Proliferation during Chronic Neurodegeneration. The Journal of Neuroscience *33*, 2481-2493.

Guo, Q., Owen, D.R., Rabiner, E.A., Turkheimer, F.E., and Gunn, R.N. (2012). Identifying improved TSPO PET imaging probes through biomathematics: The impact of multiple TSPO binding sites in vivo. NeuroImage *60*, 902-910.

Guo, Q., Owen, D.R., Rabiner, E.A., Turkheimer, F.E., and Gunn, R.N. (2014). A graphical method to compare the in vivo binding potential of PET radioligands in the absence of a reference region: application to [C]PBR28 and [F]PBR111 for TSPO imaging. J Cereb Blood Flow Metab.

Hannestad, J., DellaGioia, N., Gallezot, J.-D., Lim, K., Nabulsi, N., Esterlis, I., Pittman, B., Lee, J.-Y., O'Connor, K.C., Pelletier, D.*, et al.* (2013). The neuroinflammation marker translocator protein is not elevated in individuals with mild-to-moderate depression: A [(11)C]PBR28 PET study. Brain, behavior, and immunity *33*, 131-138.

Hannestad, J., Gallezot, J.-D., Schafbauer, T., Lim, K., Kloczynski, T., Morris, E.D., Carson, R.E., Ding, Y.-S., and Cosgrove, K.P. (2012). Endotoxin-induced systemic inflammation activates microglia: [11C]PBR28 positron emission tomography in nonhuman primates. NeuroImage *63*, 232-239.

Hofstetter, C.B., K.A., Hoegl, S., Flondor, M., Scheller, B., Muhl, H. ... Zwissler, B. (2007). Norepinephrine and vasopressin counteract anti-inflammatory effects of isoflurane in endotoxemic rats. . International Journal of Molecular Medicine, *20,* , 597-604. .

Hou, Y., Wu, C.F., Yang, J.Y., He, X., Bi, X.L., Yu, L., and Guo, T. (2006). Effects of clozapine, olanzapine and haloperidol on nitric oxide production by lipopolysaccharide-activated N9 cells. Progress in Neuro-Psychopharmacology and Biological Psychiatry *30*, 1523-1528.

Howes, B., Turkheimer, (2011). Dopamine Synthesis Capacity Before Onset of Psychosis: A Prospective [18F]-DOPA PET Imaging Study. Am J Psychiatry *2011;168:1311-1317. 10.1176*.

Howes, O., McCutcheon, R., and Stone, J. (2015). Glutamate and dopamine in schizophrenia: An update for the 21st century. Journal of Psychopharmacology *29*, 97-115.

Howes, O.D., and Kapur, S. (2009). The Dopamine Hypothesis of Schizophrenia: Version III—The Final Common Pathway. Schizophrenia Bulletin *35*, 549-562.

Howes, O.D., and Murray, R.M. (2014). Schizophrenia: an integrated sociodevelopmental-cognitive model. The Lancet *383*, 1677-1687.

Hu, X., Zhou, H., Zhang, D., Yang, S., Qian, L., Wu, H.-M., Chen, P.-S., Wilson, B., Gao, H.-M., Lu, R.-b.*, et al.* (2011). Clozapine Protects Dopaminergic Neurons from Inflammation-Induced Damage by Inhibiting Microglial Overactivation. Journal of Neuroimmune Pharmacology, 1-15.

Imaizumi, M., Kim, H.-J., Zoghbi, S.S., Briard, E., Hong, J., Musachio, J.L., Ruetzler, C., Chuang, D.-M., Pike, V.W., Innis, R.B.*, et al.* (2007). PET imaging with [11C]PBR28 can localize and quantify upregulated peripheral benzodiazepine receptors associated with cerebral ischemia in rat. Neuroscience Letters *411*, 200-205.

Ito, D., Imai, Y., Ohsawa, K., Nakajima, K., Fukuuchi, Y., and Kohsaka, S. (1998). Microglia-specific localisation of a novel calcium binding protein, Iba1. Molecular Brain Research *57*, 1-9.

Jones, C.A., Watson, D.J.G., and Fone, K.C.F. (2011). Animal models of schizophrenia. British Journal of Pharmacology *164*, 1162-1194.

Jones, S.R., Carley, S., and Harrison, M. (2003). An introduction to power and sample size estimation. Emergency Medicine Journal *20*, 453-458.

Juckel, G., Manitz, M.P., BrÃ¼ne, M., Friebe, A., Heneka, M.T., and Wolf, R.J. (2011). Microglial activation in a neuroinflammational animal model of schizophrenia â€" a pilot study. Schizophrenia Research *131*, 96-100.

Kapur, S., VanderSpek, S.C., Brownlee, B.A., and Nobrega, J.N. (2003). Antipsychotic Dosing in Preclinical Models Is Often Unrepresentative of the Clinical Condition: A Suggested Solution Based on in Vivo Occupancy. Journal of Pharmacology and Experimental Therapeutics *305*, 625-631.

Karlstetter, M., Nothdurfter, C., Aslanidis, A., Moeller, K., Horn, F., Scholz, R., Neumann, H., Weber, B.H., Rupprecht, R., and Langmann, T. (2014). Translocator protein (18kDa) (TSPO) is expressed in reactive retinal microglia and modulates microglial inflammation and phagocytosis. Journal of Neuroinflammation *11*, 3.

Karperien, A., Ahammer, H., and Jelinek, H.F. (2013). Quantitating the subtleties of microglial morphology with fractal analysis. Frontiers in Cellular Neuroscience *7*, 3.

Kato, T., Mizoguchi, Y., Monji, A., Horikawa, H., Suzuki, S.O., Seki, Y., Iwaki, T., Hashioka, S., and Kanba, S. (2008). Inhibitory effects of aripiprazole on interferon-γ-induced microglial activation via intracellular Ca2+ regulation in vitro. Journal of Neurochemistry *106*, 815-825.

Kato, T., Monji, A., Hashioka, S., and Kanba, S. (2007). Risperidone significantly inhibits interferon-Î³-induced microglial activation in vitro. Schizophrenia Research *92*, 108-115.

Kato, T.A., Monji, A., Yasukawa, K., Mizoguchi, Y., Horikawa, H., Seki, Y., Hashioka, S., Han, Y.-H., Kasai, M., Sonoda, N.*, et al.* (2011). Aripiprazole inhibits superoxide generation from phorbol-myristate-acetate (PMA)-stimulated microglia in vitro: Implication for antioxidative psychotropic actions via microglia. Schizophrenia Research *129*, 172-182.

Kay, S.R., Fiszbein, A., and Opler, L.A. (1987). The Positive and Negative Syndrome Scale (PANSS) for Schizophrenia. Schizophrenia Bulletin *13*, 261-276.

Kenk, M., Selvanathan, T., Rao, N., Suridjan, I., Rusjan, P., Remington, G., Meyer, J.H., Wilson, A.A., Houle, S., and Mizrahi, R. (2015). Imaging Neuroinflammation in Gray and White Matter in Schizophrenia: An In-Vivo PET Study With [18F]-FEPPA. Schizophrenia Bulletin *41*, 85-93.

Kettenmann, H., Banati, R., and Walz, W. (1993). Electrophysiological behavior of microglia. Glia *7*, 93-101.

Kettenmann, H., Hanisch, U.-K., Noda, M., and Verkhratsky, A. (2011). Physiology of Microglia. Physiological Reviews *91*, 461-553.

Kettenmann, H., Kirchhoff, F., and Verkhratsky, A. (2013). Microglia: New Roles for the Synaptic Stripper. Neuron *77*, 10-18.

Khandaker, G.M., Pearson, R.M., Zammit, S., Lewis, G., and Jones, P.B. (2014). Association of serum interleukin 6 and c-reactive protein in childhood with depression and psychosis in young adult life: A population-based longitudinal study. JAMA Psychiatry *71*, 1121-1128.

Kobayashi, K., Imagama, S., Ohgomori, T., Hirano, K., Uchimura, K., Sakamoto, K., Hirakawa, A., Takeuchi, H., Suzumura, A., Ishiguro, N.*, et al.* (2013). Minocycline selectively inhibits M1 polarization of microglia. Cell Death Dis *4*, e525.

Koguchi, K., Nakatsuji, Y., Okuno, T., Sawada, M., and Sakoda, S. (2003). Microglial cell cycle-associated proteins control microglial proliferation in vivo and in vitro and are regulated by GM-CSF and density-dependent inhibition. Journal of Neuroscience Research *74*, 898-905.

Kondo, S., Kohsaka, S., and Okabe, S. (2011). Long-term changes of spine dynamics and microglia after transient peripheral immune response triggered by LPS in vivo. Molecular Brain *4*, 27.

Kornbrot, D. (2005). Spearman's Rho. In Encyclopedia of Statistics in Behavioral Science (John Wiley & Sons, Ltd).

Kowalski, J., Labuzek, K., and Herman, Z.S. (2003). Flupentixol and trifluperidol reduce secretion of tumor necrosis factor-α and nitric oxide by rat microglial cells. Neurochemistry International *43*, 173-178.

Kozlowski, C., and Weimer, R.M. (2012). An Automated Method to Quantify Microglia Morphology and Application to Monitor Activation State Longitudinally In Vivo. PLoS ONE *7*, e31814.

Kraepelin, E. (1893). Ein Kurzes Lehrbuch der Psychiatrie. 4 Aufl. Barth, Lepzig.

Kreisl, W.C., Fujita, M., Fujimura, Y., Kimura, N., Jenko, K.J., Kannan, P., Hong, J., Morse, C.L., Zoghbi, S.S., Gladding, R.L.*, et al.* (2010). Comparison of [11C]-(R)-PK 11195 and [11C]PBR28, two radioligands for translocator protein (18 kDa) in human and monkey: Implications for positron emission tomographic imaging of this inflammation biomarker. NeuroImage *49*, 2924-2932.

Kreisl, W.C., Jenko, K.J., Hines, C.S., Hyoung Lyoo, C., Corona, W., Morse, C.L., Zoghbi, S.S., Hyde, T., Kleinman, J.E., Pike, V.W.*, et al.* (2013). A genetic polymorphism for translocator protein 18 kDa affects both in vitro and in vivo radioligand binding in human brain to this putative biomarker of neuroinflammation. J cereb blood flow metab.

Kyrylkova, K., Kyryachenko, S., Leid, M., and Kioussi, C. (2012). Detection of Apoptosis by TUNEL Assay. In Odontogenesis: Methods and Protocols, C. Kioussi, ed. (Totowa, NJ: Humana Press), pp. 41-47.

Labuzek, K., Kowalski, J., Gabryel, B., and Herman, Z.S. (2005). Chlorpromazine and loxapine reduce interleukin-1β and interleukin-2 release by rat mixed glial and microglial cell cultures. European Neuropsychopharmacology *15*, 23-30.

Laruelle, M., Slifstein, M., and Huang, Y. (2002). Positron emission tomography: imaging and quantification of neurotransporter availability. Methods *27*, 287-299.

Lassance, L., Haghiac, M., Minium, J., Catalano, P., and Mouzon, S.H.-d. (2015). Obesity-Induced Down-Regulation of the Mitochondrial Translocator Protein (TSPO) Impairs Placental Steroid Production. The Journal of Clinical Endocrinology & Metabolism *100*, E11-E18.

Lawson, L., Perry, V.H., Dri, P., and Gordon, S. (1990). Heterogeneity in the distribution and morphology of microglia in the normal adult mouse brain. Neuroscience *39*, 151-170.

Lawson, L.J., Perry, V. H. Dri, P., Gordon, S., (1990;). Heterogeneity in the distribution and morphology of microglia in the normal adult mouse brain. Neuroscience *39(1): 151–170.*

Lercher, M.J., and Wienhard, K. (1994). Scatter correction in 3-D PET. Medical Imaging, IEEE Transactions on *13*, 649-657.

Levene, H. (1960). Robust tests for equality of variances. In Ingram Olkin, Harold Hotelling, et alia Stanford University Press pp 278–292.

Lim, A., and Marsland, A. (2013). Peripheral Pro-inflammatory Cytokines and Cognitive Aging: The Role of Metabolic Risk. In The Wiley-Blackwell Handbook of Psychoneuroimmunology (John Wiley & Sons Ltd), pp. 330-346.

Liskowsky, D.R., and Potter, L.T. (1987). Dopamine D2 receptors in the striatum and frontal cortex following chronic administration of haloperidol. Neuropharmacology *26*, 481-483.

Llorente, M.D., and Urrutia, V. (2006). Diabetes, Psychiatric Disorders, and the Metabolic Effects of Antipsychotic Medications. Clinical Diabetes *24*, 18-24.

Lloyd-Burton, S.M., York, E.M., Anwar, M.A., Vincent, A.J., and Roskams, A.J. (2013). SPARC Regulates Microgliosis and Functional Recovery following Cortical Ischemia. The Journal of Neuroscience *33*, 4468-4481.

Lockhart, A., Davis, B., Matthews, J.C., Rahmoune, H., Hong, G., Gee, A., Earnshaw, D., and Brown, J. (2003). The peripheral benzodiazepine receptor ligand PK11195 binds with high affinity to the acute phase reactant alpha1-acid glycoprotein: implications for the use of the ligand as a CNS inflammatory marker. Nucl Med Biol *30*, 199-206.

Loggia, M.L., Chonde, D.B., Akeju, O., Arabasz, G., Catana, C., Edwards, R.R., Hill, E., Hsu, S., Izquierdo-Garcia, D., Ji, R.-R*., et al.* (2015). Evidence for brain glial activation in chronic pain patients.

Lyoo, C.H., Ikawa, M., Liow, J.-S., Zoghbi, S.S., Morse, C.L., Pike, V.W., Fujita, M., Innis, R.B., and Kreisl, W.C. (2015). Cerebellum Can Serve As a Pseudo-Reference Region in Alzheimer Disease to Detect Neuroinflammation Measured with PET Radioligand Binding to Translocator Protein. Journal of Nuclear Medicine *56*, 701-706.

Maeda, J., Zhang, M.-R., Okauchi, T., Ji, B., Ono, M., Hattori, S., Kumata, K., Iwata, N., Saido, T.C., Trojanowski, J.Q., *et al.* (2011). In vivo positron emission tomographic imaging of glial responses to amyloid-β and tau pathologies in mouse models of Alzheimer's disease and related disorders. The Journal of neuroscience : the official journal of the Society for Neuroscience *31*, 4720-4730.

Marsman, A., van den Heuvel, M.P., Klomp, D.W.J., Kahn, R.S., Luijten, P.R., and Hulshoff Pol, H.E. (2013). Glutamate in Schizophrenia: A Focused Review and Meta-Analysis of 1H-MRS Studies. Schizophrenia Bulletin *39*, 120-129.

Martin, A., Boisgard, R., Theze, B., Van Camp, N., Kuhnast, B., Damont, A., Kassiou, M., Dolle, F., and Tavitian, B. (2009). Evaluation of the PBR/TSPO radioligand [lsqb]18F[rsqb]DPA-714 in a rat model of focal cerebral ischemia. J Cereb Blood Flow Metab *30*, 230-241.

Martín, A., Boisgard, R., Thézé, B., Van Camp, N., Kuhnast, B., Damont, A., Kassiou, M., Dollé, F., and Tavitian, B. (2010). Evaluation of the PBR/TSPO radioligand [(18)F]DPA-714 in a rat model of focal cerebral ischemia. Journal of Cerebral Blood Flow and Metabolism: Official Journal of the International Society of Cerebral Blood Flow and Metabolism *30*, 230-241.

Martins-de-Souza, D., Schmitt, A., Röder, R., Lebar, M., Schneider-Axmann, T., Falkai, P., and Turck, C.W. (2010). Sex-specific proteome differences in the anterior cingulate cortex of schizophrenia. Journal of Psychiatric Research *44*, 989-991.

McGlashan, T.H., and Hoffman, R.E. (2000). Schizophrenia as a disorder of developmentally reduced synaptic connectivity. Arch Gen Psychiatry *57*, 637-648.

McGrath, J., Saha, S., Chant, D., and Welham, J. (2008). Schizophrenia: A Concise Overview of Incidence, Prevalence, and Mortality. Epidemiologic Reviews *30*, 67-76.

Mead, E.L., Mosley, A., Eaton, S., Dobson, L., Heales, S.J., and Pocock, J.M. (2012). Microglial neurotransmitter receptors trigger superoxide production in microglia; consequences for microglial–neuronal interactions. Journal of Neurochemistry *121*, 287-301.

Meisenzahl EM, R.D., Kirner A (2001). Association of an interleukin-1β genetic polymorphism with altered brain structure in patients with schizophrenia. . Am J Psychiatry *158: 1316–1319.*

Miller, B.J., Buckley, P., Seabolt, W., Mellor, A., and Kirkpatrick, B. (2011). Meta-Analysis of Cytokine Alterations in Schizophrenia: Clinical Status and Antipsychotic Effects. Biological Psychiatry *70*, 663-671.

Mittelbronn, M., Dietz, K., Schluesener, H. J. & Meyermann, R. (2001). Local distribution of microglia in the normal adult human central nervous system differs by up to one order of magnitude. . Acta Neuropathol (Berl) *101, 249–255*.

Miyamoto, S., Duncan, G.E., Marx, C.E., and Lieberman, J.A. (2004). Treatments for schizophrenia: a critical review of pharmacology and mechanisms of action of antipsychotic drugs. Mol Psychiatry *10*, 79-104.

Miyamoto, S., Miyake, N., Jarskog, L.F., Fleischhacker, W.W., and Lieberman, J.A. (2012). Pharmacological treatment of schizophrenia: a critical review of the pharmacology and clinical effects of current and future therapeutic agents. Mol Psychiatry.

Miyaoka, T.M., PhD; Yasukawa, Rei MD, PhD; Yasuda, Hideaki MD; Hayashida, Maiko MD; Inagaki, Takuji MD, PhD; Horiguchi, Jun MD, PhD (2008). Minocycline as Adjunctive Therapy for Schizophrenia: An Open-Label Study. Clinical Neuropharmacology *31(5):287-292*.

Montgomery, A.J., Thielemans, K., Mehta, M.A., Turkheimer, F., Mustafovic, S., and Grasby, P.M. (2006). Correction of Head Movement on PET Studies: Comparison of Methods. Journal of Nuclear Medicine *47*, 1936-1944.

Moorhead, T.W.J., McKirdy, J., Sussmann, J.E.D., Hall, J., Lawrie, S.M., Johnstone, E.C., and McIntosh, A.M. (2007). Progressive Gray Matter Loss in Patients with Bipolar Disorder. Biological Psychiatry *62*, 894-900.

Morkuniene, R., Cizas, P., Jankeviciute, S., Petrolis, R., Arandarcikaite, O., Krisciukaitis, A., and Borutaite, V. (2015). Small Aβ1–42 oligomer-induced membrane depolarization of neuronal and microglial cells: Role of N-methyl-D-aspartate receptors. Journal of Neuroscience Research *93*, 475-486.

Morrison, H.W., and Filosa, J.A. (2013). A quantitative spatiotemporal analysis of microglia morphology during ischemic stroke and reperfusion. Journal of Neuroinflammation *10*, 4-4.

Müller, N., Riedel M, Scheppach C, Brandstätter B, Sokullu S, Krampe K, Ulmschneider M, Engel RR, Möller HJ, Schwarz MJ (2002). Beneficial antipsychotic effects of celecoxib add-on therapy compared to risperidone alone in schizophrenia. Am J Psychiatry *159*, 1029-1034.

Näkki, R., Nickolenko, J., Chang, J., Sagar, S.M., and Sharp, F.R. (1996). Haloperidol Prevents Ketamine- and Phencyclidine-Induced HSP70 Protein Expression but Not Microglial Activation. Experimental Neurology *137*, 234-241.

Narendran, R., Lopresti, B.J., Mason, N.S., Deuitch, L., Paris, J., Himes, M.L., Kodavali, C.V., and Nimgaonkar, V.L. (2014). Cocaine Abuse in Humans Is Not Associated with Increased Microglial Activation: An 18-kDa Translocator Protein Positron Emission Tomography Imaging Study with [(11)C]PBR28. The Journal of Neuroscience *34*, 9945-9950.

Nasrallah, H.A., Schwarzkopf, S.B., Olson, S.C., and Coffman, J.A. (1990). Gender Differences in Schizophrenia on MRI Brain Scans. Schizophrenia Bulletin *16*, 205-210.

Natesan, S., Ashworth, S., Nielsen, J., Tang, S.P., Salinas, C., Kealey, S., Lauridsen, J.B., Stensbøl, T.B., Gunn, R.N., Rabiner, E.A.*, et al.* (2014). Effect of chronic antipsychotic

treatment on striatal phosphodiesterase 10A levels: a [(11)C]MP-10 PET rodent imaging study with ex vivo confirmation. Translational Psychiatry *4*, e376.

Neumann, H., Kotter, M.R., and Franklin, R.J.M. (2009). Debris clearance by microglia: an essential link between degeneration and regeneration. Brain *132*, 288-295.

Nimmerjahn, A., Kirchhoff, F., and Helmchen, F. (2005). Resting Microglial Cells Are Highly Dynamic Surveillants of Brain Parenchyma in Vivo. Science *308*, 1314-1318.

Norden, D.M., and Godbout, J.P. (2013). Microglia of the Aged Brain: Primed to be Activated and Resistant to Regulation. Neuropathology and applied neurobiology *39*, 19-34.

Nunes, S.O.V., Matsuo, T., Kaminami, M.S., Watanabe, M.A.E., Reiche, E.M.V., and Itano, E.N. (2006). An autoimmune or an inflammatory process in patients with schizophrenia, schizoaffective disorder, and in their biological relatives. Schizophrenia Research *84*, 180-182.

O'Sullivan, D., Green, L., Stone, S., Zareie, P., Kharkrang, M., Fong, D., Connor, B., and La Flamme, A.C. (2014). Treatment with the Antipsychotic Agent, Risperidone, Reduces Disease Severity in Experimental Autoimmune Encephalomyelitis. PLoS ONE *9*, e104430.

Ochoa, S., Usall, J., Jesús Cobo,2 Xavier Labad,3 and Jayashri Kulkarni4 (2012). Gender Differences in Schizophrenia and First-Episode Psychosis: A Comprehensive Literature Review. Schizophrenia Research and Treatment *2012*, 9.

Ortiz-Gil, J., Pomarol-Clotet, E., Salvador, R., Canales-RodrÃguez, E.J., SarrÃ³, S., Gomar, J.s.J., Guerrero, A., Sans-Sansa, B., Capdevila, A., JunquÃ©, C.*, et al.* (2011). Neural correlates of cognitive impairment in schizophrenia. The British Journal of Psychiatry *199*, 202-210.

Otsu (1979). A Threshold Selection Method from Gray-Level Histograms. Systems, Man and Cybernetics, IEEE Transactions on *9*, 62-66.

Owen, D.R., Guo, Q., Kalk, N.J., Colasanti, A., Kalogiannopoulou, D., Dimber, R., Lewis, Y.L., Libri, V., Barletta, J., Ramada-Magalhaes, J.*, et al.* (2014). Determination of [C]PBR28 binding potential in vivo: a first human TSPO blocking study. J Cereb Blood Flow Metab.

Owen, D.R., Howell, O.W., Tang, S.-P., Wells, L.A., Bennacef, I., Bergstrom, M., Gunn, R.N., Rabiner, E.A., Wilkins, M.R., Reynolds, R.*, et al.* (2010). Two binding sites for [lsqb]3H[rsqb]PBR28 in human brain: implications for TSPO PET imaging of neuroinflammation. J Cereb Blood Flow Metab *30*, 1608-1618.

Owen, D.R., Yeo, A.J., Gunn, R.N., Song, K., Wadsworth, G., Lewis, A., Rhodes, C., Pulford, D.J., Bennacef, I., Parker, C.A.*, et al.* (2011). An 18-kDa Translocator Protein (TSPO) polymorphism explains differences in binding affinity of the PET radioligand PBR28. J Cereb Blood Flow Metab *32*, 1-5.

Paans, A.M.J., van Waarde, A., Elsinga, P.H., Willemsen, A.T.M., and Vaalburg, W. (2002). Positron emission tomography: the conceptual idea using a multidisciplinary approach. Methods *27*, 195-207.

Pantelis, C., Velakoulis, D., McGorry, P.D., Wood, S.J., Suckling, J., Phillips, L.J., Yung, A.R., Bullmore, E.T., Brewer, W., Soulsby, B.*, et al.* (2003a). Neuroanatomical abnormalities before and after onset of psychosis: a cross-sectional and longitudinal MRI comparison. The Lancet *361*, 281-288.

Pantelis, C., Velakoulis, D., McGorry, P.D., Wood, S.J., Suckling, J., Phillips, L.J., Yung, A.R., Bullmore, E.T., Brewer, W., Soulsby, B.*, et al.* (2003b). Neuroanatomical abnormalities before and after onset of psychosis: A cross-sectional and longitudinal MRI comparison. Lancet *361*, 281-288.

Paolicelli, R.C., Bolasco, G., Pagani, F., Maggi, L., Scianni, M., Panzanelli, P., Giustetto, M., Ferreira, T.A., Guiducci, E., Dumas, L.*, et al.* (2011). Synaptic Pruning by Microglia Is Necessary for Normal Brain Development. Science *333*, 1456-1458.

Papadopoulos, V., Amri, H., Boujrad, N., Cascio, C., Culty, M., Garnier, M., Hardwick, M., Li, H., Vidic, B., Brown, A.S.*, et al.* (1997). Peripheral benzodiazepine receptor in cholesterol transport and steroidogenesis. Steroids *62*, 21-28.

Park, E., Gallezot, J.-D., Delgadillo, A., Liu, S., Planeta, B., Lin, S.-F., O'Connor, K., Lim, K., Lee, J.-Y., Chastre, A.*, et al.* (2015a). 11C-PBR28 imaging in multiple sclerosis patients and healthy controls: test-retest reproducibility and focal visualization of active white matter areas. European Journal of Nuclear Medicine and Molecular Imaging *42*, 1081-1092.

Park, Y., Franklin, J.M., Schneeweiss, S., Levin, R., Crystal, S., Gerhard, T., and Huybrechts, K.F. (2015b). Antipsychotics and Mortality: Adjusting for Mortality Risk Scores to Address Confounding by Terminal Illness. Journal of the American Geriatrics Society, n/a-n/a.

Parkhurst, C.N., Yang, G., Ninan, I., Savas, J.N., Yates, J.R., 3rd, Lafaille, J.J., Hempstead, B.L., Littman, D.R., and Gan, W.B. (2013). Microglia promote learning-dependent synapse formation through brain-derived neurotrophic factor. Cell *155*, 1596-1609.

Perego, C., Fumagalli, S., and De Simoni, M.-G. (2011). Temporal pattern of expression and colocalization of microglia/macrophage phenotype markers following brain ischemic injury in mice. Journal of Neuroinflammation *8*, 174.

Perkins, D.O., Jeffries, C.D., Addington, J., Bearden, C.E., Cadenhead, K.S., Cannon, T.D., Cornblatt, B.A., Mathalon, D.H., McGlashan, T.H., Seidman, L.J.*, et al.* (2014). Towards a Psychosis Risk Blood Diagnostic for Persons Experiencing High-Risk Symptoms: Preliminary Results From the NAPLS Project. Schizophrenia Bulletin.

Pisa, F.E., Cosano, G., Giangreco, M., Giorgini, T., Biasutti, E., and Barbone, F. (2014). Prescribing practice and off-label use of psychotropic medications in post-acute brain injury rehabilitation centres: A cross-sectional survey. Brain Injury *0*, 1-9.

Pocock, J.M., and Kettenmann, H. (2007). Neurotransmitter receptors on microglia. Trends in Neurosciences *30*, 527-535.

Politis, M., Pavese, N., Tai, Y.F., Kiferle, L., Mason, S.L., Brooks, D.J., Tabrizi, S.J., Barker, R.A., and Piccini, P. (2011). Microglial activation in regions related to cognitive function predicts disease onset in Huntington's disease: A multimodal imaging study. Human Brain Mapping *32*, 258-270.

Radewicz, K., Garey LJ, Gentleman SM, Reynolds R (2000). Increase in HLA-DR immunoreactive microglia in frontal and temporal cortex of chronic schizophrenics. J Neuropathol Exp Neurol *59:*, 137–150.

Radua, J., Borgwardt, S., Crescini, A., Mataix-Cols, D., Meyer-Lindenberg, A., McGuire, P.K., and Fusar-Poli, P. (2012). Multimodal meta-analysis of structural and functional brain changes in first episode psychosis and the effects of antipsychotic medication. Neuroscience & Biobehavioral Reviews *36*, 2325-2333.

Ransohoff, R.M., and Cardona, A.E. (2010). The myeloid cells of the central nervous system parenchyma. Nature *468*, 253-262.

Reilhac, A., Tomeï, S., Buvat, I., Michel, C., Keheren, F., and Costes, N. (2008). Simulation-based evaluation of OSEM iterative reconstruction methods in dynamic brain PET studies. NeuroImage *39*, 359-368.

Reuben, D.B., Cheh, A.I., Harris, T.B., Ferrucci, L., Rowe, J.W., Tracy, R.P., and Seeman, T.E. (2002). Peripheral Blood Markers of Inflammation Predict Mortality and Functional Decline in High-Functioning Community-Dwelling Older Persons. Journal of the American Geriatrics Society *50*, 638-644.

Rey-Villamizar, N., Somasundar, V., Megjhani, M., Xu, Y., Lu, Y., Padmanabhan, R., Trett, K., Shain, W., and Roysam, B. (2014). Large-scale automated image analysis for computational profiling of brain tissue surrounding implanted neuroprosthetic devices using Python. Frontiers in Neuroinformatics *8*, 39.

Rissanen, E., Tuisku, J., Rokka, J., Paavilainen, T., Parkkola, R., Rinne, J.O., and Airas, L. (2014). In Vivo Detection of Diffuse Inflammation in Secondary Progressive Multiple Sclerosis Using PET Imaging and the Radioligand 11C-PK11195. Journal of Nuclear Medicine *55*, 939-944.

Rizzo, G., Veronese, M., Tonietto, M., Zanotti-Fregonara, P., Turkheimer, F.E., and Bertoldo, A. (2014). Kinetic modeling without accounting for the vascular component impairs the quantification of [lsqb]11C[rsqb]PBR28 brain PET data. J Cereb Blood Flow Metab.

Samaha, A.-N.l., Reckless, G.E., Seeman, P., Diwan, M., Nobrega, J.N., and Kapur, S. (2008). Less Is More: Antipsychotic Drug Effects Are Greater with Transient Rather Than Continuous Delivery. Biological Psychiatry *64*, 145-152.

Sandu, A.-L., Rasmussen Jr, I.-A., Lundervold, A., Kreuder, F., Neckelmann, G., Hugdahl, K., and Specht, K. (2008). Fractal dimension analysis of MR images reveals grey matter structure irregularities in schizophrenia. Computerized Medical Imaging and Graphics *32*, 150-158.

Savchenko, V.L., Nikonenko, I.R., Skibo, G.G., and McKanna, J.A. (1997). Distribution of microglia and astrocytes in different regions of the normal adult rat brain. Neurophysiology *29*, 343-351.

Schmued, L.C., and Hopkins, K.J. (2000). Fluoro-Jade: Novel Fluorochromes for Detecting Toxicant-Induced Neuronal Degeneration. Toxicologic Pathology *28*, 91-99.

Schnieder, T.P.P., Trencevska, I.M.P.H., Rosoklija, G.M.D.P., Stankov, A.M.D., Mann, J.J.M.D., Smiley, J.P., and Dwork, A.J.M.D. (2014). Microglia of Prefrontal White Matter in Suicide. Journal of Neuropathology & Experimental Neurology *73*, 880-890.

Schuitemaker, A., Kropholler, M.A., Boellaard, R., van der Flier, W.M., Kloet, R.W., van der Doef, T.F., Knol, D.L., Windhorst, A.D., Luurtsema, G., Barkhof, F.*, et al.* (2013). Microglial activation in Alzheimer's disease: an (R)-[11C]PK11195 positron emission tomography study. Neurobiology of Aging *34*, 128-136.

Schuitemaker, A., van der Doef, T.F., Boellaard, R., van der Flier, W.M., Yaqub, M., Windhorst, A.D., Barkhof, F., Jonker, C., Kloet, R.W., Lammertsma, A.A.*, et al.* (2012). Microglial activation in healthy aging. Neurobiology of Aging *33*, 1067-1072.

Seeman, P., and Kapur, S. (2000). Schizophrenia: More dopamine, more D(2) receptors. Proceedings of the National Academy of Sciences of the United States of America *97*, 7673-7675.

Seki, Y., Kato, T.A., Monji, A., Mizoguchi, Y., Horikawa, H., Sato-Kasai, M., Yoshiga, D., and Kanba, S. (2013). Pretreatment of aripiprazole and minocycline, but not haloperidol, suppresses oligodendrocyte damage from interferon-γ-stimulated microglia in co-culture model. Schizophrenia Research *151*, 20-28.

Sengupta, P. (2013). The Laboratory Rat: Relating Its Age With Human's. International Journal of Preventive Medicine *4*, 624-630.

Setiawan, E., Wilson, A.A., Mizrahi, R., and et al. (2015). ROle of translocator protein density, a marker of neuroinflammation, in the brain during major depressive episodes. JAMA Psychiatry *72*, 268-275.

Shapiro, S., Wilk, M. B. (1965). An analysis of variance test for normality (complete samples). Biometrika *52*, 591-611.

Sheridan, G.K., and Murphy, K.J. (2013). Neuron–glia crosstalk in health and disease: fractalkine and CX3CR1 take centre stage. Open Biology *3*.

Sheridan, G.K., Wdowicz, A., Pickering, M., Watters, O., Halley, P., O'Sullivan, N., Mooney, C., O'Connell, D.J., O'Connor, J.J., and Murphy, K.J. (2014). CX3CL1 is up-regulated in the

rat hippocampus during memory-associated synaptic plasticity. Frontiers in Cellular Neuroscience *8*.

Singh, M., Sumien, N., Kyser, C., and Simpkins, J.W. (2008). ESTROGENS AND PROGESTERONE AS NEUROPROTECTANTS: WHAT ANIMAL MODELS TEACH US. Frontiers in bioscience : a journal and virtual library *13*, 1083-1089.

Spinks, T.J., Jones, T., Bloomfield, P.M., Bailey, D.L., Miller, M., Hogg, D., Jones, W.F., Vaigneur, K., Reed, J., Young, J., Newport, D., Moyers, C., Casey, M.E., Nutt, R., (2000). Physical characteristics of the ECAT EXACT3D positron tomograph. Phys Med Biol *45, 2601-2618*.

Spitzer, R.L., Williams, J.W., Gibbon, M., and First, M.B. (1992). The structured clinical interview for dsm-iii-r (scid): I: history, rationale, and description. Archives of General Psychiatry *49*, 624-629.

Staniland, A.A., Clark, A.K., Wodarski, R., Sasso, O., Maione, F., D'Acquisto, F., and Malcangio, M. (2010). Reduced inflammatory and neuropathic pain and decreased spinal microglial response in fractalkine receptor (CX3CR1) knockout mice. Journal of Neurochemistry *114*, 1143-1157.

Steiner, J., Bielau, H., Brisch, R., Danos, P., Ullrich, O., Mawrin, C., Bernstein, H.-G., and Bogerts, B. (2008). Immunological aspects in the neurobiology of suicide: Elevated microglial density in schizophrenia and depression is associated with suicide. Journal of Psychiatric Research *42*, 151-157.

Steiner, J., Mawrin, C., Ziegeler, A., Bielau, H., Ullrich, O., Bernstein, H.-G., and Bogerts, B. (2006). Distribution of HLA-DR-positive microglia in schizophrenia reflects impaired cerebral lateralization. Acta Neuropathol *112*, 305-316.

Stence, N., Waite, M., and Dailey, M.E. (2001). Dynamics of microglial activation: A confocal time-lapse analysis in hippocampal slices. Glia *33*, 256-266.

Stone, J.M., Howes, O.D., Egerton, A., Kambeitz, J., Allen, P., Lythgoe, D.J., O'Gorman, R.L., McLean, M.A., Barker, G.J., and McGuire, P. (2010). Altered Relationship Between Hippocampal Glutamate Levels and Striatal Dopamine Function in Subjects at Ultra High Risk of Psychosis. Biological Psychiatry *68*, 599-602.

Takano, A., Arakawa, R., Ito, H., Tateno, A., Takahashi, H., Matsumoto, R., Okubo, Y., and Suhara, T. (2010). Peripheral benzodiazepine receptors in patients with chronic schizophrenia: a PET study with [11C]DAA1106. The International Journal of Neuropsychopharmacology *13*, 943-950.

Taylor, R.A., and Sansing, L.H. (2013). Microglial Responses after Ischemic Stroke and Intracerebral Hemorrhage. Clinical and Developmental Immunology *2013*, 10.

Taylor, S.T., Julie Markham, and Jim Koenig (2009). Animal Models of Schizophrenia. Schizophrenia Research Forum.

Thaler, J.P., Guyenet, S.J., Dorfman, M.D., Wisse, B.E., and Schwartz, M.W. (2013). Hypothalamic Inflammation: Marker or Mechanism of Obesity Pathogenesis? Diabetes *62*, 2629-2634.

Thompson, P.M., Vidal, C., Giedd, J.N., Gochman, P., Blumenthal, J., Nicolson, R., Toga, A.W., and Rapoport, J.L. (2001). Mapping adolescent brain change reveals dynamic wave of accelerated gray matter loss in very early-onset schizophrenia. Proceedings of the National Academy of Sciences *98*, 11650-11655.

Tonietto, M., Rizzo G, Veronese M, Zanotti-Fregonara P, Fujita M, and Bertoldo A. (2014). Optimal metabolite curve fitting for [ 11 C]PBR28. NeuroReceptor Mapping, Amsterdam, 21-24 May.

Tost, H., Braus, D.F., Hakimi, S., Ruf, M., Vollmert, C., Hohn, F., and Meyer-Lindenberg, A. (2010). Acute D2 receptor blockade induces rapid, reversible remodeling in human cortical-striatal circuits. Nat Neurosci *13*, 920-922.

Tremblay, M.-Ã.v., Lowery, R.L., and Majewska, A.K. (2010). Microglial Interactions with Synapses Are Modulated by Visual Experience. PLoS Biol *8*, e1000527.

Tremblay, M.-Ã.v., Stevens, B., Sierra, A., Wake, H., Bessis, A., and Nimmerjahn, A. (2011). The Role of Microglia in the Healthy Brain. The Journal of Neuroscience *31*, 16064-16069.

Turkheimer, F.E., Edison, P., Pavese, N., Roncaroli, F., Anderson, A.N., Hammers, A., Gerhard, A., Hinz, R., Tai, Y.F., and Brooks, D.J. (2007). Reference and target region modeling of [11C]-(R)-PK11195 brain studies. Journal of nuclear medicine : official publication, Society of Nuclear Medicine *48*, 158-167.

Turkheimer, Federico E., Rizzo, G., Bloomfield, Peter S., Howes, O., Zanotti-Fregonara, P., Bertoldo, A., and Veronese, M. (2015). The methodology of TSPO imaging with positron emission tomography. Biochemical Society Transactions *43*, 586-592.

Turner, R., and Jones, T. (2003). Techniques for imaging neuroscience. British Medical Bulletin *65*, 3-20.

Turtzo, L., Lescher, J., Janes, L., Dean, D., Budde, M., and Frank, J. (2014). Macrophagic and microglial responses after focal traumatic brain injury in the female rat. Journal of Neuroinflammation *11*, 82.

Tziortzi, A.C., Searle, G.E., Tzimopoulou, S., Salinas, C., Beaver, J.D., Jenkinson, M., Laruelle, M., Rabiner, E.A., and Gunn, R.N. (2011). Imaging dopamine receptors in humans with [11C]-(+)-PHNO: Dissection of D3 signal and anatomy. NeuroImage *54*, 264-277.

van Berckel, B.N., Bossong, M.G., Boellaard, R., Kloet, R., Schuitemaker, A., Caspers, E., Luurtsema, G., Windhorst, A.D., Cahn, W., Lammertsma, A.A.*, et al.* (2008). Microglia Activation in Recent-Onset Schizophrenia: A Quantitative (R)-[11C]PK11195 Positron Emission Tomography Study. Biological Psychiatry *64*, 820-822.

van Haren, N.E.M., Cahn, W., Hulshoff Pol, H.E., and Kahn, R.S. (2008). Schizophrenia as a progressive brain disease. European Psychiatry *23*, 245-254.

Varga, B., Markó, K., Hádinger, N., Jelitai, M., Demeter, K., Tihanyi, K., Vas, Á., and Madarász, E. (2009). Translocator protein (TSPO 18 kDa) is expressed by neural stem and neuronal precursor cells. Neuroscience Letters *462*, 257-262.

Vernon, A.C., Crum, W.R., Lerch, J.P., Chege, W., Natesan, S., Modo, M., Cooper, J.D., Williams, S.C.R., and Kapur, S. (2014). Reduced Cortical Volume and Elevated Astrocyte Density in Rats Chronically Treated With Antipsychotic Drugs—Linking Magnetic Resonance Imaging Findings to Cellular Pathology. Biological Psychiatry *75*, 982-990.

Vernon, A.C., Natesan, S., Modo, M., and Kapur, S. (2011). Effect of Chronic Antipsychotic Treatment on Brain Structure: A Serial Magnetic Resonance Imaging Study with Ex Vivo and Postmortem Confirmation. Biological Psychiatry *69*, 936-944.

Vgontzas, A.N., Papanicolaou, D.A., Bixler, E.O., Kales, A., Tyson, K., and Chrousos, G.P. (1997). Elevation of Plasma Cytokines in Disorders of Excessive Daytime Sleepiness: Role of Sleep Disturbance and Obesity. The Journal of Clinical Endocrinology & Metabolism *82*, 1313-1316.

Walker, M.D., Dinelle, K., Kornelsen, R., Lee, N.V., Miao, Q., Adam, M., Takhar, C., Mak, E., Schulzer, M., Farrer, M.J.*, et al.* (2015). [lsqb]11C[rsqb]PBR28 PET imaging is sensitive to neuroinflammation in the aged rat. J Cereb Blood Flow Metab *35*, 1331-1338.

Walterfang, M., McGuire, P.K., Yung, A.R., Phillips, L.J., Velakoulis, D., Wood, S.J., Suckling, J., Bullmore, E.T., Brewer, W., Soulsby, B.*, et al.* (2008). White matter volume changes in people who develop psychosis. The British Journal of Psychiatry *193*, 210-215.

Wang, M., Yoder, K.K., Gao, M., Mock, B.H., Xu, X.-M., Saykin, A.J., Hutchins, G.D., and Zheng, Q.-H. (2009). Fully automated synthesis and initial PET evaluation of [11C]PBR28. Bioorganic & Medicinal Chemistry Letters *19*, 5636-5639.

Weitz, T.M., and Town, T. (2012). Microglia in Alzheimer's Disease: It's All About Context. International Journal of Alzheimer’s Disease *2012*, 11.

Wilks, S.S. (1938). Weighting systems for linear functions of correlated variables when there is no dependent variable. Psychometrika *3*, 23-40.

Wilson, M. (2003). Haloperidol, but Not Olanzapine, Impairs Cognitive Performance After Traumatic Brain Injury in Rats. American journal of physical medicine & rehabilitation *Vol.82(11), p.871*

Wood, S.J., Pantelis, C., Velakoulis, D., Yücel, M., Fornito, A., and McGorry, P.D. (2008). Progressive Changes in the Development Toward Schizophrenia: Studies in Subjects at Increased Symptomatic Risk. Schizophrenia Bulletin *34*, 322-329.

Yan, B.C., Park, J.H., Ahn, J.H., Kim, I.H., Park, O.K., Lee, J.-C., Yoo, K.-Y., Choi, J.H., Lee, C.H., Hwang, I.K.*, et al.* (2014). Neuroprotection of posttreatment with risperidone, an

atypical antipsychotic drug, in rat and gerbil models of ischemic stroke and the maintenance of antioxidants in a gerbil model of ischemic stroke. Journal of Neuroscience Research *92*, 795-807.

Yaqub, M., van Berckel, B.N., Schuitemaker, A., Hinz, R., Turkheimer, F.E., Tomasi, G., Lammertsma, A.A., and Boellaard, R. (2012). Optimization of supervised cluster analysis for extracting reference tissue input curves in (R)-[(11)C]PK11195 brain PET studies. J Cereb Blood Flow Metab *32*, 1600-1608.

Yung, A.R., Pan Yuen, H., McGorry, P.D., Phillips, L.J., Kelly, D., Dell'olio, M., Francey, S.M., Cosgrave, E.M., Killackey, E., Stanford, C.*, et al.* (2005). Mapping the Onset of Psychosis: The Comprehensive Assessment of At-Risk Mental States. Australian and New Zealand Journal of Psychiatry *39*, 964-971.

Zhang, H., Zhang, Y., Xu, H., Wang, L., Adilijiang, A., Wang, J., Hartle, K., Zhang, Z., Zhang, D., Tan, Q.*, et al.* (2014). Olanzapine ameliorates neuropathological changes and increases IGF-1 expression in frontal cortex of C57BL/6 mice exposed to cuprizone. Psychiatry Research *216*, 438-445.

Zhang, Q., Chen, C., Lü, J., Xie, M., Pan, D., Luo, X., Yu, Z., Dong, Q., and Wang, W. (2009). Cell cycle inhibition attenuates microglial proliferation and production of IL-1β, MIP-1α, and NO after focal cerebral ischemia in the rat. Glia *57*, 908-920.

Zhang, S.-C. (2001). Defining glial cells during CNS development. Nat Rev Neurosci *2*, 840-843.

Zhao, Z.a., Luo, G.a., Liu, M.a., Guo, H.b., Xue, M.a., Wang, X.a., Li, X.-M.a.b., and He, J.a. (2014). Quetiapine reduces microglial number in the hippocampus of a transgenic mouse model of Alzheimer's disease. Neuroreport *25*, 870-874.

Zheng, L.T., Hwang, J., Ock, J., Lee, M.G., Lee, W.-H., and Suk, K. (2008). The antipsychotic spiperone attenuates inflammatory response in cultured microglia via the reduction of proinflammatory cytokine expression and nitric oxide production. Journal of Neurochemistry *107*, 1225-1235.

Zhu, F., Zheng, Y., Ding, Y.Q., Liu, Y., Zhang, X., Wu, R., Guo, X., and Zhao, J. (2014). Minocycline and risperidone prevent microglia activation and rescue behavioral deficits induced by neonatal intrahippocampal injection of lipopolysaccharide in rats. PLoS One *9*, e93966.

# Appendix 1

## *Microglial software development*

The physiology of microglia is complex, with context dependent activity observable *in vitro* and *in vivo* (Kettenmann et al., 2011). The myeloid origin of these cells makes many aspects of their physiological activity similar to that of macrophages and mononuclear cells found in the peripheral bloodstream (Ransohoff and Cardona, 2010). Well characterised roles include phagocytosis of debris (Neumann et al., 2009), migration to injured tissue (Nimmerjahn et al., 2005) and cytokine release (Davalos et al., 2005). However recent evidence has demonstrated how microglial cells are involved in mature synaptic dynamics (Tremblay et al., 2011). Indeed BDNF signalling has been demonstrated as functionally critical for microglial associated synaptic plasticity (Parkhurst et al., 2013). In these novel plastic roles, the morphology of cells is more closely related to a 'ramified' morphology (Figure 30), referred to in older literature as a resting state.

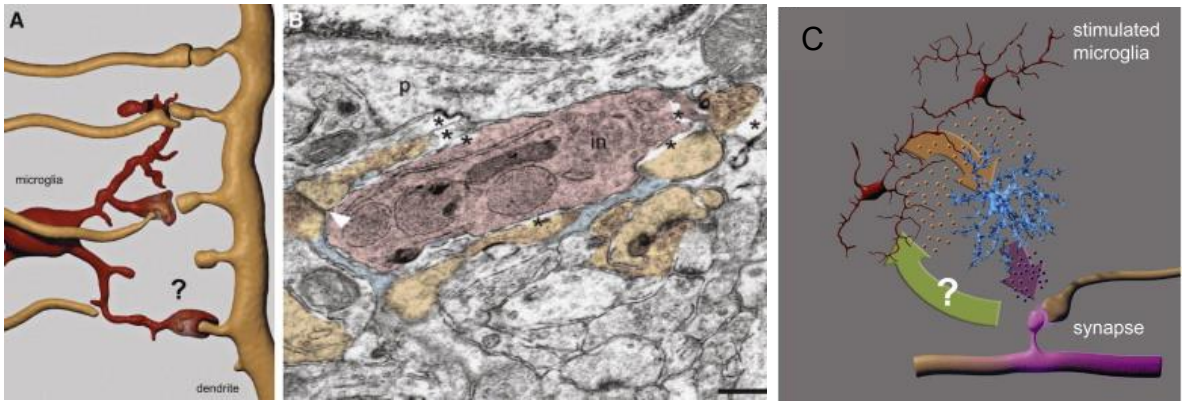


*Figure 30. Microglial processes and synapse interaction.*

Hypothesised roles for microglia, processes/synapses are physically associated through EM reconstruction (A/B) and hypothesised to play a role in synapse modulation (C). Adapted from (Kettenmann et al., 2013).

Microglial cells are particularly difficult to quantify, as the morphology of the cells varies across the cortex (Lawson et al., 1990) as well as in response to exogenous stimuli (Kondo et al., 2011). Cell density is used routinely to assess the activity of microglia, however it is very hard to draw conclusions from this type of analysis as the functions of microglia can be incredibly diverse. Morphology may suggest a specific form of activity, however the morphological response does not seem to be linear or ubiquitous. This is further illustrated by ((Rey-Villamizar et al., 2014),Figure 31) where, particularly evident in C, amoeboid cells and cells of high branch complexity are found abundantly in a close physical proximity.

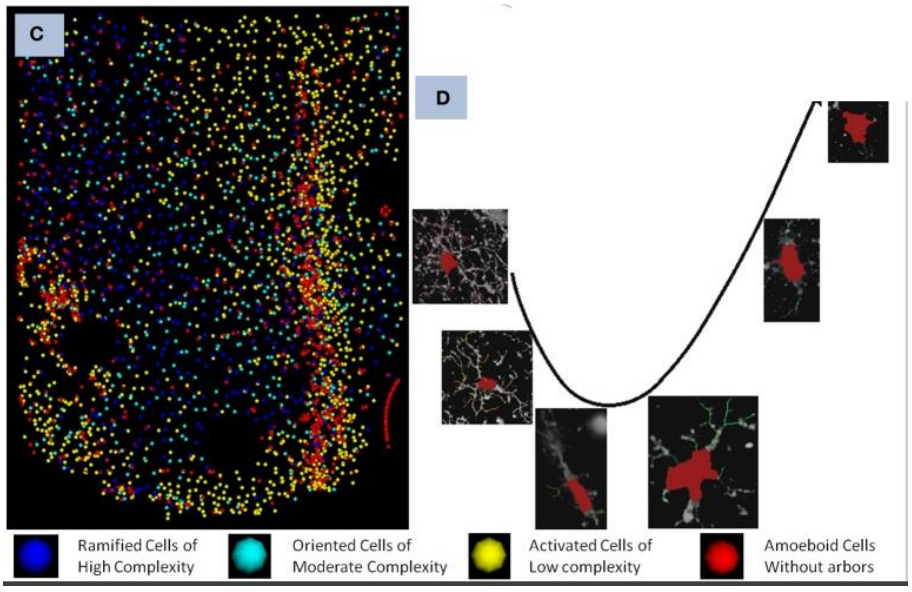


*Figure 31. Microglial morphology variation in tissue*

Distribution of microglial morphologies using python based analysis from tissue wi implanted neuroprosthetic devices. Adapted from (Rey-Villamizar et al., 2014)

Histological assessment of microglia can be conducted using many antibodies and stains, however three main cellular markers are preferred for cortical quantification, Iba-1 (ionized calcium binding adaptor protein-1), CD68 (cluster of differentiation 68) and cd11b (cluster of differentiation 11b). The cellular marker Iba-1 is one of the most commonly used markers for immunohistochemistry and is thought to represent microglial cells independent of state (Ito et al., 1998), meaning cells of all morphology type and activity state should be represented by the staining. CD68 and cd11b mark M1 type inflammatory responsive cells and microglia/macrophage cells respectively (Kobayashi et al., 2013; Perego et al., 2011). (Stence et al., 2001) used time lapse confocal imaging of microglia in hippocampal slices to demonstrate how morphological changes can occur rapidly (branch changes within minutes and cell motility occurring over hours).

*In vitro* analysis can be quite easily implemented in an automated fashion using ImageJ/FIJI (NIH, USA) or similar tools, as background signal is lower than in tissue slices (Boizeau et al., 2013). When analysing tissue samples, reliable segmentation is necessary for accurate quantification. There are a number of features of microglia which are quantified in tissue sections, including density of cells in an ROI, the coverage of the ROI by the processes and the roundness of cell (Kozlowski and Weimer, 2012). While these methods can determine broad dissimilarity between two tissue types, individually they are not particularly descriptive or sensitive to subtle changes in tissue. For example, if assessing the response of microglia to a compound, it may be the case that the density of the cells is reduced, however the morphology and process coverage may become more complex, hence using the traditional methods of counting or coverage, the context would not be described so

accurately. A number of studies have attempted to develop software to analyse microglial cells using a range of assessment criteria. Table 17 outlines the methods used and the criteria analysed in each study.

Automation is an attractive feature of most analysis techniques as it reduces bias, saves time and provides a standardised method for multiple end-users. While automation of analysis is an attractive prospect, there is the danger that serendipitous findings and familiarity with the imaged tissue may become limited when analysis is fully automated.

We designed an automated software pipeline for the analysis of microglial cells. Cell density, cell body size, cell body stain intensity and cell process complexity will be the cellular features identified in the software, as highlighted by the literature review as useful markers of microglial cells.

| Study | Software used/method of detection | Automated? | Parameters assessed | Context specificity |
|---|---|---|---|---|
| (Rey-Villamizar et al., 2014) | Python, 3D segmentation of stacks; cellular characterization | Partial | Ramified cells – high complexity; Moderately complex cells; Activated cells of low complexity; Amoeboid cells without arbours | Neuroprosthetic surgery, 4 phenotypes |
| (Karperien et al., 2013) | Image J, FracLac software | Partial | Fractal linearity ('$D_B$') | A range of cellular phenotypes |
| (Morrison and Filosa, 2013) | Image J, Analyzeskeleton and scholl analysis | Partial | Branch length Branch divisions; Area of cell spread | Ischemic stroke inflammation |
| (Kozlowski and Weimer, 2012) | Matlab, 3D segmentation of stacks; morphological quantification | Full | Cell density (with nuclear colocalization); Cell area; Roundness; Cell body size; Stain intensity | 4 acute doses of LPS |

| | | | | |
|---|---|---|---|---|
| (Paolicelli et al., 2011) | Image J 3D particle analysis plugin | Partial | Stain colocalization; Microglial cell density (with nuclear colocalization) | Developmental pruning |
| (Tremblay et al., 2010) | Single cell reconstruction, Image J tracing & Reconstruct software | No | Process area ($\mu m^2$); Colocalization of Spines and microglial processes (%) | Plasticity interactions |
| (Forero et al., 2010) | Image J, DeadEasy | Partial | Cell density (with nuclear colocalization) | Drosophilla mitotic glia |

*Table 17. Studies quantifying microglial cells*

Description of detection, automation status, parameters of assessment and demonstration of context specific sensitivity.

## *Software development.*

After assessing the software reported in the literature (**Error! Reference source ot found.**) we determined the following to be representative analysis parameters;

- Soma size
- Cell density
- Soma intensity
- Average branch length

We inspected images of microglia and, as proposed by (Kozlowski and Weimer, 2012), determined that a more accurate way to represent cell density was by using a DAPI channel colocalisation detection process. This ensures that all the cells quantified in the ROIs are indeed whole cells rather than larger clusters of processes captured in the volume.

Images were acquired for a batch of slides in a single session, this was to prevent error in laser drift and changes in gain between sesions. Images acquired in different sessions would be produced from batches of slides with control animal tissue included to ensure comparison can be accurately made (it is important to image control samples with experimental groups in imaging, particularly for the intensity based quantification).

Following acquisition, image files were converted to.tif image format as a maximum projection of the 11 plane stack. As a standardised identifyer, a suffix of _ch0 was added to low gain red channel images _ch1 was added to high gain red channel images and _ch2 was added to the DAPI images.

## Cell Profiler Software pipeline steps

1. **Load images** – Individual images were loaded from a source folder, with the DAPI channel and CY3 channel distinguishable for each image in the set. _ch0 and _ch2 image sets are given a RED or DAPI identifyer respectively.
2. **Correct illumination determination** – RED images are normalized to a standard illumination to account for variation in field of view brightness variation (image brightness drops off in the corners as the objective has a circular aperture). The illumination is scaled according to a standardised polynomial.
3. **Correct illumination application** – The illumination scaling is then applied to the RED image.
4. **Identify primary objects** – Microglial associated staining in the image is then identified from the illumination corrected image, the lower threshold for cell detection is 9 pixels in diameter and the upper bound for inclusion is 50 pixels in diameter. These values were based on cell sizes reported in the literature (Karperien et al., 2013; Kozlowski and Weimer, 2012) as well as preliminary testing with our image files. Objects outside this diameter were discarded, as were cells in contact with the border of the image (this was to prevent analysis of incomplete cells). In this module, Otsu Adaptive thresholding (Otsu, 1979) was performed to distinguish cellular staining from background, with 0.25-1.0 bounds on threshold. Clumped objects were distingushed in the red channel and the outlines of the red cells were overlaid on the illumination corrected image (Figure 32).

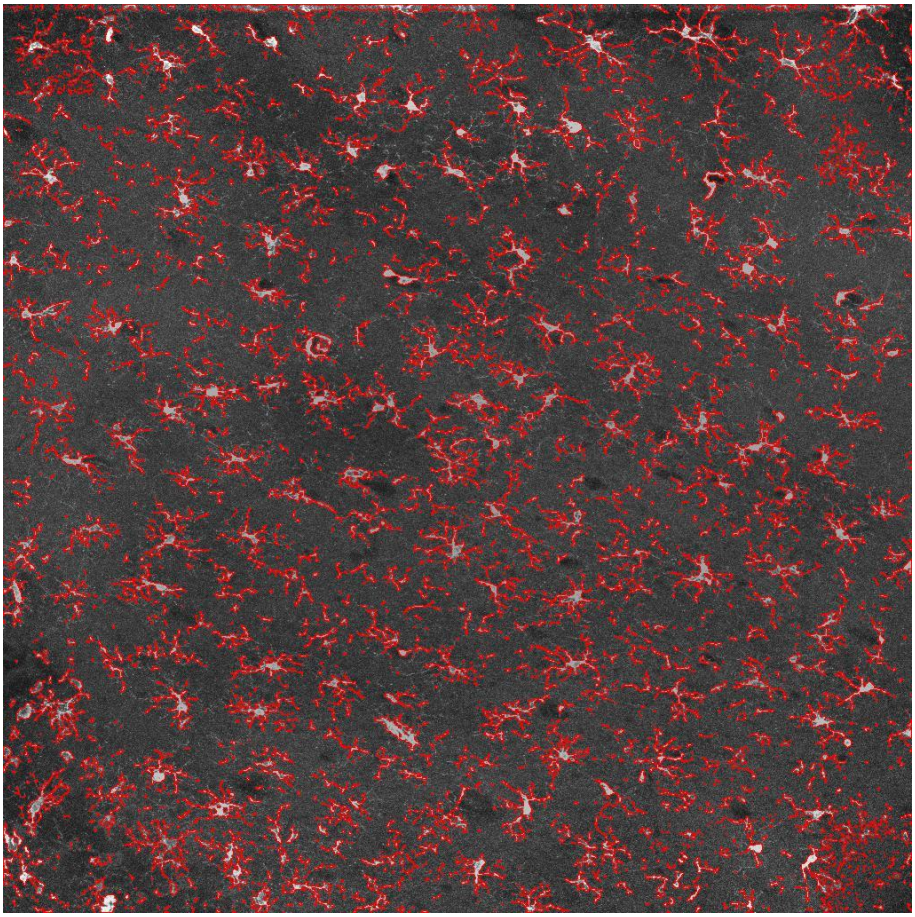

*Figure 32. Microglial process area detection*

Resulting detection image produced from pipeline step 4: Identify primary objects.

5. **Measure object size & shape** – The size and shape of the identified red objects are measured in this module.
6. **Filter objects** – The red objects identified are then further filtered so that a minimum measurement of size is retained for subsequent analysis, this step ensures that smaller clusters of cell processes are not later counted as cells when colocalisation with DAPI is implemented.

*The next three steps are implemented in the same manner for the DAPI channel as the red, however thresholds for identifying nuclei are marginally different.*

7. **Correct illumination calculate** – Same as red
8. **Correct illumination apply** – Same as red
9. **Identify primary objects** – The lower threshold for diameter is 5 pixels and the lower bound for thresholding is 0.08, ensuring all nuclei were detected. Clustered nuclei were identified through shape recognition. Outlines are then overlaid and a nuclear outline image is saved.
10. **Pause cell profiler** – At this stage the pipeline either pauses or continues, this step was implemented for the testing of software so that the full analysis was prevented from running once object identification had occurred.
11. **Mask objects** – In this module, the nuclei are masked to create an image to analyse colocalisation from.
12. **Mask objects** – In this module, the red cells are masked from the centre point of staining to provide an area to measure the cell soma.
13. **Measure objects size shape** – This module measures the now masked red cells prior to colocalisation with DAPI nuclei to gain a could of stain density. This is to compare the accuracy of nuclear colocalisation, as previous methods reported in the literature often do not confirm whole cell presence with a nuclear channel.
14. **Filter objects** – This module is a further size filter to ensure masked objects retain threshold criteria.
15. **Overlay outlines** – The filtered red cell outlines and masked nuclei are overlaid in this module to produce a visual output of colocalization. The whole

cell spread including processess are outlined in white, the filtered cells are outlined in green and the nuclei are outlined in blue (Figure 33).

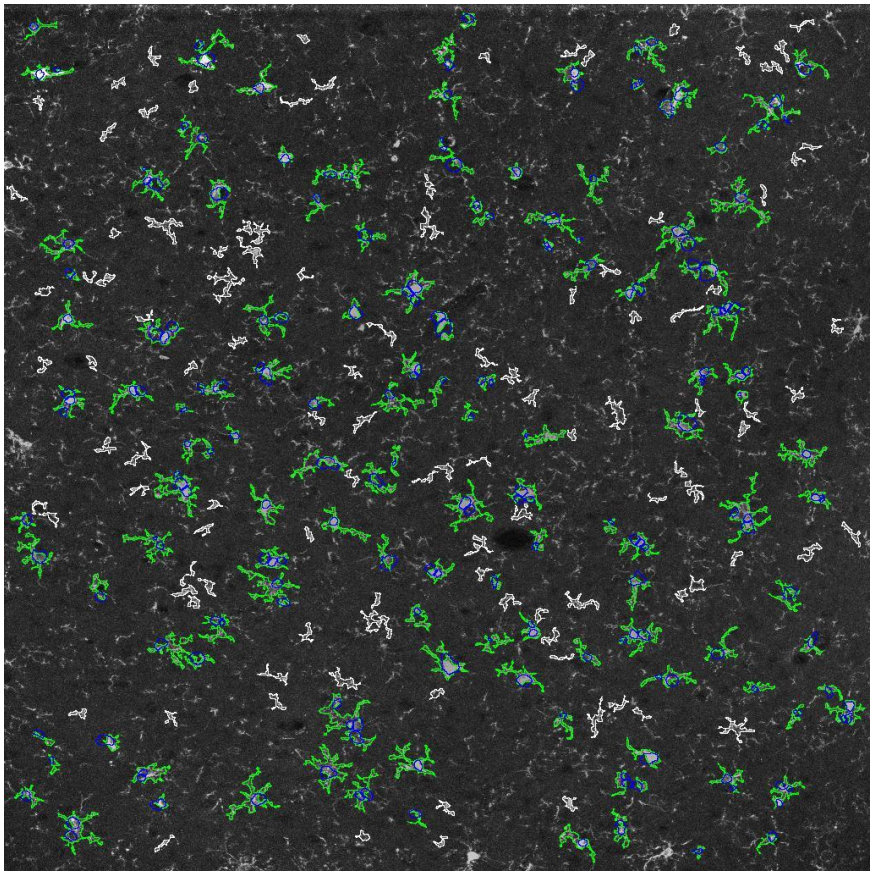

*Figure 33. Co-localised nuclear detection*

Overlaid nuclei and microglial cell stain processes from step 15: Overlay outlines

16. **Identify primary objects** – This module assess the area in the image occupied by cell processes, as this method has previously been used as a criteria for quantifying cortical microglial cells.
17. **Measure objects size shape** – The red cell process size and shape is quantified in this module.
18. **Measure object intensity** – In this module, the intensity of the masked red cell soma intensity is quantified.

19. **Overlay outlines** – In this module a final image of the red cell process coverage is produced, with a red outline of all cell process coverage.

20. **Measure image area occupied** – In this module, the full area of coverage is measured.
21. **Identify sencondary objects** – In this module, the procecess (here labelled the dendritic tree) associated with specific red cells are measured. This is to provide a quantification of whole cell spread rather than all process occupancy in the image.
22. **Measure object size shape** – The dendritic tree size and shape is measured.
23. **Overlay outlines** – Overlay images of the dendritic tree are produced and added to the cell soma images, where the tree has a red outline, the soma has a green outline and the nucleus a blue outline.
24. **Save images** – Cell body overlays are saved.
25. **Save images** – Cell process image overlays are saved.
26. **Save images** – Dendritic tree overlays are saved.
27. **Overlay outlines** – In this module nuclear DAPI overlaid images are generated.
28. **Save images** – DAPI nuclear outlined overlays are saved in this module (Figure 34).

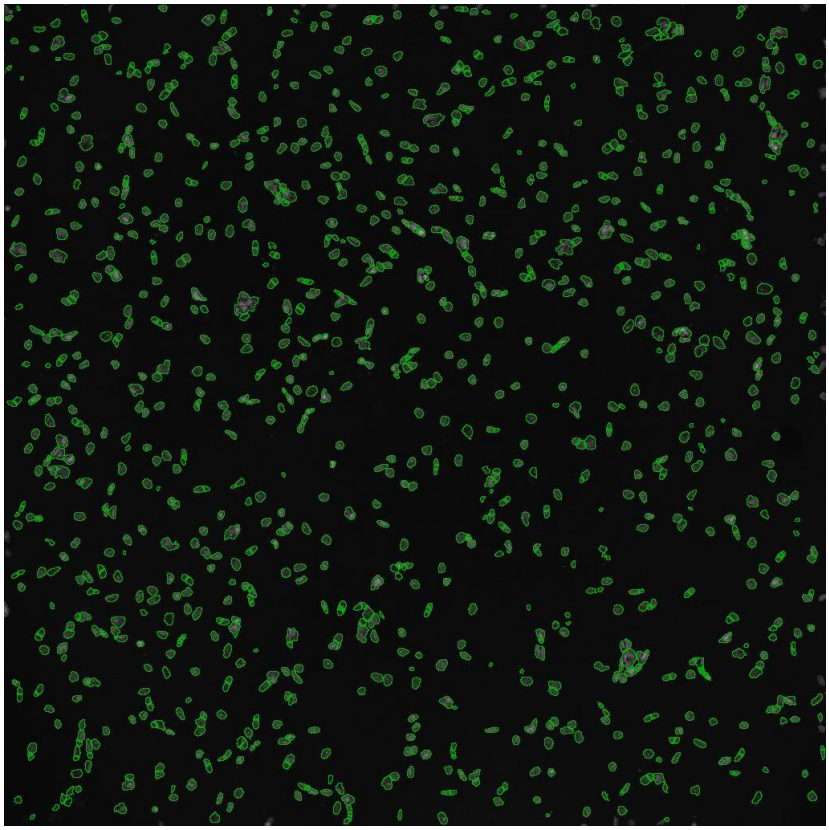

*Figure 34. Nuclear count detection*

DAPI Nuclei counting module image from stage 28: Save images.

29. **Export to spreadsheet** – The measurements are exported to a comma seprated (.csv) spreadsheet for analysis, with the output in Figure 35;

| | A | B | C | D | E | F | G | H | I | J |
|---|---|---|---|---|---|---|---|---|---|---|
| 1 | AreaOccu | AreaOccu | Count_Ce | Count_Fil | Count_Ma | Count_Nu | FileName | PathName_DAPI | | |
| 2 | 112820 | 1048576 | 93 | 115 | 93 | 1601 | 101_1_ch2 | P:\Analysis\Cell Profiler\10_8_14 | | |
| 3 | 101826 | 1048576 | 60 | 83 | 60 | 1685 | 101_2_ch2 | P:\Analysis\Cell Profiler\10_8_14 | | |
| 4 | 105958 | 1048576 | 135 | 218 | 136 | 2001 | 201_1_ch2 | P:\Analysis\Cell Profiler\10_8_14 | | |
| 5 | 105499 | 1048576 | 113 | 165 | 113 | 2062 | 201_2_ch2 | P:\Analysis\Cell Profiler\10_8_14 | | |
| 6 | 101097 | 1048576 | 91 | 152 | 92 | 1549 | 202_1_ch2 | P:\Analysis\Cell Profiler\10_8_14 | | |
| 7 | 104804 | 1048576 | 94 | 114 | 94 | 1525 | 202_2_ch2 | P:\Analysis\Cell Profiler\10_8_14 | | |
| 8 | 104691 | 1048576 | 117 | 200 | 117 | 2221 | 301_1_ch2 | P:\Analysis\Cell Profiler\10_8_14 | | |
| 9 | 111222 | 1048576 | 129 | 243 | 129 | 1838 | 301_2_ch2 | P:\Analysis\Cell Profiler\10_8_14 | | |
| 10 | 120428 | 1048576 | 116 | 149 | 116 | 1784 | 302_1_ch2 | P:\Analysis\Cell Profiler\10_8_14 | | |
| 11 | 111354 | 1048576 | 101 | 147 | 101 | 1427 | 302_2_ch2 | P:\Analysis\Cell Profiler\10_8_14 | | |

*Figure 35. Data output spreadsheet*

An excel file from the Cell Profiler based analysis pipeline. Where column A; area occupied, is the total area of process occupancy. Column B; area Occupied_Total, is the total area of the image analysed. Column C; Count_Cells_DendriticTree, is the number of cells with a dendritic tree record (the full data for dendtritic tree is produced in a separate spreadsheet). Column D; Count_Filtered, is the number of cells identified before the DAPI colocalization is applied. Column E; Count_Masked is the number of masked red cells with a DAPI nucleus colocalised. Column F; Count Nuclei; is the total number of nuclei in the DAPI channel. Column G/H are file and directory identifiers.

## Output/data

The data is easily interpreted from a spreadsheet design and can be imported to SPSS, matlab or r studio for statistical testing.